Planning, Operation and Control of Battery Energy Storage Systems based on Repurposed Electric Vehicle Batteries

by

Talal Alharbi

A thesis
presented to the University of Waterloo
in fulfillment of the
thesis requirement for the degree of
Doctor of Philosophy
in
Electrical and Computer Engineering

Waterloo, Ontario, Canada, 2020

Examining Committee Membership

The following served on the Examining Committee for this thesis. The decision of the Examining Committee is by majority vote.

External Examiner:	Rajiv Varma Professor Dept. of Electrical and Computer Engineering, University of Western Ontario
Supervisor:	Kankar Bhattacharya Professor Dept. of Electrical and Computer Engineering, University of Waterloo
Supervisor:	Mehrdad Kazerani Professor Dept. of Electrical and Computer Engineering, University of Waterloo
Internal Member:	Magdy Salama Professor Dept. of Electrical and Computer Engineering, University of Waterloo
Internal Member:	Ramadan El-Shatshat Lecturer Dept. of Electrical and Computer Engineering, University of Waterloo
Internal-External Member:	Gordon Savage Professor Dept. of Systems Design Engineering, University of Waterloo

Author's Declaration

I hereby declare that I am the sole author of this thesis. This is a true copy of the thesis, including any required final revisions, as accepted by my examiners.

I understand that my thesis may be made electronically available to the public.

Abstract

Battery Energy Storage Systems (BESSs) play a pivotal role in facilitating the grid integration of renewable energy resources and mitigating the impact of high penetration of Electric Vehicles (EVs). The increasing number of EVs, however, would lead to stockpiling of used Electric Vehicle Batteries (EVBs) after their vehicular End-of-Life (EoL). Since high installation and capital costs of new BESS pose a barrier to their large-scale deployment, utilization of the used EVBs after repurposing can play a significant role in power systems by helping defer capacity addition in the long-term. This would also alleviate the adverse environmental impacts of manufacturing more batteries and delay the recycling process of used EVBs. There are significant benefits for the utilities, EV customers, and governments in utilizing the used EVBs, as they offer a cheaper option for energy storage applications. In this context, BESS has emerged as a promising and viable solution for utilities such as microgrids and Local Distribution Companies (LDCs) for balancing their supply and demand and implementing efficient control and operation. The thesis aims at developing models for planning, operation, and control of BESS and Repurposed Electric Vehicle Battery (REVB) in isolated microgrids and distribution systems.

The thesis first presents a comprehensive and novel framework for planning and operation of BESS based on REVBs. A systematic procedure is proposed to model and simulate the degradation of EVBs during their first life in vehicles to capture the impact on their State of Health (SoH) and hence on the number of years to reach their EoL, which are used to estimate the expected cost of installing REVBs. A generic microgrid planning model is developed to determine the optimal energy and power ratings, and year of installation and replacement of new BESSs and REVBs considering the impact of calendar and cycling degradations. The proposed planning model introduces a novel set of mathematical relations for BESS degradation and optimal year of replacement, thereby avoiding premature replacements and additional costs. The EVB degradation model is arrived at by using a real EVs drive cycle database and the microgrid planning model is validated using the CIGRE isolated microgrid test system.

The thesis then extends the earlier proposed microgrid planning model to include system adequacy requirement using a novel backward-forward propagation approach with an embedded energy sharing strategy for multiple REVB units. A novel concept of measuring the adequacy level of the microgrid in terms of REVB energy to power ratio (E/P) is presented. The novel, heuristic, adequacy check module starts from

the terminal year of the planning horizon, and propagates to the initial year, to ensure that the microgrid's capacity adequacy requirements are met in all years. To accommodate multiple installations and replacements of REVBs over the planning horizon, an energy sharing strategy among various installed REVB units is proposed to enhance the battery useful life and delay their replacements so as to minimize the total cost. The proposed models are validated on the CIGRE isolated microgrid test system.

The third part of the thesis introduces an interactive real-time Community Energy Management System (CEMS) for an REVB-based Community Energy Storage System (CESS) in a practical Low-Voltage (LV) distribution system. This is an extension (in terms of operation and control) to the first research problem, where economic viability of installing REVBs is assessed. A rule-based controller for the four-quadrant REVB-based CESS is embedded in the CEMS to reduce the loading of the distribution transformer and slow down battery degradation. The proposed controller structure can be modified based on the specific characteristics of the battery. A Hardware-in-the-Loop (HIL) simulation is carried out to validate the simulation results and illustrate the effectiveness of the proposed CEMS and its rule-based control algorithm, using actual signals from the Battery Management System (BMS) and the bidirectional charger setup.

Acknowledgements

First and foremost, I shall praise and thank Allah Almighty for giving me the strength, patience, knowledge, ability and opportunity to undertake this research journey and to persevere the successful completion of this thesis. Without his blessings, this achievement would not have been possible.

Then, I would like to take this opportunity to express my sincere gratitude and appreciation to Prof. Kankar Bhattacharya and Prof. Mehrdad Kazerani, for the invaluable guidance, continual support and encouragement which they provided throughout my graduate studies at the University of Waterloo. Without their knowledge, enthusiasm, availability for discussions at any time and, most importantly, patience, I could not have made my way through this journey. Their commitment for high quality research is an inspiration for pursuing excellence and success not only in academic endeavors but in every other aspect of life.

My appreciation and thanks are also extended to Prof. Magdy Salama, and Prof. Ramadan El-Shatshat, and Prof. Gordon Savage from the University of Waterloo, for serving on my doctoral Advisory Committee, and for their insightful comments and feedback. I am also very thankful to Prof. Rajiv Varma from University of Western Ontario, for serving as the external thesis examiner and for his careful reading, wise comments and insightful observations. Furthermore, I would like to thank Prof. David Spafford for chairing my thesis examination committee.

With deep appreciation, I would to thank Qassim University in the Kingdom of Saudi Arabia, for granting me the scholarship to pursue my graduate studies. I also would like to thank the Ministry of Education, Saudi Arabia, and the Saudi Arabian Cultural Bureau in Canada for their support. I also acknowledge the partial funding and support from the Natural Sciences and Engineering Council of Canada (NSERC) through the NSERC Energy Storage Technology (NEST) Network.

I am truly indebted to my devoted mother, Nora Alhoimli, my brothers, and my sisters all of whom have constantly given me endless love, support, encouragement, and sincere prayers. I also wish to express my deepest gratitude to my dear brother Meshary for his sincerity, friendship and encouragements during my academic journey.

Words fail me to express my deepest appreciation to my lovely wife, Afnan, for her endless love, unfailing understanding, support and encouragement during my

PhD journey. She tolerated the stressful times and shared both the ups and downs of my PhD studies. This thesis was possible only through her love and care.

Special thanks are due to all my friends and colleagues of EMSOL, Power Electronics, and GAIA Labs at the University of Waterloo for their valuable and fruitful discussions and creating a pleasant and friendly working environment. A special note of thanks goes to my dear friend Mauricio Restrepo for his friendship and for sharing his thoughts during our technical discussions.

Finally, this thesis would not have been possible without the help, support and guidance of so many friends who shared happiness and tough times with me throughout various stages of this study and for making my stay memorable. Among them, Badr Lami, Rayed Alyousef, Omar Alrumayh, Hisham Alabduljabbar, Omar and Abdullah Bin Humaid, Majed Alotaibi, Abdulaziz and Nawaf Almutairi, Hesham and Walied Alharbi, Nizar Alsharif, Omar Alarfaj, Yasser Assolami, Abdulrahman Alorinan, and Dawood Alsaedi.

Dedication

To my mother, Nora, for her unconditional love, support, and blessed prayers.

To my family who gave colors to my life.

To the soul of my father, May Allah have mercy on his soul.

Table of Contents

List of Tables

List of Figures

List of Abbreviations

ANN	Artificial Neural Network
BCDM	Battery Capacity Degradation Model
BESS	Battery Energy Storage System
BEV	Battery Electric Vehicle
BMS	Battery Management System
CAN	Controller Area Network
CESS	Community Energy Storage System
CEMS	Community Energy Management System
COPT	Capacity Outage Probability Table
C2F	Cycle-to-Failure
DoD	Depth of Discharge
EV	Electric Vehicle
EVB	Electric Vehicle Battery
EoL	End-of-Life
EMS	Energy Management System
FOR	Forced Outage Rate
GHG	Greenhouse Gas
GAMS	General Algebraic Modeling Systems
HEV	Hybrid Electric Vehicle
HIL	Hardware-in-the-Loop
LDC	Local Distribution Company
LV	Low-Voltage
LoL	Loss of Life

LDC	Local Distribution Company
LP	Linear Programming
Li-Ion	Lithium-Ion
LOLP	Loss of Load Probability
MV	Medium-Voltage
MILP	Mixed-Integer Linear Programming
MINLP	Mixed-Integer Non-Linear Programming
NASA	National Aeronautics and Space Administration
NOAA	National Oceanic and Atmospheric Administration
NPV	Net Present Value
NLP	Non-Linear Programming
O&M	Operating and Maintenance
PHEV	Plug-in Hybrid Electric Vehicle
PCS	Power Conversion System
PVF	Present Value Factor
PV	Photovoltaic
PLL	Phase-Locked Loop
QP	Quadratic Programming
REVB	Repurposed Electric Vehicle Battery
RTT	Real-Time Target
RCA	Rainflow Counting Algorithm
RES	Renweable Energy Source
SoH	State of Health
SoC	State of Charge
SMP	Symmetric Multi Processing
VLDM	Vehicle Longitudinal Dynamic Model
VSC	Voltage Source Converter
VPM	Vehicle Power-train Model
V2G	Vehicle-to-Grid
UC	Unit Commitment

Chapter 1

Introduction

1.1 Motivation

Reduction of Greenhouse Gas (GHG) emissions is a long-term government commitment of many countries around the world. Based on reports published by National Aeronautics and Space Administration (NASA) and the (US) National Oceanic and Atmospheric Administration (NOAA), the warmest year globally, since recording began in 1880, was 2015 [1]. The two main GHG emission contributors, that produce energy by the combustion of fossil fuels, are the electricity and transportation sectors. According to Environment Canada, the latter accounts for 24% of total national emissions [2]. Moreover, the transportation sector being dependent on oil, is an issue of energy security, as it means being dependent on foreign resources in the long-term.

In pursuit of addressing the aforementioned environmental challenges, many federal and provincial governments around the world have started adopting policies to promote electrification of the transportation sector, and integrating clean Renweable Energy Sources (RESs) such as wind and solar in the electricity sector which is in accordance with the Paris (climate change) Agreement of 2015. In Canada, the province of Ontario offered a package of $250 million in incentives and programs to electrify the transportation sector by 2020 [3] and Canada has set a target to reduce its 2005 GHG emission level by at least 30%, by 2030 [4]. In Norway and the Netherlands, policies have been implemented to ensure that all passenger cars purchased from 2025 onward are Electric Vehicles (EVs) [5].

It is a fact that nearly all automotive manufacturers are now producing EVs and have made significant investments in EV development to meet the demands of the market. According to the International Energy Agency (IEA) publication, *Global EV Outlook* 2018, the global EV stock exceeded 5.2 million cars in 2018 after crossing the first million threshold in 2015 [6]. In Canada, the EV market sales growth in 2018 for EVs was 125% of 2017 levels [7]. Globally, the sale of EVs will continue to grow in the coming years and is expected to touch 100 million units by 2030 [8].

When an Electric Vehicle Battery (EVB) reaches its End-of-Life (EoL), it is removed from the vehicle and replaced by new batteries in order to maintain the power and energy density require for high performance of the vehicle. There are two options for the used EVBs, recycling or repurposing. The first option is not preferred and justifiable since the used EVB still has enough energy capacity to serve in a variety of stationary applications [9]. According to [6], in Ontario, Canada, 500,000 EVs will be driven on the province′s roads by 2025.

This will result in stockpiling of a large number of used EVBs, because of the need to replace batteries periodically. The challenge of disposing of these EVBs safely at their EoL would be immense, because of the safety hazards involved, and the fact that recycling them would be wasteful due to the significant energy capacity left in the battery. Significant economic and environmental benefits can be accrued if EVBs can be reused after the end of their first life. They can either be reused directly after their EoL, or go through a process of refurbishing and repurposing before being used again in stationary energy storage applications. There is also a need for a systematic procedure to model the degradation of EVBs during their first-life.

While grid reinforcements involve high investment costs, a cheaper option, that metaphorically kills two birds with one stone, is the reuse of EVBs for this purpose. The reuse of EVB is also an opportunity for the EV owners to lower their replacement cost while helping the system ensure a secure and reliable energy supply in the grid at a much lower cost.

In recent years, Battery Energy Storage Systems (BESSs) have come in the limelight offering viable solutions to grid operators to overcome the uncertainty introduced by the growing presence of RES and the consequent need for more system reserves and deferring high upgrade costs. A lot of work has been reported in recent years [10–14] on the applications of BESS in microgrids. However, the high cost of BESS limits their large-scale deployment in stationary applications. Therefore, there is a need to explore viable solutions to potentially offset the high initial cost

of BESS and one of them is the utilization of reused or Repurposed Electric Vehicle Batteries (REVBs). REVBs can reduce the high cost of fuel transportation along with reducing the environmental impact.

However, there is a need to develop microgrid planning models which examine both REVBs and new BESS as possible options, taking into account their degradation characteristics, and arrive at the most suitable and economically viable investment decisions for the microgrids.

The ability of a microgrid to meet the demand at all times (over the plan horizon) is reflected on its adequacy. One of the means to meet adequacy requirements, is by installing REVBs. However, energy capacity of REVBs are affected by their cycling and calendar aging which significantly impacts the microgrid adequacy performance. Therefore, the microgrid planning models need to determine the optimal set of REVB investments that ensures the adequacy level of the microgrid while also capturing their degradation during the operational process over the plan horizon.

The REVB can also serve as part of a Community Energy Storage System (CESS) while being owned by the Local Distribution Company (LDC); they can also be owned by microgrid operators for various applications. CESS refers to a small grid-scale distributed energy storage located in the distribution system, which releases the stress and ensures efficient operation [15]. With significant increase in residential BESS deployment in recent years in Ontario [16], CESS designed using REVBs can provide a cost effective solution.

The utilization of REVBs with appropriate modelling and control system is worth examining. There is a need to carry out Hardware-in-the-Loop (HIL) simulations which would allow the dynamic behavior of REVB-based CESS to be realistically represented and controlled, for CESS grid integration applications.

With increasing number of EVs each year, which leads to stockpiling of used EVBs, the goal of the research presented in this thesis is to model, plan, and investigate the feasibility, economic opportunities, and technical operational aspects of integration of REVBs in stationary applications. The efficient and proper control of REVB units would lead to their large-scale deployment in grid-scale (*e.g.*, CESS) or microgrid applications. Also, it will offset the high replacement cost of batteries for EVs owners.

1.2 Literature Review

In this section an overview of the relevant research reported in the literature pertaining to EVs, BESS planning and operations in microgrids, and CESS are presented and discussed.

1.2.1 Electric Vehicles

There has been a growing interest during the last decade in the electrification of the transportation sector as a promising solution environmentally, and economically. The benefits of EVs are well understood and so are the technical and economical challenges of integrating them into the grid. To study these benefits and challenges, EV market forecast is needed in order to determine (i) the expected aggregated charging demand, and (ii) the expected storage capacity available from used EVBs.

Several studies are reported in the literature on the forecast of EV market penetration under various scenarios [6,17–19]. As stated in a recent report [20], the global sales of EVs is expected to reach 54% of the sales of new light duty vehicles in 2040. Moreover, it is estimated that 34% (530 millions EVs in total) of the global vehicle fleet on the road will be electric by 2040. With fast growing number of used EVBs, it is expected that REVBs will be readily available in the market.

1.2.1.1 Electric Vehicle Battery Degradation

Since REVBs are proposed to be used later in generic microgrid planning models, a systematic procedure to model and capture the degradation of EVBs during their first life in the vehicles, is needed. As a result, this part of the literature review focuses on the modelling of an EVB and its degradation.

The Li-Ion EVB capacity degradation takes place during operation (referred to as cycling degradation) and in its idle state (referred to as calendar degradation). The cycling and calendar degradations cause permanent energy capacity loss in the EVB, which should be captured and modeled. Thus, it is important to estimate the State of Health (SoH) of the EVB over the time of their vehicular life. Several studies in the literature developed different models estimating the degradation of Li-Ion batteries using various approaches, considering different ageing factors [21]. In [22], a practical capacity degradation model for Li-Ion batteries under different conditions

was developed; it was noted that the capacity degradation of the battery depends on several factors such as its State of Charge (SoC) and temperature. However, only the cycling effect was accounted for, while calendar degradation was not considered. Even though calendar degradation per year in Li-Ion batteries is small at room temperature, it is important to be taken into account to determine the true cost of the EVB after vehicular EoL [23] which would impact the cost of REVBs and consequently the microgrid planning decisions.

The authors in [24] apply a simple method to predict the degradation of EVBs in second-use stationary applications; the degradation model does not consider capacity losses due to calendar degradation and SoH is assumed rather than modelling and simulating the first life of EVBs to predict it.

1.2.1.2 Repurposed Electric Vehicle Battery

Researchers are examining various usages of REVBs in stationary applications, but only a few projects have been reported so far [9, 25]. To integrate REVBs in such applications, the SoH of EVBs at their EoL need be considered. The life of an EVB can be extended after vehicular use by utilizing it in secondary applications under safe and secure conditions that brings about savings for the electric utilities and reduces the overall cost of new batteries for EV owners [26, 27]. Having substantial energy capacity after its first life, EVBs can either be directly used or reconfigured and repurposed for stationary applications. The authors in [28] reported that the direct reuse of EVBs has more disadvantages than repurposing them; although direct reuse is cheaper, their reliability and safety are of concern.

Since the idea of using REVBs in stationary applications is still under research, only a few projects have been reported in the literature, while very little work is available on pricing of REVBs. Studies in [29, 30] and [25] explored various possible market prices of REVBs. The market price consists of: (i) buying the used EVBs, (ii) selling the REVBs that implicitly includes the repurposing cost, considering sorting, collecting, testing, and reassembling the used EVBs.

The market price of Li-Ion REVBs is calculated in [25] based on a facility that is adequate for testing and repurposing the used EVBs. The work in [31] extrapolated the economic evaluation model presented in [25], while changing module size, cell failure rate, and improvement in testing requirements.Various inputs are needed to determine the price of REVBs, the SoH of used EVBs being the most crucial input.

In recent years, various pilot projects for REVBs have been launched in Germany. For instance, North Rhine-Westphalia has developed an REVB of 13 MWh energy capacity, realized from 1,000 used EVBs. This makes it the largest second-use EVB in the world [26]. Another pilot project in San Diego, California, USA is in collaboration with BMW for testing the second life for EVBs. The project uses a repurposed Mini E BMW EVB for stationary energy storage application. The size of the project is 100 $kW/108$ kWh of Li-Ion based batteries. The benefits potentially achieved are reliability, RES integration, and reduction in overall cost of the EV [26].

In [32] an EVB is directly used in stationary application without repurposing; various operational topologies and their associated controls are proposed. Different types of battery chemistry were considered (including lead-acid, NiMH, and lithium) to develop a flexible interface scheme based on modular boost-multilevel buck converter. The authors concluded that a proper interface scheme with an efficient controller can tackle the widely different voltages of different chemistries.

1.2.2 BESS Planning and Operation in a Microgrid

One of many purposes of introducing BESS in a microgrid is to reduce the total investment and operating cost by overcoming the uncertainty introduced by RES and the consequent need for more system reserve, and delaying high upgrade costs. In this section some of the works reported in the literature addressing BESS planning and operation in a microgrid are discussed; the main issues being: BESS power and energy capacity sizing considering REVBs, battery degradation, BESS replacement considering degradation, BESS planning and operation considering reliability, multi-unit BESS planning, and power sharing for installed multi-unit REVBs.

Many works have been carried out in recent years [10–13] to examine the role of BESS in supporting microgrids with rising cost of fossil fuel based generation.

An optimization method was introduced in [10] to find the optimal BESS size in isolated and grid-connected microgrids. Artificial Neural Network (ANN) was used for forecasting the wind and solar generation profiles. It was found that the optimally sized BESS would reduce the total cost for an isolated microgrid and increase the total benefit of a grid-connected microgrid. The BESS lifetime was assumed to be fixed (three years), which is not accurate since the life depends on its cycling and calendar degradation.

A two-stage stochastic optimization model for a microgrid planning problem considering BESS, solar, and wind was proposed in [11]. The first stage considers investment decisions while the second seeks to minimize the microgrid's operating cost. However, the work uses a low value for the limit on BESS Depth of Discharge (DoD) which does not accurately reflect the battery degradation during its operation. A low DoD enforces the planning model to oversize the battery capacity during installation. Also, the work does not consider the replacement cost for the battery. Furthermore, battery degradation is not reflected on its energy capacity, which is important, so as to capture the true cost of operation of the microgrid.

A study on cascaded sizing of BESS in remote microgrids equipped with wind farms was carried out in [12]. Although it was noted that BESS capacity addition over time could reduce the total operating cost of the microgrid, their degradation and replacements were not considered.

In [33], a multi-stage algorithm for sizing of BESS and upgrading the geothermal generators was studied, considering the technical and economical constraints, in an isolated microgrid with high wind penetration. Battery capacity degradation was considered and the BESS would be replaced once it reaches 25% of its initial energy capacity. Although capacity degradation was considered, the model was not explained and degrading the battery to 25% capacity is not realistic.

In [34], BESS planning in microgrids was carried out considering life-cycle degradation, by accounting for the number of Cycle-to-Failure (C2F); however, the reduction in BESS energy capacity due to cycling and calendar degradations was not considered.

In [35], a stochastic optimization framework for BESS planning for isolated microgrids was proposed, wherein BESS cycling degradation was considered on a flat-rate basis, not capturing the true capacity loss during discharging, and thus over- or under-estimating the battery energy capacity. Also, a fixed replacement year was considered, leading to premature replacement decisions and hence increasing the plan cost.

BESSs involve high capital investments and can be economically unattractive in microgrid application. In such a context, REVBs can provide the same services at a fraction of the cost of a new BESS [9]. Also, by repurposing an EVB it would delay its recycling and prolong its useful life.

It should be noted that, none of the above works attempted to determine the optimal year of BESS replacement. Moreover, in most of the reported works, either

the number of C2F or the impact of cycling and calendar degradations on the size are considered, but not both, which is necessary to accurately capture the BESS energy capacity and optimal operation. Also, there is a need to connect the stages of EVB life to test the viability of REVBs in secondary applications.

For installation of either new BESS or REVBs in isolated microgrids the following important issues need be considered: a) determining the optimal year of installation, along with the optimal power and energy capacity ratings; b) optimal operation of these devices; c) proper consideration of calendar and cycling degradation of BESS and REVBs; and d) determining an optimal year of BESS replacement, considering degradation, instead of using a fixed replacement year which can lead to premature replacements and additional costs.

BESS Planning and Operation in a Microgrid Considering Reliability

There are very few reported works in the literature that consider BESS or REVB planning and operation in a microgrid taking into account system reliability. In [36], a holistic reliability model for power electronic equipment of a BESS in isolated microgrids was proposed, where equipment failure rates were calculated and the overall microgrid reliability was quantitatively determined. Degradation of the BESS was not considered, which is critical when evaluating and assessing isolated microgrid reliability.

The optimal investment plan considering BESSs and solar Photovoltaic (PV) units is determined for a microgrid in [13]. Reliability was considered using two scenarios: a sudden large change in load and a sudden change in solar irradiation intensity. It is noted that the BESS can accrue benefits to the microgrid with an appropriate capacity configuration. However, battery degradation or replacement cost was not included in the planning model, which would have significantly impacted the reliability evaluations.

In [37], the role of optimal BESS sizing on microgrid reliability is examined, although battery degradation is not considered. The BESS was assumed to be single-unit facility with a fixed life which under- or over-estimates the installed size of BESS. The degradation of battery not reflecting on the installed capacity size has an impact on reliability of the microgrid.

A BESS sizing model in a microgrid considering reliability is proposed in [38]. The model minimizes the BESS installation cost and the expected microgrid operating

cost. However, only one year of the planning horizon was assumed. No degradation of the BESS was considered, which greatly affects the adequacy of the system when it is taken into account.

In [39], a comprehensive multi-year distribution system planning model was proposed considering reliability of the system as a constraint, and using a back-propagation algorithm. However, the use of BESS was not considered.

Multi-Unit BESS Installations

The previous works pertaining to microgrid planning with BESSs and REVBs [10–13, 33–35, 40, 41] did not consider multi-unit installations. Multi-unit installations have benefits to microgrid operators since these boost the microgrid adequacy by having more units (hence more capacity) online when there are outages. Also, the discharging energy dispatched by the microgrid operator would be shared among the multi-units which ultimately reduces battery degradation. Moreover, multi-units can play a vital role in deferring the need for replacements or new installations when a proper power sharing strategy between the units of the BESS/ REVB is used.

In [42] an Energy Management System (EMS) is proposed for the short-term operation of a renewable hydrogen-based microgrid. It is noted that although the power sharing strategy is a valid approach, it is not able to optimize the performance for mid- and long-term operations. Therefore, there is a need for power sharing strategy for long-term planning models while keeping the degradation of the BESS as low as possible. When system upgrades are essentially driven by the continuously increasing demand, the simultaneous multi-unit REVB installations and a proper power sharing strategy can play a vital role in deferring the need for replacements or new installations.

Coordination of multi-unit REVB operation and planning can reduce the total cost of the microgrid. Although, in the literature, there are several studies that consider BESS in general, very few have considered planning of REVBs in isolated micrgrids considering adequacy, while no works have considered an power sharing strategy coupled with battery degradation.

It is noted from the above review that most of the reported works on sizing of BESS in a microgrid do not properly take into account battery degradation due to cycling and calendar aging. On the other hand, some degradation models reported in the literature [21, 43] are too detailed, involve non-linear functions, which makes the

BESS planning problem very difficult to solve. Therefore, there is a need to introduce a linear degradation model that can be easily implemented within a microgrid planning model. Moreover most of the works on BESS sizing, consider a fixed replacement year, which however can lead to incorrect replacement decisions and hence increase the plan cost. Therefore, it is necessary to consider BESS replacement year as a decision variable.

1.2.3 Community Energy Storage System

Introduction to CESS

The concept of CESS has gained attention amongst utilities in recent years with the possibility of deploying BESS at the distribution level [44]. Typically, CESS is defined as a utility-owned system that is connected to the LV distribution system to immunize the network against adverse impacts of increased loading, outages, and power quality issues [45]. With increasing penetration of EVs, REVBs are expected to present a viable solution to the utility and customers by facilitating the development of CESS. The use of REVBs as CESS would offset the utility cost by improving the voltage profile and mitigating distribution transformer aging.

In [46], a discrete-continuous particle swarm optimizer was used to optimally size a CESS considering solar panels and EVs to maximize the Net Present Value (NPV) of profit from the energy arbitrage. It was noted that CESS could benefit the distribution system by reducing the power losses, provide energy arbitrage and improve the voltage profile. However, the work consider neither battery degradation nor a proper EMS for CESS. EMS of CESS or, henceforth referred to, in this thesis as Community Energy Management System (CEMS), is essential as it modifies the control signals of the CESS based on the battery SoH. In [47] a CESS was proposed to mitigate the voltage rise/ drop encountered by the grid due to high PV/ EV penetration, but the work did not consider a detailed model of CESS taking into account the technical constraints.

In [48], a profit maximizing operation framework for CESS was proposed to optimally charge/ discharge the batteries taking advantage of the fluctuating electricity prices. The proposed control architecture of CESS only controls the battery active power, and if the CESS battery is degraded, the controller is not able to provide any further controller maneuvering. In [49], households with smart appliances and

CESS were assessed from the perspective of the end-consumer. Two indices were used to evaluate the CESS, the levelized cost of energy and the payback period. The proposed control constraints does not take into account the battery SoH which is important to capture CESS degradation and hence modify the charging and discharging signals accordingly. The CESS capability to provide reactive power was not considered in the proposed control.

With increasing adoption of EVs, their charging loads can lead to under-voltages at distribution system nodes, and over-loading of feeders and transformers [50]. These impacts can be alleviated by upgrading the transformers and feeders or implementing coordinated charging of EVs [46, 51–53]. Given that upgrading the transformers and feeders is not a cost-effective solution and policies and communications infrastructure for coordinated charging are not available, installing CESS in LV distribution systems [46, 54], particularly with REVBs, is a viable alternative due to the increasing availability of batteries in the market. Most of the studies on the control of distribution systems, reported in the literature, focus on Medium-Voltage (MV) and very little has been done on control of LV distribution systems or on designing a proper control for CESS [51, 53]. Therefore, there is a need for a proper controller for CESS in an LV distribution system that ensures its successful operation and takes into account the impact of battery degradation.

Currently, there are only a few projects around the world based on CESS, owned by the LDCs. The reason for utilities not installing CESS is that EV penetration has been low so far and not impacting the grid. Also, from economic standpoint, these are not viable because of the low level of EV charging demand and high cost of new batteries. A CESS using REVBs presents opportunities to provide energy to the LDC and reduce the impact of its EV charging load if a proper control strategy for CESS is introduced.

EMS for CESS

In [55], a bi-level optimization approach is proposed to solve the EMS model for communities under a distribution grid outage event. The CEMS model coupled with home energy management system of various houses was iteratively solved. The CEMS is responsible for controlling the battery charging/discharging power and reshaping decisions of the load for each house. It is noted that during grid outages, the CEMS with its CESS and home energy control can have self-powered supply capability. However, the CEMS control only provides P services to the communities.

In order to provide bidirectional P and Q services and limit battery degradation using a CESS, a four-quadrant charger is needed. Most of the bidirectional chargers reported in the literature focus on P-control from the viewpoint of EVs, but not from the point view of CESSs. Similarly, there is little work on providing Q-services by CESS [52, 56]. To this effect, a controller for a four-quadrant EV charger was proposed in [57], which took battery degradation cost into account; however, this work did not include any HIL simulations based on detailed model of the power network, and reducing the Loss of Life (LoL) impact of LV distribution transformer was not analysed.

There are challenges that have to be overcome in controlling the active and reactive powers using CESS, while seeking to reduce the adverse impact on the battery SoH. A CEMS equipped with an effective controller for the CESS would be capable of improving the flexibility of the distribution system in a cost-effective manner, while extending the life of the REVBs and the LV distribution transformer.

So far, only a few works have attempted to realize the operational benefits of a CESS employing REVBs with a properly-designed CEMS. Such a CEMS should be tested in an appropriate platform under different conditions to identify and address the issues that may appear in real-life operation. In view of this, HIL simulations become relevant in fast and accurate analysis of large and complex systems, such as an LV distribution system equipped with CEMS.

HIL Simulation

HIL simulation is a comprehensive platform which is a synergic combination of actual hardware components and computer simulation models in a closed-loop environment. One of the reasons for utilizing HIL simulations is that it allows the dynamic behavior of the battery-based CESS to be realistically represented and controlled [58]. While some works on CESS for grid integration have been reported [59], the majority of the existing works pertaining to battery-based CESS use the battery in a simulated environment, and not in an HIL environment [60]. Also, most of the reported research concentrates only on the economic side of CESS based on new batteries [35, 46, 54, 61–64], but not their implementation and control.

To the best of the author's knowledge, the use of REVB-based CESS for active and reactive power control in LV distribution networks has not been reported in the literature. The control of EVs from the LDC's standpoint has been considered for

slow residential EV charging by optimally sharing the available capacity of the LV transformer among several EV loads, which are also used as reactive power control devices [51, 52, 65]. However, compared with a Vehicle-to-Grid (V2G) scheme, the CESS can provide a better support to the grid as it is permanently connected, it is able to go beyond the limits of the LV transformer to locally supply any extra load, and can offer local voltage regulation.

It is noted that researchers have examined different simple approaches in controlling P and Q based on the V2G framework, considering merely battery degradation while tuning the controller parameters. However, to the best of the author's knowledge, a study on the integration of a CEMS in an LV distribution system using REVB in HIL environment has not been reported in the literature.

In view of the above discussions, there is a need for a real-time CEMS to control an REVB-based CESS and study its interactions with a practical LV distribution system using an HIL simulation environment.

1.3 Research Objectives

The main objectives of the research presented in this thesis are as follows:

- Develop a systematic procedure to model the degradation of EVBs for different classes of EVs during their first life in vehicles, and incorporate these characteristics to estimate the expected cost of installing REVBs. Considering multiple drive cycles of different classes of EVBs would capture the impact on their expected SoH and hence on the number of years to reach their EoL. The market price of REVBs will be obtained using the capacity of the degraded EVB units and their SoH, which will determine the economic feasibility of REVBs as compared to new BESS in the long-term energy supply planning of a remote microgrid.

- Develop a generic microgrid planning model to determine the optimal energy size, power rating, and optimal year of installation and replacement of new BESS and REVBs. The planning model should include the impact of degradation due to calendar and cycling effects on the BESS/REVBs' energy capacity, as well as on the number of C2F. The proposed model will introduce a novel set of mathematical relations for BESS degradation and optimal year of replacement, thereby avoiding premature replacements and additional costs.

- Extend the proposed microgrid planning model to include multi-unit REVBs to simultaneously determine their multiple optimal installations, power and energy sizing, replacement and investment timelines. To ensure that the microgrid's capacity adequacy requirements are met at all years, a heuristic backward-forward propagation process will be proposed.

- Develop a generic real-time CEMS to control a four-quadrant REVB-based CESS and study its interactions with a practical LV distribution system using an HIL simulation environment. The real-time CEMS will be validated with an actual setup comprised of an actual Li-ion battery pack, for HIL simulation, together with a four-quadrant charger.

1.4 Organization of the Thesis

The rest of this thesis is structured as follows:

Chapter 2 presents a brief background to the relevant topics related to this research, including a description of microgrids, the generic Unit Commitment (UC) formulation, BESS, basic concepts of EVB modelling and degradation, REVBs for secondary use applications, a review of the Rainflow Counting Algorithm (RCA), and some fundamentals of mathematical programming.

Chapter 3 presents a systematic procedure to model and simulate the degradation of EVBs and the novel framework and mathematical model for planning and operation of isolated microgrids using BESS and REVB.

Chapter 4 presents the framework and mathematical model for a novel backward-forward propagation approach with an embedded power sharing strategy for REVB units to develop a microgrid planning model taking into consideration its reliability aspects.

Finally, Chapter 5 presents a CEMS equipped with a rule-based controller for REVB-based CESS and includes detailed analysis carried out using an HIL simulation test-bed.

Chapter 6 presents the summary, concluding remarks and main contributions of this thesis, and identifies some directions for future research work. Detailed data of the test systems and other related inputs to the models used in this thesis are presented in Appendices A and B.

Chapter 2

Background

This chapter presents a brief background review of the main topics and tools relevant to the research proposed herein. The microgrid concept is presented, followed by an overview of the BESS and its services. An overview of EVs and their models are discussed, followed by a review of REVB for second-use applications. A typical two-stage bidirectional converter topology is explained and the distribution transformer degradation estimation is briefly discussed. Finally, a review of the RCA and some fundamentals of mathematical programming are presented.

2.1 Nomenclature

Indices

g	Index for generating units	$g \in G$
t	Index for operation-steps, [hour]	$t \in T$
i	Index for operation-steps, [second]	$i \in I$

Parameters

CUP_g	Start-up cost generating unit	[$]
CDN_g	Shut-down cost generating unit	[$]
$\underline{P_g}$	Minimum generator power limit	[kW]
$\overline{\overline{P_g}}$	Maximum generator power limit	[kW]
$Pd_{y,t}$	Isolated microgrid demand	[kW]
RUP_g	Maximum ramp-up generator	[kW]
RDN_g	Maximum Ramp-down generator	[kW]

Variables

P_t^{Res}	Isolated microgrid reserve demand	[kW]
$U_{g,t}$	Start-up binary decision [1 or 0]	
$V_{g,t}$,	Shut-down binary decision [1 or 0]	
$W_{g,t}$	Unit-commitment binary decision [1: ON or 0: OFF]	

2.2 Microgrid

A *microgrid* is defined as a cluster of loads and small-generation technologies operating as a single controllable entity that provides both power and heat to its local area. Microgrids can operate either in grid-connected mode, where there is a point of common coupling, or in isolated mode [66]. The general architecture of a microgrid is shown in Figure 2.1. Microgrids include conventional diesel generators, wind turbines, micro-turbines, PV panels, and energy storage systems, *e.g.*, batteries, ultracapacitors, and fuel cells.

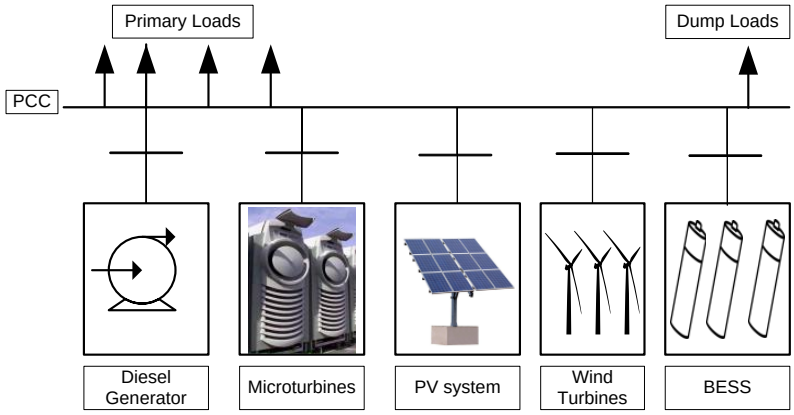

Figure 2.1: Schematic diagram of an islanded microgrid

The operation of microgrids has to be economically viable and technically reliable [67]; the challenges are greater for isolated microgrids. With increasing deployment of RES to reduce the fossil fuel dependency and reduce operation cost, particularly in isolated microgrids, energy storage systems are essential as these can help the isolated microgrids achieve better economy of operation.

The connection modes of a microgrid are of two types: grid-connected mode or islanded/isolated mode. There are many examples of islanded/isolated microgrids

around the world, and in Canada there are around 280 isolated microgrids [68]. These microgrids do not have interconnection with the main electric grid primarily because of geographical reasons.

Microgrid: Basic Scheduling Model

The basic scheduling model used in a microgrid essentially deals with committing the available generating resources in close to real-time, and is similar to a traditional UC model. The objective is to minimize the microgrid operation cost while meeting the load and satisfying the generator limits and other system constraints [69, 70]. Several optimization methods have been proposed to solve the UC problem [69, 70]. A general UC mathematical model is presented in [70]. The formulation of the UC objective function and constraints are discussed in detail next.

Objective Function:

The objective function is the total generation cost of the available generating resources over the operation horizon:

$$J = \sum_{g \in G} \sum_{t \in T} \Big[C_g(P_{g,t})\, W_{g,t} + CUP_g\, U_{g,t} + CDN_g\, V_{g,t} \Big] \tag{2.1}$$

where the first term of (2.1) represents the generation cost from the thermal units; the cost function $C(.)$ can either be a linear or a quadratic function. The second and third terms respectively represent the start-up and shut-down costs, associated with the thermal generators. Minimization of the objective function is subjected to several constraints, of which, the most relevant ones are presented below [70]:

- Upper and lower limits of generation:

$$\underline{P_g}\, W_{g,t} \leq P_{g,t} \leq W_{g,t} \overline{P_g} \qquad \forall t \tag{2.2}$$

- Supply-Demand Balance: Total system demand at each hour should be supplied by the power generated.

$$\sum_{g \in G} P_{g,t} = Pd_t \qquad \forall t \tag{2.3}$$

- Spinning Reserve Constraint: Reserves are important for isolated microgrids to maintain a secure and flexible operation. Therefore, a constraint on system spinning reserve is imposed at all time periods.

$$\sum_{g \in G} \left(\overline{P_g} \, W_{g,t} - P_{g,t} \right) \geq \; P_t^{Res} \qquad \forall t \qquad (2.4)$$

$$P_t^{Res} = 10\% \; Pd_t \qquad \forall t \qquad (2.5)$$

- Ramp Up/Down Constraints: The increase or decrease in the generation between two consecutive time intervals is subjected to ramp-up and ramp-down limits, respectively.

$$P_{g,t} \leq \; P_{g,t-1} + RUP_g \qquad \forall g, t; t \neq 1 \qquad (2.6)$$

$$P_{g,t} \geq \; P_{g,t-1} - RDN_g \qquad \forall g, t; t \neq 1 \qquad (2.7)$$

Concept of Adequacy

The system adequacy is defined as the ability to meet the peak demand in a steady state condition [71].

2.3 Battery Energy Storage System (BESS)

Energy storage systems such as batteries have the capability to improve the performance of the system and also contribute to several applications. Table 2.1 presents the range of applications of energy storage systems to power systems [72]; it is to be noted that many of applications are relevant to isolated microgrids also.

The BESS generally comprises the following main components: battery modules, BMS, Power Conversion System (PCS) including bi-directional converters, controller, and transformers, and EMS that controls the bi-directional flow of energy between the grid and the BESS, as shown in Figure 2.2.

One of the challenges that the BESS can address is smoothening the output generation profile of RES. When surplus energy is generated by PV or wind, it can be stored in BESS, to be used later. On the other hand, when there is insufficient

Table 2.1: Power System Applications of Energy Storage Systems

Category	Description	Category	Description
Bulk energy service	Electric energy time-shift (arbitrage) Power supply capacity RES curtailment	Ancillary services	Frequency regulation Load following Voltage support Black start provision Reserve Capacity
Transmission services	Transmission upgrade deferral Transmission congestion relief		
Distribution services	Distribution upgrade deferral Voltage support Outage mitigation Distribution congestion relief	Customer services	Power quality Power reliability Time-shift Demand charge management

energy to supply the demand, the stored energy in a BESS can be discharged to make up for the deficit [73].

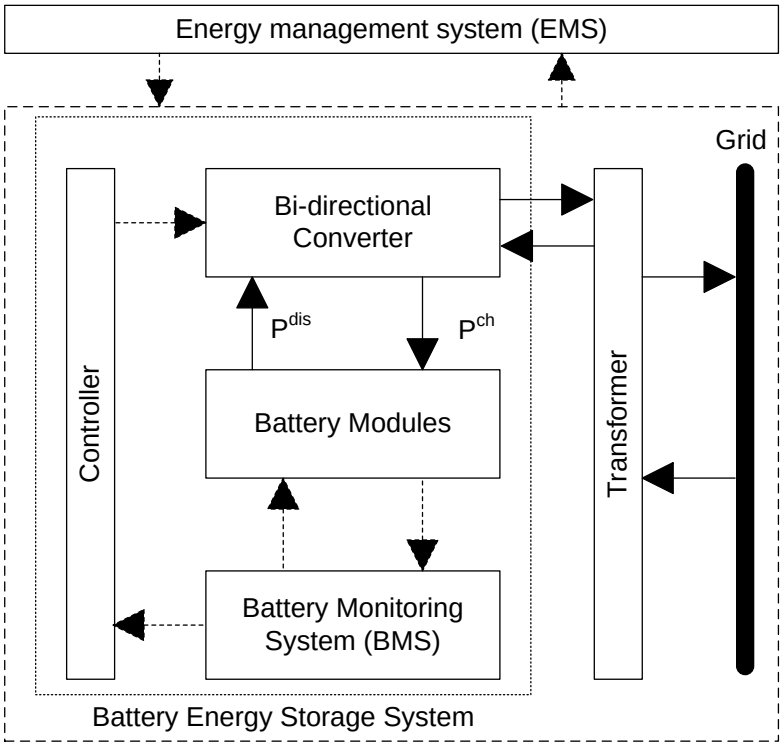

Figure 2.2: General block diagram of a BESS

The deployment of BESS can either be in small-scale, at the distribution systems level and microgrids, or in large-scale at the transmission level. The small-scale BESS is known as CESS [61]; an example of a CESS is the Li-Ion based facility of 25/50 (kW/kWh) [74] DTE battery CESS project in Detroit, Michigan, USA.

According to [75], BESSs have been installed and used in distribution networks and isolated microgrids all over the world, to provide services such as demand-supply balancing. The microgrid projects discussed in [13] have BESS as one of the main energy sources. The largest BESS installed in an isolated microgrid, is in China and it is rated at 44.3 MWh. Since the costs associated with RES are decreasing; thus introducing them in microgrids would be of great value, economically and environmentally, and will make remote communities less dependent on fossil-fuel based generators. It has been claimed that a Li-Ion based BESS is more economical as compared to an inefficient peaking power plant [75].

In Canada, there are about 280 remote communities that house 200,000 people and their main source of energy is diesel generators. The idea of installing wind and solar energy is being pursued by the government and local utilities, in order to reduce the dependency on diesel, reduce GHG emission, and harness free and clean energy [76]. In this context, BESS can facilitate the penetration of RES, which can eventually reduce the overall cost of electricity in the remote microgrids. According to [76], electricity tariffs in many of the Northern remote microgrids in Canada are in the range of 0.45 \$/kWh and 2.5 \$/kWh which is significantly higher than what a retail customer pays in a Canadian city.

There are several configurations for deploying the energy storage systems [77]; for example, large BESS, owned and controlled by an industrial entity, utility, or aggregator, and small privately owned BESS, controlled by an aggregator, or owned and controlled by an aggregator.

Definitions

Several terms are used to represent the battery characteristics and operational states, which are given below:

- Rated or nominal energy capacity: the initial energy capacity at the time of installation, given in Ah or Wh.
- Rated power capacity: the initial power capacity at the time of installation, given in W.

- Lost battery capacity: the energy capacity lost, in Wh, due to calendar and cycle degradations.
- Current energy capacity: the initial energy capacity minus lost battery capacity, given in Ah or Wh.
- Energy to Power (E/P) ratio: the ratio between energy and power capacities of a battery. The power rating measures the instantaneous demand the battery is able to supply. At the time of installation, E/P is determined from the rated power and energy sizes. However, after the battery is operated, E/P is determined from the instantaneous power and energy sizes considering degradation. Depending on the application of the battery, the E/P ratio can take values either below or greater than unity.
- SoC: the available charge or energy left in the battery during operation based on the current capacity taking into account degradation of the battery.
- DoD: the percentage of discharged energy between various combination of transitions- charging, discharging, and battery idle mode.
- SoH: the condition of a battery; a zero SoH means that the battery is not capable of delivering the minimum required power and energy for intended applications [78], while an SoH of 100% means the battery is at its rated capacity. The SoH can be mathematically represented as follows:

$$\text{SoH} = 1 - \frac{\text{Lost Capacity}}{\text{Rated Capacity}} \tag{2.8}$$

  Let us assume that the battery has an initial capacity of 16 kWh, and it degrades to 14.4 kWh, through a number of years of operation. Hence, the battery has an SoH of 90%.
- Energy density: the available energy in a battery per unit of volume.
- Power density: the available power in a battery per unit of volume.
- Battery cycle: is divided into two types, semi-cycle and full-cycle. Semi-cycle refers to one single charge or discharge when the battery changes its SoC status from the previous SoC. On the other hand, full-cycle is the summation of two identical half-cycles of the the same DoD but in a opposite direction. When determining the degradation, full-cycles are usually used and the cycles are calculated using, for example the RCA, as explained in Section 2.8. When the number of charging and discharging cycles, which corresponds to various ranges of DoD, reaches its limits, it is said that the battery has reached its EoL.

2.4 Electric Vehicles

A schematic diagram of the power-train of an EV is presented in Figure 2.3, which is used to model the mechanical traction power demand, referred to as Vehicle Longitudinal Dynamic Model (VLDM), and the electrical traction power demand, referred to as Vehicle Power-train Model (VPM). The EV is comprised of four main units: the EVB, the dc/ac converter, the electric motor, and transmission system. Basically, the power needed to drive the vehicle is drawn from the battery unit and then processed by the electric motor that is controlled via the dc/ac converter to generate the traction propulsion power at the wheels through the transmission system [79].

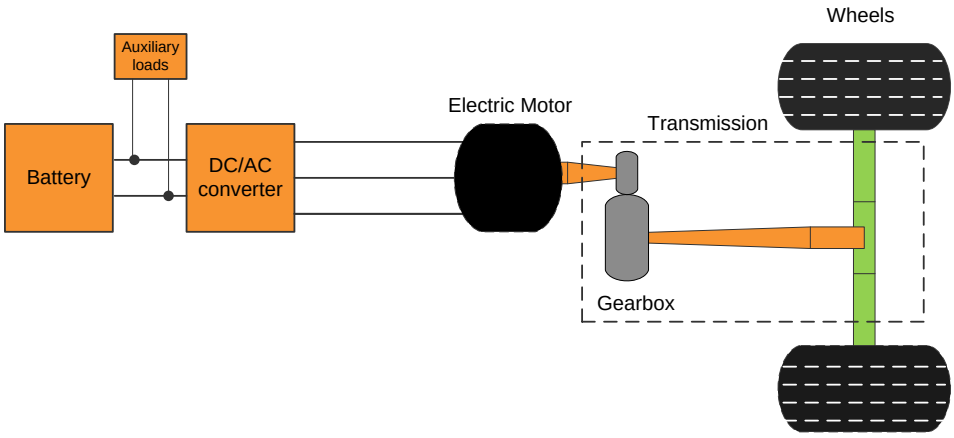

Figure 2.3: Traction power-train of EV

The VLDM determines the vehicle mechanical traction power demand based on the power that the vehicle needs, to meet the instantaneous velocity and acceleration of a given driving cycle. The vehicle mechanical traction power demand is obtained from the traction force (FT_t), which is comprised of: aerodynamic drag (F_t^{ad}), rolling resistance (F_t^r), gradient resistance (F_t^g), and the vehicle′s inertia (F_t^i), and drive cycle, as given by (2.9). Equations (2.10) and (2.11) show the structure of traction force [79]. The relationship between the traction force and the drive cycle are given below:

$$P_t^d = FT_t \; v_t \tag{2.9}$$

$$FT_t = F_t^{ad} + F_t^r + F_t^g + F_t^i \tag{2.10}$$

$$FT_t = \left[\left(\frac{1}{2}\,\rho\; A_f\; C_D\; v_t^2\right) + (M_t\; g\; C_r \cos\alpha) + (M_t\; g\;\; \sin\alpha) + \left(M_t\; \frac{dv}{dt}\right)\right] \tag{2.11}$$

The VPM is comprised of the traction dc/ac converter, electric motor, and transmission system, which determines the electrical traction power demand drawn from the EVB. The commonly used dc/ac converter for passenger EVs is a three-leg IGBT Voltage Source Converter (VSC), which inverts the required dc power to ac at the electric motor side. The transmission system has the responsibility to step up the mechanical torque of the motor in order to rotate the vehicle wheels. Two types of EV traction motors are commonly available in the market: the induction machine and the permanent magnet synchronous machine. The first type is the most popular in passenger EVs since their cost is low and are lightweight; they produce high torque and power [78, 79]. The equations governing the electrical traction power demand P_t^{ed} at the dc bus of the traction inverter are given below:

$$P_t^{ed} = P_t^{td} + P_t^{aux} = \begin{cases} \dfrac{P_t^{td}}{\eta_{tr} \cdot \eta_m} & \text{if} \quad P_t^{td} \geq 0 \\ P_t^{td} \cdot \eta_{tr} \cdot \eta_m & \text{otherwise} \end{cases} \tag{2.12}$$

where P_t^{aux} is the auxiliary demand of the vehicle, η_{tr} is the transmission efficiency [79], and η_m is the combined traction inverter and motor efficiency [80]. The parameters used in (2.9) to (2.12) are reported in Table A1 and A2 in Appendix A.

2.4.1 Electric Vehicle Battery Modelling

Currently, five types of EVBs are commercially available: the nickel-cadmium (NiCd) battery, nickel-metal hydride (NiMH) battery, Sodium-Nickel Chloride or Zeolite Battery Research Africa (ZEBRA), lead-acid, and Lithium-Ion (Li-Ion) [81]. Two types of EVBs are commonly used in EVs and Hybrid Electric Vehicles (HEVs), Li-Ion and Nickel-Metal Hydride (NiMH) [82].

According to [81], NiMH battery has a relatively high specific power and low specific energy, and is commonly used in HEVs. Toyota Prius is an example, that uses NiMH batteries because of their lower cost per Watt ($/W) compared to the Li-Ion battery.

Different types of Li-Ion batteries are dominating the EV, HEV, and Plug-in Hybrid Electric Vehicle (PHEV) markets today: the lithium iron phosphate ($LiFePO_4$), lithium titanate ($Li_4Ti_5O_{12}$), lithium manganese oxide ($LiMn_2O_4$), lithium nickel manganese oxide (NMC), and lithium nickel cobalt aluminum oxide ($LiNiCoAlO_2$) [83]. The principle of operation of the Li-Ion battery is simple. When the bat-

Table 2.2: Li-Ion Battery Capacity and Electric Range of Common EV Models

Model	Type	Capacity kWh	EV Range (km)	Battery Type
Volkswagen e-Golf	Battery Electric Vehicle (BEV)	35.8	201	Li-Ion
BMW i3	BEV	22	130	Li-Ion
Chevrolet Bolt EV	BEV	60	383	Li-Ion
Chevrolet Volt	PHEV	16	85	Li-Ion
Ford C-Max Energi	PHEV	8	32	Li-Ion
Ford Focus Electric	BEV	23	122	Li-Ion
KIA Soul EV	BEV	27	149	Li-Ion
Mitsubishi i-MiEV	BEV	16	100	Li-Ion
Nissan Leaf	BEV	24	128	Li-Ion
Smart Fortwo	BEV	17	145	Li-Ion
Tesla Model S	BEV	90	435	Li-Ion
Tesla Model X	BEV	90	413	Li-Ion
Tesla Roadstar	BEV	53	393	Li-Ion
Toyota Prius	PHEV	4.4	23	Li-Ion & NiMH

tery charges, Li-Ions in the cell move from the positive electrodes to the negative electrodes, and in the opposite direction when discharging [84].

Six metrics are used to differentiate among the battery types: specific power, specific energy, lifespan, safety, performance, and cost [78]. Li-Ion battery types are currently used in EVs such as Tesla, Nissan Leaf, and Chevrolet Volt, as seen in Table 2.2 [85]. Compared with other battery types mentioned before, Li-Ion batteries have the highest specific energy and specific power for the least weight, with a low self discharge, thus making them the best and obvious choice for EVs [83].

Electric and Thermal Models of a Battery

The modelling of batteries is classified under two categories, electrochemical models and electrical equivalent circuit-based models. The former describes the electrochemical processes occurring in the battery cell while the latter is circuit based, which model the behaviour of the cell rather than the electrochemical processes in the cell. The latter describes the electrical equivalent performance of the battery using voltage sources, resistors and capacitors, which is the focus of the present research. The electrical model is mostly used in circuit simulations with other circuits and systems.

There are many models that have been proposed to model the electrical behavior of the battery. Among these, there are three different models for electrical equivalent circuit-based: Thevenin's equivalent, ac model, and runtime-based model [86]. Thevenin's equivalent model is able to capture transients, but cannot predict the battery runtime information nor the dc response of the battery cell [22, 86, 87]. The ac model, also called the impedance-based electrical model, is able to capture the ac response of the battery behavior over a large range of frequencies. However, this model is only able to perform under a fixed SoC and temperature setting [86, 88]. The last basic model is runtime-based model that is able to capture the dc response as well as the battery runtime information but fails to capture the ac response due to limited transient capability [86, 89].

Some models, referred to as a complete model, such as the one presented in [86], combined the three main models into a complete equivalent circuit-based model combining the advantages of each model. The complete model of the electric circuit is able capture all the battery characteristics such as ac response, open circuit voltage dependence on SoC, transient behavior, and battery runtime. The equivalent circuit-based complete model for a single Li-Ion cell has been developed in [86] to capture the battery terminal I-V characteristics, and the same is adopted in this thesis. The complete electrical circuit model of the Li-Ion battery is shown in Figure 2.4 [86].

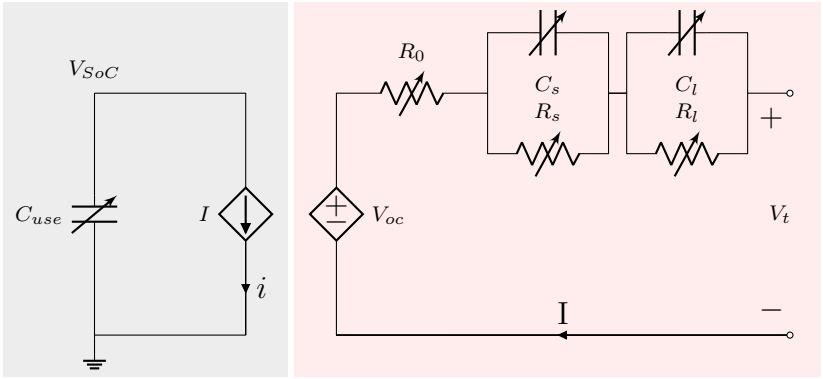

Figure 2.4: Complete electrical model of Li-Ion battery

The passive parameters are functions of SoC, temperature and the direction of the current. The cylindrical battery cell ANR26650 manufactured by A123 Systems [90] is widely used, and adopted in this work; the governing equations of its passive components and dependent voltage source are identified in [90] and used in this

thesis. The behaviour of each impedance element, resistance and capacitance (RC), in the model are different for charging and discharging, leading to two equations per impedance element [90].

It should be noted that when the battery pack is constructed, multiple battery cells are connected in series and multiple battery strings are connected in parallel that conforms to the electrical needs of a particular application.

The lumped thermal equivalent model [90] is used in this thesis to simulate the temperature, which is a function of the passive parameters of the electrical equivalent circuit model. The power loss, which is dissipated heat, is assumed to be generated at the core of the battery cell and is calculated, as shown below, by multiplying the battery cell current with the voltage drop across the internal impedance:

$$Q^h = (V_{oc} - V_{batt})\ I_{batt} \tag{2.13}$$

The dynamic relationship between the core temperature (T_c) and the surface temperature (T_s) in $^\circ C$ are expressed as follows:

$$C_c \frac{dT_c}{dt} = Q^h + \frac{T_s - T_c}{R_c} \tag{2.14}$$

$$C_S \frac{dT_S}{dt} = \frac{T_f - T_s}{R_u} + \frac{T_s - T_c}{R_c} \tag{2.15}$$

The inputs in (2.14)-(2.15) are the inlet air coolant temperature (T_f) and the heat generation (Q^h), which are determined using the electrical model. It should be noted that R_u represents a convection thermal resistance modeled between the surface and the surrounding coolant to account for convective cooling. The dynamics of the battery thermal model is equivalently modeled by the equivalent electrical circuit in Figure 2.5.

Battery Capacity Degradation Model

SoH is a subjective term used to indicate how much battery energy capacity has degraded during cycling and storage in percentages, over time. The battery SoH is 100% when it is new while its EoL is reached when the SoH is 0%. It should be noted that a zero SoH means that the battery is not capable of delivering the minimum required power and energy for the intended application [78].

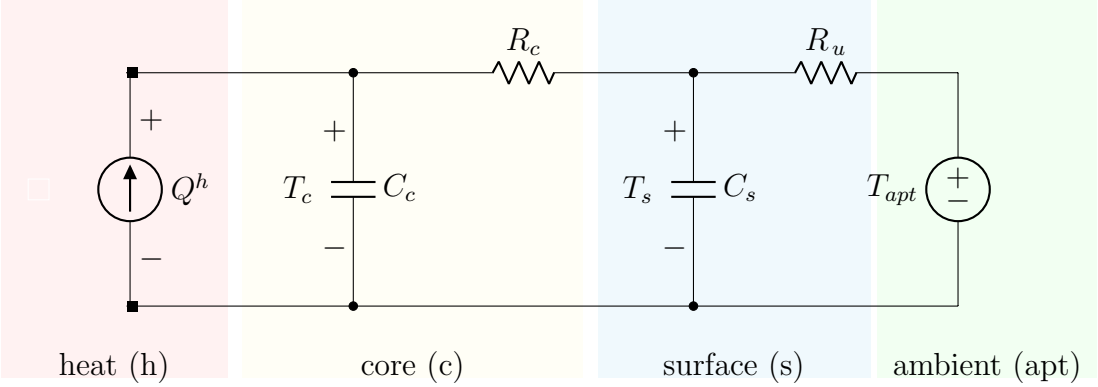

Figure 2.5: Electrical equivalent circuit of battery cell thermal model

The changes in useable capacity (C_{use}) of a battery can be the result of either irreversible or reversible capacity loss. Irreversible capacity loss, widely known as capacity degradation, is a result of cell ageing due to cycling and storage or refereed to as calendar. The capacity loss of the battery is calculated considering the Ah processed [22].

There are many approaches and models to estimate the capacity degradation of an EVB based on the intended application [91]. Therefore, an empirical model capable of representing the capacity degradation in EVBs is used in this thesis based on [22]. The capacity degradation for an $LiFePO_4$ battery is calculated from Ah processed, at each instant. Various factors greatly affect capacity degradation: the average SoC (SoC_{avg}), the standard deviation of SoC (SoC_{dev}), and temperature. Based on experimental results reported in [22], a mathematical model for capacity degradation was introduced to capture battery fading during cycling, as given below:

$$\zeta\left(T, SoC^{ev}_{avg}, SoC^{ev}_{dev}, Ah\right) = \sum_i \left[\left(K_{s1}\ SoC^{ev}_{dev,i}\ e^{K_{s2}SoC^{ev}_{avg,i}}\ R_{s2_*} + K_{s3}\ e^{K_{s4}SoC^{ev}_{dev,i}}\right) e^{\left[-\frac{E_a}{R}\left(\frac{1}{T_i} - \frac{1}{T_{ref}}\right)\right]}\right] Ah_i \tag{2.16}$$

It should be noted that in (2.16), the degraded capacity ζ is calculated only when there is a change in the temperature. The battery temperature in $^\circ K$ is found by the thermal model. The activation energy (E_a) has a value of $78,060\ mol/J$. The ideal gas constant R is $8.314\ J/mol{\cdot}K$. The T_{ref} is $298\ K$. The rest of the constant parameters are as follows: k_{s1} = -4.092×$\times 10^{-4}$, $k_{s2} = -2.167$, $k_{s3} = 1.408\times 10^{-5}$,

and $k_{s4} = 6.130$ [22].

After Ah processed is determined, the C_{use} can be calculated as follows [22]:

$$C_{use} = C_{use}(T, \zeta) = \left(Q^{ini} - \zeta\right) e^{k_1 \left(\frac{1}{T - k_2} - \frac{1}{T_{ref} - k_2}\right)} \tag{2.17}$$

where Q^{ini} is the initial true capacity at reference temperature (T_{ref}) and ζ the capacity degraded in Ah. The measured temperature (T) and T_{ref} are in $^{\circ}K$. The parameters k_1 and k_2 are constants [22].

2.5 Repurposing EVB for Second Use Applications

EVBs are designed to supply the power and energy needed by a vehicle. When an EVB is no longer capable of providing at least 80% of the energy required for the full driving range of the EV, and at least 80% of the power that a new battery would supply, it is considered to have reached its EoL [83]. However, when an EVB is not able to meet the performance requirements of the vehicle, it may still be able to provide energy and power for less demanding applications [92]. Therefore, there is a need to repurpose the EVB after its EoL by re-engineering it for stationary energy storage applications.

The process of repurposing the used EVB starts by removing it from the EV power-train. Before the used EVB is repurposed, its remaining capacity is identified using one of three methods [92]:

1. Measuring its capacity directly at the point of repurposing: This method is simple but needs special equipment and time for processing.

2. Measuring the SoH and other parameters of the used EVB after applying a drive cycle on the vehicle close to the time of replacement of the battery.

3. Installing a recording device that collects important information about the battery at the beginning of its life.

After the capacity degradation of the used EVB and several parameters are obtained, the used EVB buying cost, that is paid to the EV owner, need be determined. The used EVB buying cost can be considered to be a salvage value for the EV owner. It should be noted that the cost of repurposing will vary across facilities depending on the level of disassembling of the battery packs, modules, or cells required. Therefore, the deeper the level of disassembling, the higher are the costs incurred. After disassembling, the battery modules are reconfigured to meet the requirements of secondary use applications. Once the used EVBs are repurposed, refurbished, and reconfigured, the battery can be called an REVB. The cost of repurposing and of buying the used EVB will decide the selling price of the REVB in the market.

2.6 Bidirectional Converter

Bidirectional converter of an EVB is referred to as a four-quadrant converter which is capable of operating in all four quadrants of the PQ plane with different combinations of real and reactive power, as follows: charging and capacitive, charging and inductive, discharging and capacitive, and discharging and inductive. A general schematic diagram of the two-stage converter is shown in Figure 2.6 [52, 65].

The converter is capable of exchanging active power between the grid and the battery through the ac-dc and dc-dc converters. Basically, the bidirectional converter of a battery is comprised of two stages, the first stage is a single-phase full-/half-bridge ac/dc bidirectional converter that is able to charge and regulate the capacitor voltage of the dc-link as well as setting the reactive power dispatch if needed, proportional to the capacity of the converter. The second stage is a bidirectional dc/dc converter based on a buck-boost topology capable of controlling the battery current according to the setting of the controller for charging or discharging. The bidirectional converter takes the advantage of the dc-link capacitor to inject/absorb reactive power to/from the grid. It should be noted that the ability of the bidirectional converter to provide reactive power will not have an impact on battery degradation.

2.7 Transformer Loss of Life

To estimate the distribution transformer degradation, an LoL index is estimated using the thermal model proposed by IEEE C57.91-2011 [93], by first determining

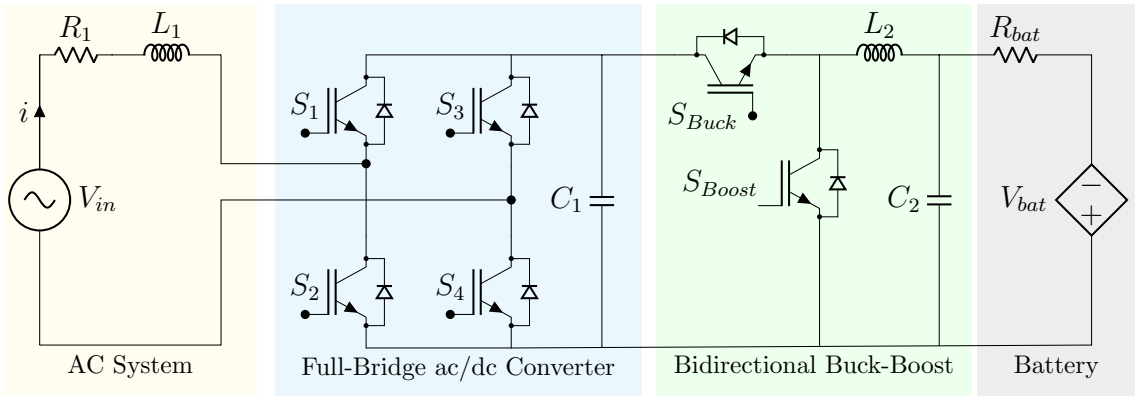

Figure 2.6: A general schematic diagram of the two-stage bidirectional converter

the winding hottest-spot temperature, which is the main factor accelerating the deterioration of the transformer insulation. This hottest-spot temperature depends on the daily ambient air temperature, the transformer's oil rise over ambient air temperature, and the transformer's winding hot-spot rise over top-oil temperature [93, 94]. Thereafter, the transformer aging acceleration factor is determined and aggregated over all time intervals of the study (F_{EQA}).

Finally, the distribution transformer's daily LoL can be estimated as follows:

$$LoL(\%) = \frac{F_{EQA} \times t}{\alpha} \times 100 \tag{2.18}$$

where α is the normal insulation life of the transformer [93]. According to IEEE C57.91-2011, in order to avoid premature transformer replacement, the LoL during normal operation should not exceed a specific threshold [93].

2.8 Rainflow Counting Algorithm (RCA)

Any physical system or equipment with an operational cycle is subject to degradation in its life due to fatigue and stress. The RCA is a lifetime estimation method that determines the number of the cycles of operation that causes reduction in the life of the equipment [91, 95, 96]. To capture battery capacity degradation accurately and the replacement year, the RCA is used to count the number of discharge and charge cycles and their corresponding DoD from its SoC profiles. There are different

ways to count the cycles using the RCA as explained in [95–97]. Each range of DoD corresponds to a specific number of cycles to failure, that is provided by a battery manufacturer, as shown in Figure 2.7 [98].

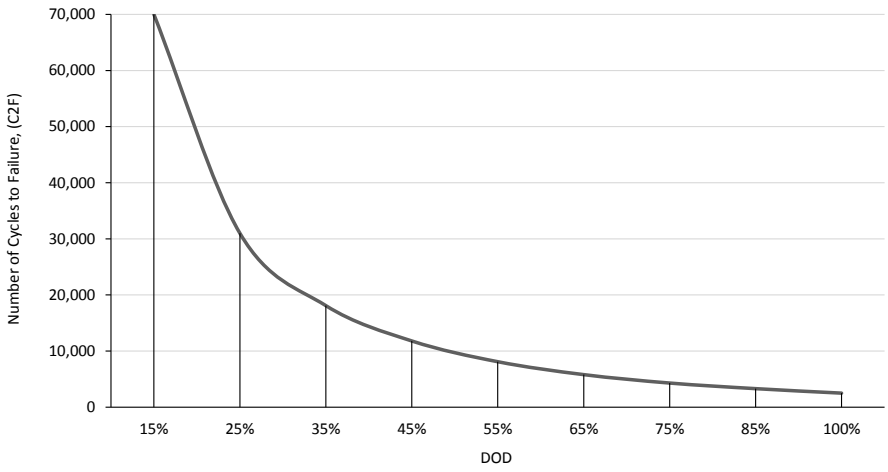

Figure 2.7: Cycles to failure of Li-Ion battery *vs* DoD

The RCA analyzes a daily SoC profile of the battery, starting with a discharge process. The counting begins at the highest peak and continues until it identifies the lowest SOC value [97]. The *discharging path* (shown by the dark-blue line in Figure 2.8) of the SoC profile seeks to determine a continuously decreasing path to the lowest value of the SoC without overlapping with the obtained first path. The method is

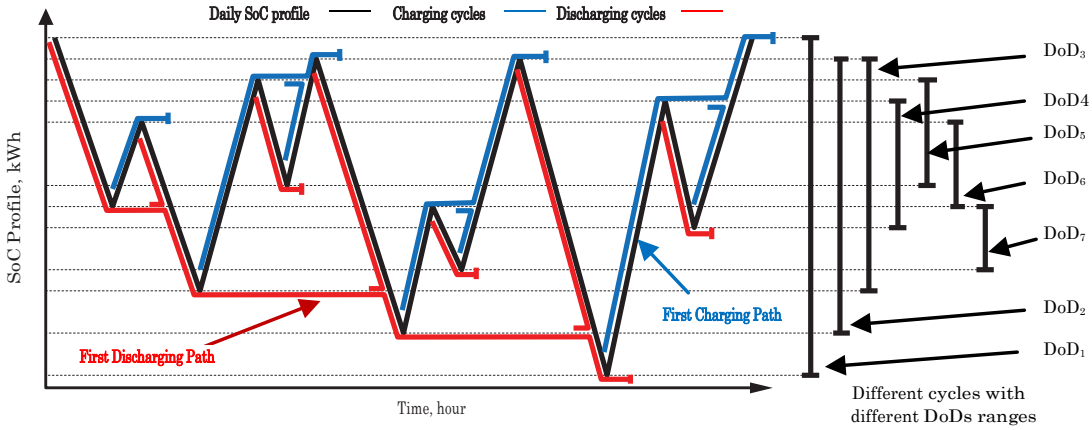

Figure 2.8: Rain-Flow Cycling Counting During Charging and Discharging

repeated, starting from the next highest peak of the SoC until it determines the next lowest valley and the corresponding discharge path. This counting will be repeated until all the discharge paths of the SoC are determined, as presented in Figure 2.8.

The RCA will follow the same process to capture all the charging cycles. Therefore, it begins from the lowest valley of the SoC profile and proceeds to identify the highest peak and hence determines a continuously increasing path to the highest value of the SoC, referred to as, *charging path* (shown by the red line in Figure 2.8). The process will be repeated until all the charging paths are determined, as shown in Figure 2.8.

Finally, the obtained semi-cycles of the charging and discharging paths are matched to count the complete cycles that correspond to various ranges of DoD, as presented in Figure 2.8.

Based on the matched cycles and the respective DoD, and using the data provided by the battery manufacturer, the lifetime of the battery can hence be determined.

2.9 Mathematical Programming

An optimization problem is a mathematical process that can either maximize or minimize an objective function that is subjected to constraints. Examples of types of optimization problems are [99, 100]: Linear Programming (LP), Quadratic Programming (QP), Non-Linear Programming (NLP), Mixed-Integer Linear Programming (MILP), and Mixed-Integer Non-Linear Programming (MINLP).

Linear Programming (LP)

The LP problem is a linear optimization problem that has a linear objective function subject to linear equality/inequality constraints. An LP problem can be mathematically stated as follows:

$$\begin{array}{ll} \max \ / \ \min & f(x) \\ \text{subject to} & g(x) = 0 \\ & h(x) \leq 0 \\ & x \geq 0 \end{array} \tag{2.19}$$

where $f(x)$ is a linear objective function to either be maximized or minimized, $g(x)$ denotes a linear function describing the equality constraint, and $h(x)$ represents a linear function describing the inequality constraint [100].

Non-Linear Programming (NLP)

NLP is similar to the LP explained earlier. However, the mathematical model is non-linear either in the objective function or equality/inequality constraints or both [100].

Mixed-Integer Non-Linear Programming (MINLP)

When a nonlinear optimization problem has both discrete and continuous variables, the problem is referred to as an MINLP problem. These problems are difficult to solve and solutions can be obtained either by using decomposition techniques or linearizing the non-linear variables and equations [100].

MINLP problems that have bilinear variables, as given by (2.20), can be linearized and relaxed using the concept of McCormick envelop relaxation [101] to obtain an LP problem.

$$\begin{array}{rlcccl} \min & xy & & & & \\ \text{s.t.} & x^L & \leq & x & \leq & x^U \\ & y^L & \leq & y & \leq & y^U \\ & x, y & \geq & 0 & & \end{array} \tag{2.20}$$

First, the bilinear variables are replaced with a new variable $xy = w$. Then, several derived equations are introduced to create an LP problem. The new linearized optimization problem will be as follows:

$$\begin{array}{rlr} \min & w & \\ \text{s.t.} & & \\ x^L y + y^L x - x^L y^L & \leq w \leq & x^U y + y^U x - x^U y^L \\ x^U y + y^U x - x^U y^U & \leq w \leq & x^L y + y^U x - x^L y^U \\ x^L & \leq w \leq & x^U \\ y^L & \leq w \leq & y^U \\ & w \geq 0 & \end{array} \tag{2.21}$$

In (2.21), x^L and y^L are lower bound values and x^U and y^U are upper bound values of their respective variables x and y. The NLP problem in (2.20) hence becomes an LP problem as seen in (2.21) which can be easily solved. McCormick envelopes relaxation can be applied to any problem with a bilinear variable to invert the non-convex function into a convex function.

2.10 Summary

In this chapter, a general description and operations model for a microgrid was presented. General concepts of an EV and its battery model including the thermal model and capacity degradation model were explained. Repurposing EVB for second use applications was presented, followed by an overview of the basic bidirectional converter in batteries, and transformer LoL to estimate their aging. The RCA to estimate battery degradation was explained in brief. Finally, a brief discussion on mathematical programming was presented.

Chapter 3

Planning and Operation of Isolated Microgrids Based on Repurposed Electric Vehicle Batteries*

3.1 Nomenclature

Indices

g	Index for generating units	$g \in G$
t	Index for operation-steps, [hour]	$t \in T$
y	Index for planning-steps, [year]	$y \in Y$

Parameters

C^{UNS}	Cost of unserved demand	[$/kWh]
C^{v}_{E}, C^{v}_{pb}	BESS variable installation costs of energy and power capacities, respectively	[$/kWh, $/kW]
C^{fx}	Fixed installation cost of REVB and new BESS	[$]
OMC^{fx}	Fixed O&M cost of the REVB and new BESS	[$/kW]
OMC^{v}	Variable O&M cost of REVB and new BESS	[$/kW]
$Pd_{y,t}$	Isolated microgrid demand	[kW]
$P^{PV}_{y,t}$	Solar power output forecast	[kW]
$P^{W}_{y,t}$	Wind power output forecast	[kW]

*Parts of this chapter have been published as a paper in: T. Alharbi, K. Bhattacharya and M. Kazerani, "Planning and Operation of Isolated Microgrids Based on Repurposed Electric Vehicle Batteries," IEEE Transactions on Industrial Informatics, vol. 15, no.7, pp.4319-4331, July 2019.

RC	Replacement Cost	[$/kWh]
M	Large number	
TND	Total number of days in a year	
FCI	Fuel cost increase	[%]
η_{ch}, η_{dch}	BESS charging and discharging efficiencies, respectively	[%]

Variables

AC_y	BESS added capacity at replacement year	[kWh]
B_y	BESS installation decision [1 or 0]	
CRB_y	BESS remaining energy capacity with respect to 80% of the rated capacity [+, 0 , -]	[kWh]
CRB_y^+	CRB_y value when it is positive only	[kWh]
CRB_y^-	CRB_y value when it is negative or zero	[kWh]
CF_y^+	Binary variable when CRB_y value is positive	
CF_y^-	Binary variable when CRB_y value is negative	
E_y^{ini}	Initial energy capacity of BESS at installation	[kWh]
$\underline{E_y}$	Minimum BESS capacity	[kWh]
$\overline{E_y}$	Current BESS energy capacity	[kWh]
$Edeg_y^{Cyc}$	Capacity Degradation due to cycling effect	[kWh]
$Edeg_y^{Cal}$	Capacity Degradation due to calendar effect	[kWh]
LC_y	BESS capacity loss due to degradation	[kWh]
LRY_y	Bi-linear variable used to replace the product of two variables, replacement year and initial BESS capacity	[kWh]
$P_{y,t}^{UNS}$	Unserved demand	[kW]
$Pba_{y,t}$	BESS Charging (-)/discharging (+) power	[kW]
$P_{g,y,t}$	Power output of generator	[kW]
$P_{y,t}^{Res}$	Reserved demand	[kW]
Pb_y^{ini}	BESS power rating at initial installation	[kW]
Pb_y	Current BESS power rating	[kW]
RY_y^v	Replacement year	[year]
$SoC_{y,t}$	SoC of battery	[kWh]
$SRB_{y,t}$	Reserve provided to the system by BESS	[kW]
TED	Total discharged energy by BESS in one day	[kWh]
$U_{y,g,t}$	Start-up binary decision [1 or 0]	
$V_{y,g,t}$,	Shut-down binary decision [1 or 0]	
$W_{y,g,t}$	Unit-commitment binary decision [1: generation i is online, 0: otherwise]	
$X_{y,t}^{ch/dch}$	Binary decision [1: BESS is charging or discharging, 0: otherwise]	
Z_y^{RY}	BESS replacement year binary decision variable	
ζ	Total capacity loss due to cycling and calendar degradation of the EVB (Stage-I)	

ζ_t^{Cyc} Total capacity loss due to cycling degradation (Stage-I)
ζ_t^{Cal} Total capacity loss due to calendar degradation (Stage-I)

3.2 Introduction

The increasing penetration of EVs raises concerns of stockpiling of used EVBs after their vehicular EoL [6, 102]. The retired EVBs, after repurposing, can serve as an alternative option to new batteries in a BESS. Utilization of used EVBs, after repurposing, can play a significant role in isolated microgrids in alleviating the need for costly new BESS or diesel generators in the long-term, which is beneficial, both economically and environmentally. REVBs can provide the same services at a fraction of the cost of a new BESS [9]; also, repurposing an EVB would delay its recycling and prolong its useful life.

For installation of new BESS or REVBs in isolated microgrids the following issues need to be considered: a) determining the optimal year of installation, along with the optimal power and energy capacity ratings; b) optimal operation of these devices; c) proper consideration of calendar and cycling degradations of BESS and REVBs; and d) determining an optimal year of BESS replacement, considering degradation, instead of using a fixed replacement year which can lead to premature replacements and additional costs.

This chapter presents a comprehensive and novel framework and mathematical model for planning and operation of BESS based on REVBs. Various new, modified and linearized operational constraints for the new BESS and REVBs have been included in the planning model to ensure their replacement years are optimally determined. Several classes of EVs with multiple drive cycles are clustered and integrated within the proposed framework. Therefore, the main objectives of this chapter are as follows:

- Develop a systematic procedure to model the degradation of EVBs for different classes of EVs during their first life in vehicles, and hence incorporate these characteristics to estimate the expected cost of installing REVBs.
- Develop a generic microgrid planning model to determine the optimal energy size, power rating, and optimal year of replacement of new BESS and REVBs. The model needs to include the impact of degradation due to calendar and cycling effects on the BESS/REVBs' energy capacity, as well as on the number

of C2F. The proposed model will introduce a novel set of mathematical relations for BESS degradation and optimal year of replacement, thereby avoiding premature replacements and additional costs.

- Consider multiple drive cycles of different classes of EVs to capture their impact on the expected SoH of the EVBs and hence on the number of years until they reach their EoL. This leads to developing an expected degradation model of EVBs for each class, for inclusion in the generic microgrid planning model proposed earlier, to study the impact of uncertainties.

The structure of the chapter is as follows: Section 3.3 describes the proposed framework, as well as the detailed mathematical models of each stage. In Section 3.4, the proposed framework is simulated and the results are presented to demonstrate the effectiveness of the proposed models with the exploration of various scenarios. Section 3.5 presents a discussion on the algorithms used and their computational aspects. Finally, conclusions are drawn in Section 3.6.

3.3 Proposed Microgrid Planning Framework and Mathematical Models

In this section, a novel systematic framework is proposed for modelling of BEVs during their first-use and subsequently their utilization as BESS in isolated microgrids for various second-use applications. The framework comprises three stages, presented in Figure 3.1 which are discussed in detail in the following sub-sections; the important inputs to, and outputs from, each stage are clearly identified in the figure, and all assumptions are stated.

Stage-I: EVB Capacity Degradation During Vehicular Life

A comprehensive flowchart of Stage-I is shown in Figure 3.1. This stage simulates the performance of an EVB during its first-life in an EV and determines its SoH at any instant, and the number of years it takes for the battery to degrade to its SoH threshold [103], considering cycling and calendar degradations. There is a need for real and detailed drive cycle data of different EV classes to accurately estimate the outputs.

This stage includes the following three models (Figure 3.1):

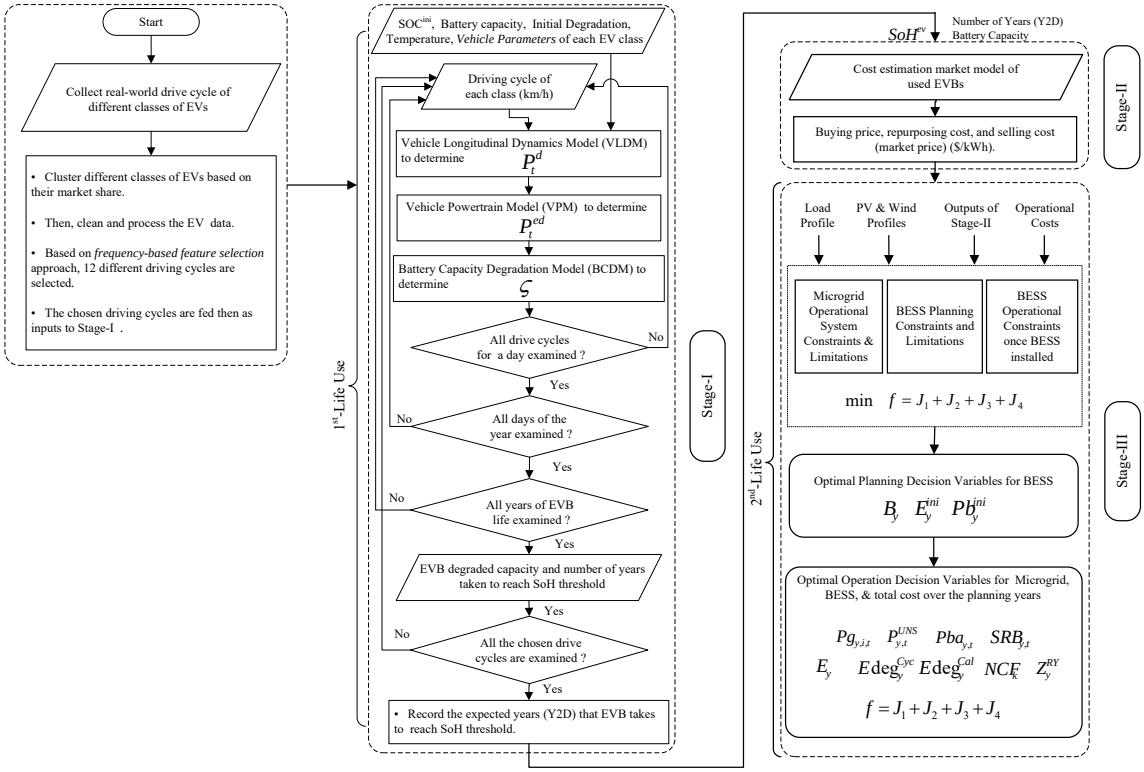

Figure 3.1: Flowchart of the proposed systematic framework of REVBs utilization

- VLDM [80],
- VPM [80], and
- Battery Capacity Degradation Model (BCDM) [22].

The simulation starts with reading all the parameters as inputs, which are then fed, together with the EV drive cycle, to the VLDM, to calculate the mechanical traction power, P_t^d. This power is transferred to the VPM to determine the electrical traction power demand, P_t^{ed}, needed from the battery. From P_t^{ed}, the SoC and temperature of the battery are calculated using the electrical and thermal models of the EVB, as explained in [90]; the EVB's capacity degradation and SoH are determined from the BCDM [22]. It should be noted that [22] only accounts for degradation due to cycling (ζ^{Cyc}), while this work, besides cycling degradation, considers a linear calendar degradation rate (ζ^{Cal}) as well. The initial SoC is 90% and the EVB is recharged to 90% at the end of each drive cycle.

In this work, Li-Iron-Phosphate ($LiFePO_4$)-based EVBs are considered; the BCDM of $LiFePO_4$ EVBs is expressed as a function of different stress factors, as follows:

$$\zeta = \zeta_t^{Cyc}(T, SoC_{avg}^{ev}, SoC_{dev}^{ev}, Ah) + \zeta_t^{Cal}. \tag{3.1}$$

where ζ is the total capacity loss due to cycling degradation of the EVB pack (ζ_t^{Cyc}) and calendar degradation of the EVB battery pack (ζ_t^{Cal}). The total capacity loss due to cycling depends on EVB temperature T, the average value and standard deviation of SoC, SoC_{avg}^{ev} and SoC_{dev}^{ev}, respectively. It should be noted that the inputs to BCDM are results of EVB simulation based on a given drive cycle. The SoH of the EVB is calculated as follows [22],

$$\text{SoH} = \big(1 - \frac{\zeta}{(\text{EVB size})}\big) \tag{3.2}$$

Stage-I provides two main outputs that will have an impact on Stage-II and Stage-III, the SoH and the number of years it takes to degrade to 80% SoH threshold. The latter determines how many years REVB will stay in second life applications (microgrid applications).

Stage-II: Post Vehicular Life Assessment and Cost Estimation

Adopting the economic model from [104], the outputs of Stage-I (*i.e.*, SoH and number of years) are used to estimate the cost of an REVB, which includes the monetary value of the used EVB and the cost of repurposing; this is used to determine the economic feasibility of REVB as compared to new BESS in the long-term. The cost of an REVB is dependent on module properties, cell failure rates, the used battery SoH, as well as initial and degraded capacities of the EVB.

3.3.1 Stage-III: Microgrid Planning Model

The proposed planning model for isolated microgrids determines the optimal power rating and energy capacity of BESS, as well as optimal year of installation and replacement, taking into account the inherent cycling and calendar degradations. Accounting for degradation ensures realistic operational decisions and an optimal replacement year, thereby avoiding premature replacements and additional costs. Two different options for BESS are considered, *i.e.*, REVBs and new BESS.

3.3.1.1 Objective Function

The objective function, J to be minimized, is the NPV of the total cost, given as follows:

$$J = J_1 + J_2 + J_3 + J_4. \tag{3.3}$$

In (3.3), the microgrid operation cost, J_1, is comprised of the cost of unserved demand, generation cost and start-up/shut-down costs, respectively, as given below.

$$J_1 = TND \sum_{g\in G}\sum_{y\in Y}\sum_{t\in T}\left\{\frac{1}{(1+R)^y}\Big[P^{\text{UNS}}_{y,t}\cdot C^{\text{UNS}}_{y,t} + (1+FCI)^{y-1} \right.$$
$$\left.(P_{y,g,t}\ b_g + c_g W_{y,g,t}) + SUP_g U_{y,g,t} + SDN_g V_{y,g,t}\Big]\right\}. \tag{3.4}$$

The BESS installation cost in (3.3), J_2, is composed of power capacity cost, energy capacity cost, and a fixed installation cost, given as follows:

$$J_2 = \sum_{y\in Y}\left[\frac{1}{(1+R)^y}\left(Pb^{ini}_y C^v_{pb} + E^{ini}_y C^v_E + B_y C^{fx}\right)\right]. \tag{3.5}$$

The O&M cost component in (3.3), J_3, is composed of the fixed and variable O&M costs of the BESS, which vary across technologies and types, as given below.

$$J_3 = \underbrace{\sum_{y\in Y}\left[\frac{OMC^{fx}}{(1+R)^y}\left(Pb_y\right)\right]}_{\text{Fixed O\&M Cost of the Battery}} +$$
$$\underbrace{TND\sum_{y\in Y}\sum_{t\in T}\left[\frac{OMC^v}{(1+R)^y}\left(\frac{\eta_{ch}}{1-\eta_{dch}\cdot\eta_{ch}}(-Pba_{y,t})\right)\right]}_{\text{Variable O\&M Cost of the Battery}}. \tag{3.6}$$

The BESS replacement cost in (3.3), J_4, is included only when BESS reaches its EoL and has to be replaced, as given below.

$$J_4 = \left[\frac{1}{(1+R)^{RY}} + \frac{1}{(1+R)^{2RY}} + ..\right]\left(E^{ini}RC\right). \tag{3.7}$$

The replacement year (RY) is initially considered a fixed parameter, as in all studies reported in the literature. When the optimal year of replacement is determined, it is a variable (RY_y^v), and (3.7) is modified, as the Present Value Factor (PVF), given below, is no longer a constant.

$$PVF = \frac{1}{(1+R)^{RY_y^v}} \qquad \forall y. \tag{3.8}$$

The PVF in (3.8) is nonlinear, which can be linearized as an infinite series using binomial expression, as follows:

$$PVF = \left(1 - RY_y^v \cdot R\right) + \frac{(RY_y^v)^2}{2!} - \frac{(RY_y^v)^3}{3!} + \cdots \quad . \tag{3.9}$$

By replacing the sum of higher-order terms of (3.9) with an equivalent parameter ε_y, which is calculated by subtracting the first term of the binomial expression, $\left(1 - RY_y^v \cdot R\right)$, from the original PVF of (3.8), a new representation of the PVF can be derived as follows:

$$PVF = \left(1 - RY_y^v \cdot R\right) + \varepsilon_y \qquad \forall y. \tag{3.10}$$

It is noted that the PVFs obtained using (3.9) and the linearized version (3.10) are exactly matched, as seen in Figure 3.2, and hence (3.10) helps avoid the nonlinear terms created by the higher order terms in (3.9). The BESS replacement cost, after introducing the replacement year as a variable, is then given as follows:

$$J_4 = \left(1 - R \cdot RY_y^v\right) E_y^{ini}\ RC + \varepsilon_y \left(E_y^{ini} \cdot RC\right). \tag{3.11}$$

3.3.1.2 Model Constraints

• *Change in SoC:* In order to include BESS degradation, the change in SoC ($\Delta SOC_{y,t}$), when the BESS is charging or discharging, is given as follows.

$$\Delta SOC_{y,t} = \left\{(SOC_{y,t+1} - SOC_{y,t})\ \Delta_{y,t}^{+}\right\} + \left\{(SOC_{y,t+1} - SOC_{y,t})\ \Delta_{y,t}^{-}\right\} \quad \forall y, t. \tag{3.12}$$

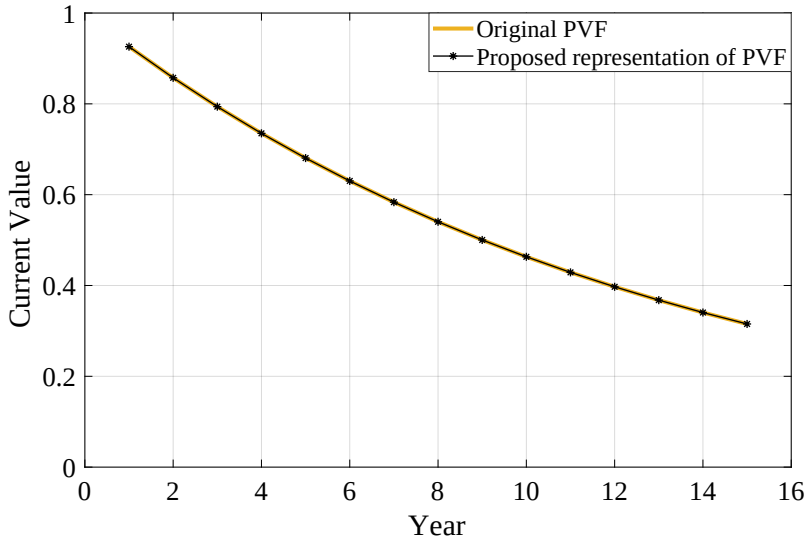

Figure 3.2: PVF values over number of years

Equation (3.12) is linearized to reduce the computational burden. New relations for positive and negative changes in SoC, $\Delta SOC^{+}_{y,t}$, $\Delta SOC^{-}_{y,t}$, respectively, are presented below.

$$\Delta SOC_{y,t} = SOC_{y,t+1} - SOC_{y,t} \qquad \forall y,t \tag{3.13}$$

$$-M\ \Delta^{-}_{y,t} \leq \Delta SOC_{y,t} \leq M\ \Delta^{+}_{y,t} \qquad \forall y,t \tag{3.14}$$

$$\Delta^{+}_{y,t} + \Delta^{-}_{y,t} \leq \sum_{y=1}^{y=T} B_y \qquad \forall y,t \tag{3.15}$$

$$\sum_{y=1}^{N} B_y = 1 \qquad \forall y. \tag{3.16}$$

Constraint (3.14) ensures that $\Delta^{+}_{y,t}$ is unity when $\Delta SOC_{y,t}$ is positive and zero otherwise; furthermore, $\Delta^{-}_{y,t}$ is unity when $\Delta SOC_{y,t}$ is negative and zero otherwise. Equation (3.15) enforces the coordination between $\Delta^{+}_{y,t}$ and $\Delta^{-}_{y,t}$, which are binary variables. Equation (3.16) is a binary constraint for BESS installation, and is applied only once during the planning horizon. Furthermore, $\Delta SOC_{y,t}$ is split into two

variables $\Delta^{+}_{y,t}$ and $\Delta^{-}_{y,t}$, to explicitly calculate BESS degradation due to cycling.

$$-BM\ \Delta^{-}_{y,t} \leq \Delta SOC^{-}_{y,t}\ \leq\ 0 \qquad \forall y. \tag{3.17}$$
$$\Delta SOC^{-}_{y,t} \leq \Delta SOC_{y,t} + (1-\Delta^{-}_{y,t})\ M \qquad \forall y. \tag{3.18}$$
$$\Delta SOC^{-}_{y,t} \geq \Delta SOC_{y,t} - (1-\Delta^{-}_{y,t})\ M \qquad \forall y. \tag{3.19}$$

Constraint (3.17) forces $\Delta SOC^{-}_{y,t}$ to be equal to zero if $\Delta^{-}_{y,t}$ is zero, and negative otherwise. The inequality constraints (3.18) and (3.19) ensure that $\Delta SOC^{-}_{y,t}$ is equal to $\Delta SOC_{y,t}$ if $\Delta^{-}_{y,t}$ is unity. The inequality constraints associated with $\Delta SOC^{+}_{y,t}$ are similar to (3.17)−(3.19), with the exception that $\Delta SOC^{+}_{y,t}$ must be positive if $\Delta^{+}_{y,t}$ is unity and zero otherwise.

• *BESS Sizing With Degradation:* The BESS energy capacity and year of replacement are determined optimally considering degradation due to calendar and cycling factors, and number of C2F, as follows:

$$E_y = \begin{cases} E^{ini}_{y} + Edeg^{\text{Cyc}}_{y} & ; y = 1 \\ E_{y-1} + Edeg^{\text{Cyc}}_{y} - Edeg^{\text{Cal}}_{y} + AC_y \forall y, y \neq 1. \end{cases} \tag{3.20}$$

$$Edeg^{\text{Cyc}}_{y} = TND \cdot \sum_{t=1}^{24} \left(K \cdot \Delta SOC^{-}_{y,t}\right) \qquad \forall y. \tag{3.21}$$

$$B_y \leqslant E^{ini}_{y}\ \leqslant M \cdot B_y \qquad \forall y. \tag{3.22}$$

Note from (3.20) that the BESS energy capacity at the year of installation does not consider calendar aging. The capacity lost by degradation during operation is accounted for in (3.20) by introducing a negative variable $Edeg^{\text{Cyc}}_{y}$. Degradation due to cycling is calculated during discharging in (3.21), where K is a degradation factor [105] obtained using lab measurements. The value of K is chosen as 3×10^{-4} and varies based on BESS technology [105]. Note that the degradation approach in [105] only considers cycling degradation, whereas this work includes both cycling and calendar degradations, as reflected in (3.20). It should be noted that $Edeg^{\text{Cal}}_{y}$ of the REVBs depends on the Y2D values for each class of EVs.

B_y is a binary variable, taking the value of unity when a BESS is installed at year y, and zero otherwise; the initial BESS energy capacity is assigned optimally using (3.22).

• *Limit on Capital Budget of BESS:* This imposes an upper limit on how much capital the microgrid operator can invest in BESS, over the planning horizon. Accordingly,

$$\sum_{y=1}^{N} \left[\frac{1}{(1+R)^y} \left(Pb_y^{ini} C_{pb}^{v} + E_y^{ini} C_{pb}^{v} + B_y C^{fx} \right) \right] \leqslant BL. \tag{3.23}$$

The first and second terms in (3.23) denote the costs associated with the installed power rating and energy capacity, respectively, and the third term represents the fixed installation cost.

• *Battery Energy to Power Ratio Constraints:* To maintain the energy to power ratio $\left(\frac{E}{P}\right)$ of the installed BESS within acceptable limits for the chosen technology, the following constraint is introduced:

$$\underline{\left(\frac{E}{P}\right)} Pb_y \leqslant E_y \leqslant Pb_y \overline{\left(\frac{E}{P}\right)} \qquad \forall y = 1. \tag{3.24}$$

• *Standardization of BESS Power and Energy Ratings:* The BESS energy and power capacity ratings need to follow available market standards, as follows:

$$E_y^{ini} = n1_y \cdot \Lambda^E \quad \& \quad Pb_y^{ini} = n2_y \cdot \Lambda^P. \tag{3.25}$$

It should be noted that $n1_y$ and $n2_y$ are integer variables, and Λ is the standard unit power and energy rating available on the market. In this work, Λ^P and Λ^E are assumed to be 50 kW and 50 kWh, respectively.

• *Linearization of Battery Capacity Degradation:* As per common practice of BESS manufacturers [106], the battery is warranted to provide desired performance until a SoH of 80% of its rated capacity. Beyond that, the battery is recommended to be replaced, as the manufacturer is no longer responsible for any malfunction that could occur. In view of the above, the same assumption is used in this work, as follows:

$$\underline{E_y} = 0.8E^{ini} \qquad \forall y. \tag{3.26}$$

$$\overline{CRB_y} = E_y - \underline{E_y} \qquad \forall y. \tag{3.27}$$

E^{ini} is the rated capacity of the BESS; note that (3.26) imposes the lower limit of BESS capacity before replacement. The value of CRB_y represents the remaining energy capacity with respect to replacement threshold of the rated capacity. It should be noted that if the value of $CRB_y = 0$ or negative in (3.27), the BESS replacement is due.

$$-M \cdot CF_y^- \leq CRB_y \leq M \cdot CF_y^+ \qquad \forall y. \tag{3.28}$$

$$CF_y^+ + CF_y^- \leq \sum_{y=1}^{y=T} B_y \qquad \forall y. \tag{3.29}$$

Constraint (3.28) ensures that CF_y^+ is unity when CRB_y is positive, and zero otherwise; similarly, CF_y^- is unity when CRB_y is negative and zero otherwise. Equation (3.29) enforces the coordination between CF_y^+ and CF_y^-. The CRB_y^+ represents the positive value of CRB_y and its associated constraints given below make sure that the obtained value is correct.

$$0 \leq CRB_y^+ \leq M \cdot CF_y^+ \qquad \forall y. \tag{3.30}$$

$$CRB_y^+ \leq CRB_y + (1 - CF_y^+)\, M \qquad \forall y. \tag{3.31}$$

$$CRB_y^+ \geq CRB_y - (1 - CF_y^+)\, M \qquad \forall y. \tag{3.32}$$

The inequality constraint (3.30) states that CRB_y^+ is zero if CF_y^+ is zero, and positive, less than "M" value, otherwise. The inequality constraint (3.31) ensures that CRB_y^+ is equal to CRB_y if CF_y^+ is unity.

$$-M \cdot CF_y^- \leq CRB_y^- \leq 0 \qquad \forall y. \tag{3.33}$$

$$CRB_y^- \leq CRB_y + (1 - CF_y^-)\, M \qquad \forall y. \tag{3.34}$$

$$CRB_y^- \geq CRB_y - (1 - CF_y^-)\, M \qquad \forall y. \tag{3.35}$$

The inequality constraints (3.33)−(3.35) are similar to (3.30)−(3.32), with the exception that negative CRB_y^- is considered. The logic-of-status changes, given below, ensure the transitions of states from 0 to 1 when the BESS capacity degrades to the minimum limit; Z_y^{RY} is a binary variable and becomes unity when BESS reaches its year of replacement.

$$Z_{y+1}^{RY} = CF_{y+1}^- - CF_y^- \quad \forall y, y \neq 1 \;:\; Z_y^{RY} = 0; y = 1. \tag{3.36}$$

The replacement year is obtained from the constraint below, when Z_y^{RY} is unity.

$$RY_y^v = Z_y^{RY} \times ord_y \qquad \forall y. \tag{3.37}$$

In (3.37), ord_y is the relative position of each year in the set.

• *Replacement Year Bi-linear Relations:* As shown in (3.11), BESS replacement cost is a bi-linear term (product of two continuous variables), not acceptable in MILP problems. The McCormick method [101] is applied to solve the bi-linear term, obtained from multiplication of the two variables RY_y^v and E^{ini}, by replacing $\left(RY_y^v \cdot\ E^{ini}\right)$ with a new variable, LRY_y, which is linked with the two variables, and introducing the inequality constraints (3.38)−(3.43). Also, the upper and lower bounds for the two variables of the bi-linear term are chosen appropriately to reduce the search space of the linearized problem (3.43).

$$
\begin{aligned}
LRY_y &\geq \underline{E^{ini}}\ RY_y^v + E^{ini}\ RY_y^v - \underline{E^{ini}}\ RY_y^v && \forall y. && (3.38)\\
LRY_y &\geq \overline{E^{ini}}\ RY_y^v + E^{ini}\ \overline{RY_y^v} - \overline{E^{ini}}\ \overline{RY_y^v} && \forall y. && (3.39)\\
LRY_y &\leq \overline{E^{ini}}\ RY_y^v + E^{ini}\ RY_y^v - \overline{E^{ini}}\ RY_y^v && \forall y. && (3.40)\\
LRY_y &\leq E^{ini} RY_y^v + \overline{RY_y^v}\ \underline{E^{ini}} - \underline{E^{ini}}\ \overline{RY_y^v} && \forall y. && (3.41)\\
\underline{E^{ini}} &\leq E^{ini} \leq \overline{E^{ini}} && \forall y. && (3.42)\\
\underline{RY_y^v} &\leq RY_y^v \leq \overline{RY_y^v} && \forall y. && (3.43)
\end{aligned}
$$

Finally, the linearized form of (3.11) is obtained as follows:

$$J_4 = \left(\ E_y^{ini} - R \cdot LRY_y\right) \cdot RC + \varepsilon_y \cdot \left(E_y^{ini} \cdot RC\right). \tag{3.44}$$

In order to ensure convergence for this linearized model, the constraint relaxation has to be controlled using an appropriate relative optimality gap.

• *Linearization of BESS Replacement Year:* The BESS energy capacity lost due to degradation, at year y, is given by:

$$LC_y = \ E^{ini} - E_y \qquad \forall y. \tag{3.45}$$

At the replacement year, the variable AC_y, below, ensures that the BESS capacity is equal to E^{ini}; accordingly, the various linearized relations are given as:

$$
\begin{aligned}
AC_y &\geq\ 0 && \forall y. && (3.46)\\
AC_y &\leq\ M\ Z_y^{RY} && \forall y. && (3.47)\\
AC_y &\geq\ LC_y + (1 - Z_y^{RY})\ M && \forall y. && (3.48)\\
AC_y &\leq\ LC_y - (1 - Z_y^{RY})\ M && \forall y. && (3.49)
\end{aligned}
$$

• *BESS Power Sizing:* Note that BESS power capacity is assumed to remain

constant throughout the planning horizon; degradation essentially affects the energy capacity, as follows:

$$Pb_y = \begin{cases} Pb_y^{ini} & ; y = 1. \\ Pb_{y-1} & \forall y, y \neq 1. \end{cases} \tag{3.50}$$

$$B_y \leqslant Pb_y^{ini} \leqslant M \cdot B_y \quad \forall y. \tag{3.51}$$

The constraint (3.51) ensures that BESS power capacity constraints are in effect, once the BESS is installed.

• *BESS Operational Constraints:* The energy balance of BESS is given below, where the charging/discharging operations determine the SoC level [107]:

$$Pba_{y,t} \cdot \left[\frac{(X_{y,t}^{dch})}{\eta_{dch}} + (X_{y,t}^{ch})\eta_{ch} \right] = SoC_{y,t} - SoC_{y,t-1} \qquad \forall y, t. \tag{3.52}$$

Since the proposed planning problem is solved as an MILP optimization problem, it is essential that (3.52), which is also nonlinear, is linearized using "Big-M" method. The linearized equations of charging/discharging constraints can be found in [107]. To force the binary variables associated with the charging and discharging processes to be properly activated, several constraints are used and can found in [35, 107].

$$-M\ X_{y,t}^{ch} \leqslant Pba_{y,t} \leqslant M\ X_{y,t}^{dch} \qquad \forall y, t. \tag{3.53}$$

$$X_{y,t}^{dch} + X_{y,t}^{ch} \leqslant \sum_{y=1}^{N} B_y \qquad \forall y, t. \tag{3.54}$$

The constraint (3.53) ensures that $X_{y,t}^{dch}$ is unity when discharging and zero otherwise; it also ensures that $X_{y,t}^{ch}$ is unity when charging and zero otherwise. It is assumed that the chosen Li-Ion battery has a round-trip efficiency of 90% [108]. The coordination between charging and discharging ensures that decision variables are attained, and that BESS does not charge and discharge simultaneously, as per (3.54).

The SoC of the BESS is bound by lower and upper limits; the lower limit depends on the DoD, as given below.

$$E_y \cdot \left(1 - \overline{DoD}\right) \leqslant\ SoC_{y,t}\ \leqslant\ E_y \qquad \forall y \in Y, t \in T. \tag{3.55}$$

It should be noted that $SoC_{y,t}$ varies over time, and depends on BESS capacity degradation. The maximum allowable DoD of a BESS is denoted by $\overline{DoD}$.

– *Charging and Discharging Operational Relations:* In order to capture the O&M cost of the BESS in (3.3), BESS discharge needs to be calculated accurately. The total energy discharged (TED) is given as follows [35]:

$$\text{TED} = \left(\frac{\eta_{ch}}{1-\eta_{dch}\ \eta_{ch}}\right)\ \sum_{t=1}^{T} -Pba_{y,t}\ \Delta t \qquad \forall y \in Y, t \in T. \tag{3.56}$$

– *Cycling Operations Constraints:* The maximum number of C2F of BESS, N_{C2F}, is obtained from the manufacturer as "*Wöhler Curve*", which captures the effect of BESS cycling degradation on the operations, as follows [34, 35]:

$$TND \cdot \sum_{t \in T} X_{y,t}^{dch} + X_{y,t}^{ch} = Cyc_y \qquad \forall y \in Y, t \in T. \tag{3.57}$$

$$\sum_{y \in Y} Cyc_y \leqslant N_{C2F} \qquad \forall y \in Y. \tag{3.58}$$

Cyc_y is number of operational cycles of the BESS in year y; the value of N_{C2F} is provided by [108]. Note that Cyc_y can be obtained more accurately by implementing the rainflow algorithm [96], by counting the operation cycles and grouping them in various ranges of DoD, which is beyond the scope of this work.

• *System Operational Constraints:* The system demand-supply balance is given as follows:

$$\sum_{i=1}^{G} P_{y,i,t} + Pba_{y,t} + P_{y,t}^{PV} + P_{y,t}^{W} + P_{y,t}^{UNS} = (1+\Gamma)^{y-1} Pd_t \tag{3.59}$$

Reserve constraints ensure that enough capacity is committed from generators and BESS to meet the system peak demand and maintain a reserve capacity margin, given as follows [35].

$$\sum_{g \in G} \left(\overline{P_g} W_{y,g,t} - P_{y,g,t}\right) + SRB_{y,t} \geq \chi\big[(1+\Gamma)^{y-1} (Pd_{y,t} - P_{y,t}^{UNS}) + P_{y,t}^{Solar} + P_{y,t}^{Wind}\big] \qquad \forall y, t. \tag{3.60}$$

In (3.60), Γ is the annual rate of demand increase and χ is a reserve allocation factor to be maintained taking into account the uncertainty of RESs.

All standard unit commitment constraints are considered for generating units, such as ramp-up/ramp-down constraints, minimum-up/minimum-down time constraints, and binary coordination constraints, which are discussed in [70].

3.4 Results and Discussions

3.4.1 Input Data, Assumptions, and Test System

3.4.1.1 Stage-I

In the deterministic case, one class of EV (EV2), as presented in Table 3.1, with two realistic drive cycles, FTP-75 and EPA-Highway, are considered to obtain the degradation using the BCDM, by emulating a realistic urban-highway-urban round trip [109]. The FTP-75 drive cycle has three phases: cold-start, stabilized, and hot-start, whereas the EPA-Highway drive cycle has only one phase. The total driving distance is 68.16 miles, with an average speed of 34.22 km/h.

On the other hand, for a stochastic case study, three different classes of EV are considered (EV1, EV2, and EV3), with twelve drive cycles for each class of EV, selected based on a *frequency-based feature selection* approach [110]; real-world data is collected and preprocessed, and the drive cycles have been clustered based on EV classes. Table 3.1 presents the general data for the three classes of EV considered in the studies. The EV drive cycles data [§§] is based on the actual data collected for three EV classes from the Region of Waterloo, Ontario, Canada, over a period of three years.

The vehicle parameters used to calculate the traction power using VLDM and VPM, are presented in Table 3.2 for EV2 class [80]. Similar parameters for the other classes of EVs can be found in [79]. It is assumed that the EVB packs for all the EV classes are fully charged at the beginning of the drive cycle, and their SoC is allowed to vary between 20% and 90% during operation.

[§§]The data was collected in the Drive4Data program, led by Waterloo Institute for Sustainable Energy (WISE). More information is available at: `https://wise.uwaterloo.ca/drive4data`.

Table 3.1: EV Participants Database Summary

	Model	Size (kWh)	Datalogging interval
EV1	Ford Focus	23	2013-2016
EV2	Nissan Leaf	24	2013-2016
EV3	Chevrolet Volt	16	2013-2016

Table 3.2: Nissan Leaf Vehicle (EV2) and other Parameters

Parameters	Value	Unit	Parameters	Value	Unit
Effective vehicle frontal area (A_f)	2.59	m^2	Air density (ρ)	1.225	(kg/m^3)
Aerodynamic drag coefficient (C_D)	0.28	-	Gearbox ratio (N_g)	7.94	-
Gravitational acceleration (g)	9.81	$(m/s^{2)}$	Vehicle mass (m)	1,177	(kg)
Rolling resistance coefficient (C_r)	0.0125	-	Wheel radius (r_w)	0.3	m

It should be noted that the battery type of all EV classes is Li-ion pack as per information given by their manufactures.

3.4.1.2 Stage-II and Stage-III

The Li-Ion battery is considered for both new and repurposed BESS, whose costs are given in Table 3.3. The microgrid has a total investment budget of $2.5 million. The maximum DoD is assumed to be 80%, whereas the $\frac{E}{P}$ ratio is between 1 and 4 [108]. The energy cost of REVBs is obtained in Stage-II, which is multiplied by different factors obtained from [108] to estimate the different cost components of an REVB system. Note that the cost of installing an REVB as a BESS is assumed to be the same as installing a new BESS.

Table 3.3: System Costs of New and Repurposed Li-Ion BESS

	C^v_{pb}	C^v_E	OMC^{fx}	OMC^v	RC	Energy-Unit	Power-Unit
	$/kW	$/kWh	$/kWh	$/kWh	$/kWh	$/kWh	$/kW
New	1,859	901	13.2	0.0014	1,560	445	525
Repurposed	1,334	456	13.2	0.0018	1,115	200	236

The proposed BESS planning model is validated and tested on the CIGRE isolated microgrid benchmark system [67], which features the following components: 3

diesel generator units with ratings of 2,500 kW (DG1), 1,400 kW (DG2) and 800 kW (DG3); a 310 kW CHP-diesel unit (DG4); a 500 kW gas-microturbine (DG5); and 8 PV units and 4-wind turbine units, with total installed capacities of 840 kW and 1,450 kW, respectively [67]. These dispatchable and non-dispatchable units supply the peak demand of 5.29 MW in the first year, which increases annually at the rate 2% over a 10-year planning horizon [67]. A 3% annual fuel cost increase (FCI) is assumed. The proposed BESS sizing model is executed based on forecasted profiles of average power demand, and solar and wind generation, shown in Figure 3.3 and Figure 3.4 [67]. The operating reserve requirement of the isolated microgrid is 13%

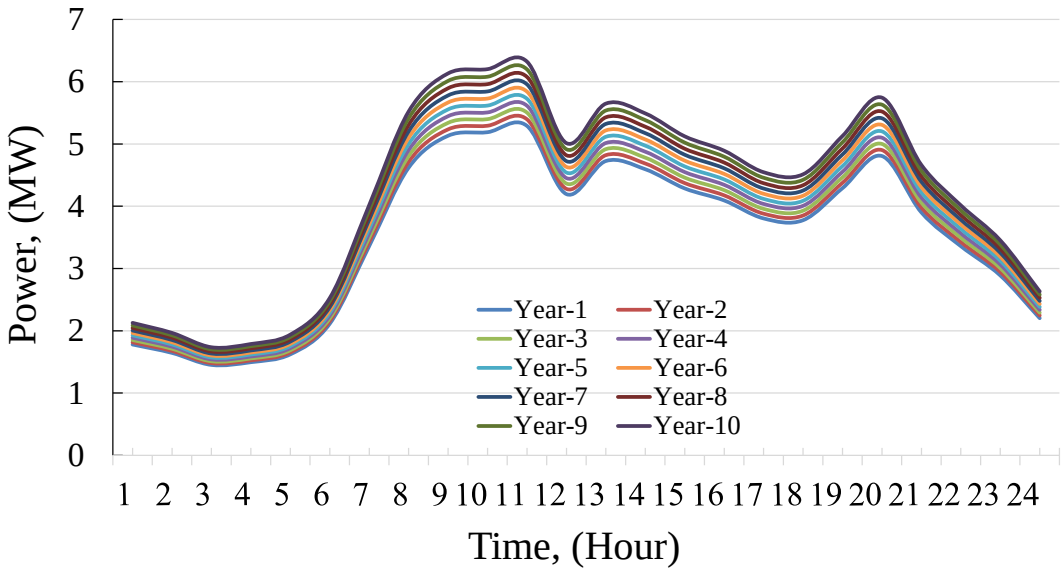

Figure 3.3: Isolated microgrid hourly demand profile of each year (Pd_t)

of the hourly demand. The fixed installation cost is $\$20,000$, which is incurred only once. When the replacement year of the BESS is assumed to be fixed, the BESS is replaced every 5 years. The discount rate (R) of the planning problem is assumed to be 8%, and the maximum BESS energy capacity and power rating that can be installed are 10 MWh and 10 MW, respectively. It should be noted that the Big-M value is set to be 10,000 which is similar to the maximum BESS energy capacity.

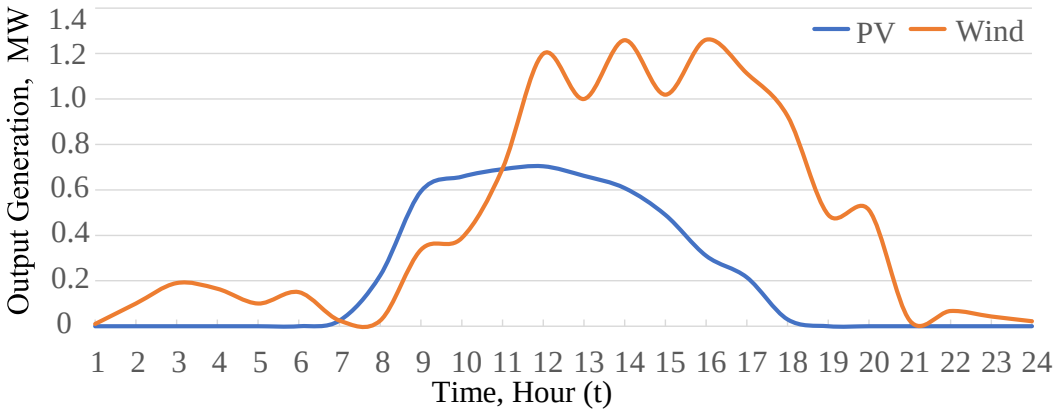

Figure 3.4: PV and wind hourly generation profiles

3.4.2 Results and Analysis

3.4.2.1 Stage-I

Deterministic Case Study: The Stage-I models are solved for a realistic urban-highway-urban round trip drive cycle which results in degradation of the EVB pack to an SoH of 80.2% of the original capacity of 24 kWh (EV2 class), with $\zeta = 4.752\,kWh$. The degraded capacity after one daily drive cycle is 0.00775% of the initial capacity (Figure 3.5(a)), and it is noted that the EVB reaches an SoH of 80.2% after 7 years on the road (Figure 3.5 (b)). Assuming that the EVBs have a calendar life of 15 years [111], 7 years on the road means that they have a remaining calendar life of 8-years.

Stochastic Case Study: First, each EV class parameters described in Table 3.1 and their 12-selected drive cycles were simulated. The number of driving cycles to reach the threshold of SoH (80%) is then determined. Figure 3.6(a)-Figure 3.6(c) show the number of driving cycles required by each class of EV to reach an SoH of 80%. Each EVB reaches its 80% SoH depending on how harsh the acceleration and braking events were for that vehicle's drive cycle. Since each drive cycle represents a one-day driving operation, the number of years that it takes for the EVB to degrade to an SoH of 80%, denoted by Y2D, can be calculated as follows:

$$\text{Y2D} = \text{Number of Drive Cycles to 80\% SOH}/TND \tag{3.61}$$

After determining the Y2D of each drive cycle, it is then multiplied by a uniform prob-

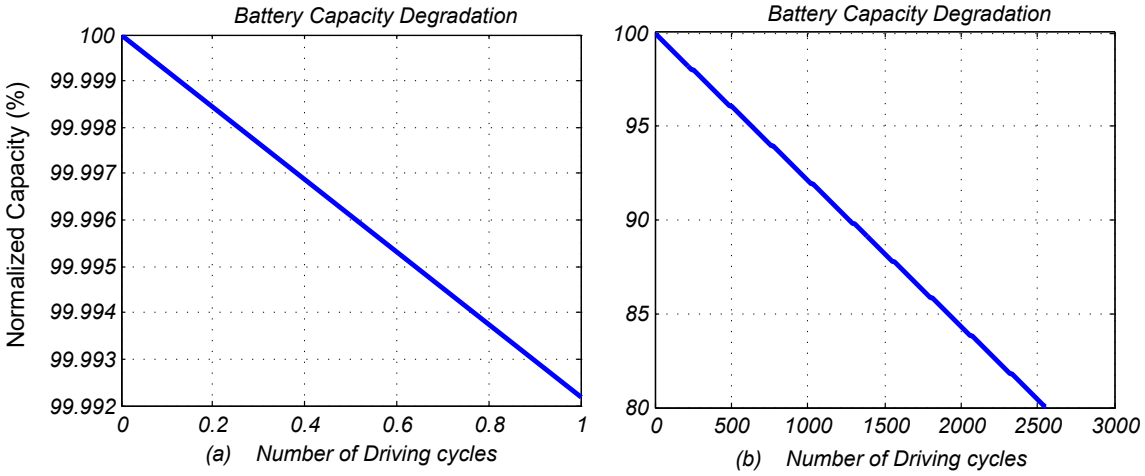

Figure 3.5: (a) EVB normalized capacity for one-day driving (b) EVB normalized capacity for 7-Years driving

ability distribution function to determine the expected Y2D, denoted by E(Y2D), for each EV class, which will impact Stage-II and Stage-III. The remaining life of an EVB will impact the cost of REVBs , and later will influence their replacement year in the microgrid planning model. For the drive cycles considered in this work, it is noted that the value of E(Y2D) is 5.6 years for class EV1, 5.1 years for class EV2 is, and 5 years for class EV3. These values are less than those in the deterministic case because of the presence of numerous real data scenarios of the drive cycles. Accordingly, there would be early replacements for EVBs during their first-life, and longer calendar years for REVBs in microgrid applications.

The stochastic studies demonstrate how to capture and represent the heterogeneity of REVBs in the real-world (e.g., different charging / discharging coefficients, different remaining capacities for second-life purpose in microgrids, and different characteristics) by clustering and integrating within the proposed planning model.

Thus, modelling the performance of the EVB on the road over a number of years until it reaches its 80% SoH provides the inputs needed for Stage-II. It should be noted that varying drive cycles, initial SoC, and other parameters of an EVB would result in a different SoH, and, in turn, a different REVB cost, as presented in the stochastic case.

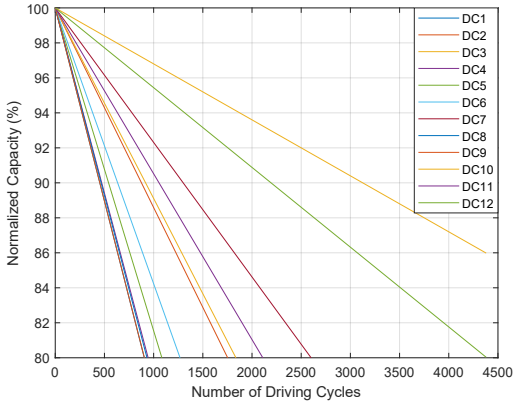

(a) EV1

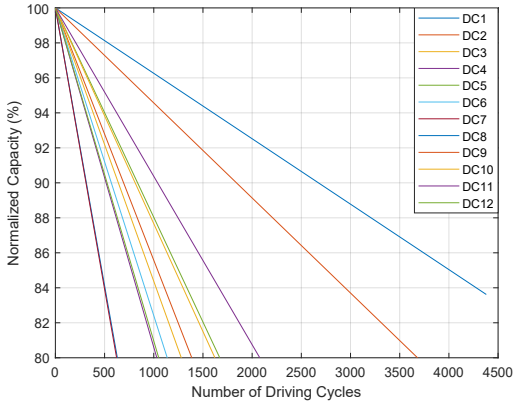

(b) EV2

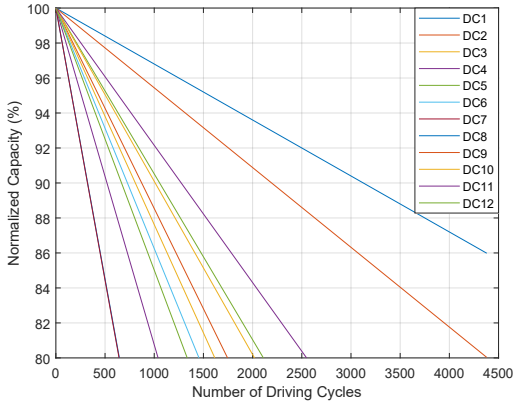

(c) EV3

Figure 3.6: EVB normalized capacity for different drive cycles and EV classes

3.4.2.2 Stage-II and Stage-III

The outputs of Stage-I of the deterministic case, are introduced as inputs to Stage-II; the results show that the cost of the used Li-Ion EVB of 80.2% SoH is 141 $/kWh and the effective repurposing cost is 59 $/kWh. The total cost of the REVB is therefore 200 $/kWh. These values are compared with those for a new Li-Ion BESS (Table 3.3), and introduced as inputs to Stage-III. It should be noted that the REVB cost is based on EV2 class of the Nissan Leaf battery capacity of 24 kWh. In order to examine the suitability of the proposed BESS planning model, the following cases are considered:

- Base Case: No BESS installation.
- Case I: With REVB as BESS.
- Case II: With new BESS.

For Cases I and II, the following four scenarios pertaining to the BESS are studied:

(a) Fixed year of replacement, no degradation.

(b) Fixed year of replacement, considering degradation.

(c) Variable replacement year, considering degradation.

(d) Variable replacement year, considering degradation, with no C2F constraints.

The microgrid operator has the option to install BESS, either new or REVB, with the objective of lowering the total NPV of costs, and thereby increasing its participation in the system reserve service provisions and discharging energy during peak periods. Also, the microgrid operator will optimally replace the BESS based on the introduced set of constraints to avoid premature replacement and additional costs. As shown in Table 3.4, for Case-I, Scenario-*a*, the total cost of the microgrid is $60,501,295, which is considerably lower than that without BESS (Base Case), when the cost is $82,097,474. The size of BESS as an REVB is optimally determined in Case-I(a) to be 800 kWh with power rating of 600 kW; since degradation effect is not taken into account, the BESS size is determined based on the terminal year requirements, which implicitly satisfies previous year requirements as well. The operation of microgrid for one day in year-5 of Case-I(a) is highlighted in Figure 3.7, which presents the supply-demand balance where the supply is represented by stacked areas including

Table 3.4: Optimal Battery Sizing Solutions (REVB)

	Base Case	**Case-I**: with REVBs			
Scenario-	-	*a*	*b*	*c*	*d*
Deg./RY.*	-	**No/ Fixed**	**Yes/ Fixed**	**Yes/Variable**	**Yes/Variable**
J, \$	**82,097,474**	**60,501,295**	**61,370,432**	**60,563,632**	**60,371,250**
J_1, \$	82,097,474	58,329,594	58,774,730	59,235,576	57,756,013
J_2, \$	-	1,097,407	1,202,963	1,328,056	1,640,000
J_3, \$	-	54,045	53,663	58,095	71,638
J_4, \$	-	1,020,249	1,339,077	780,710	903,600
RY_y [year]	-	every 5 years		7	8
Pb_y [kW]	-	600	600	650	800
E_y [kWh]	-	800	1,050	1,200	

*Deg./RY. denotes degradation and replacement year, respectively.

two discharging events of REVBs and the total load of the microgrid is represented by a solid line.

In Case-I, Scenario-*b*, which considers BESS calendar and cycling degradations, a 1,050 kWh / 600 kW REVB is optimally determined for the BESS in the microgrid. Even though the total microgrid cost is increased, the incremental cost of

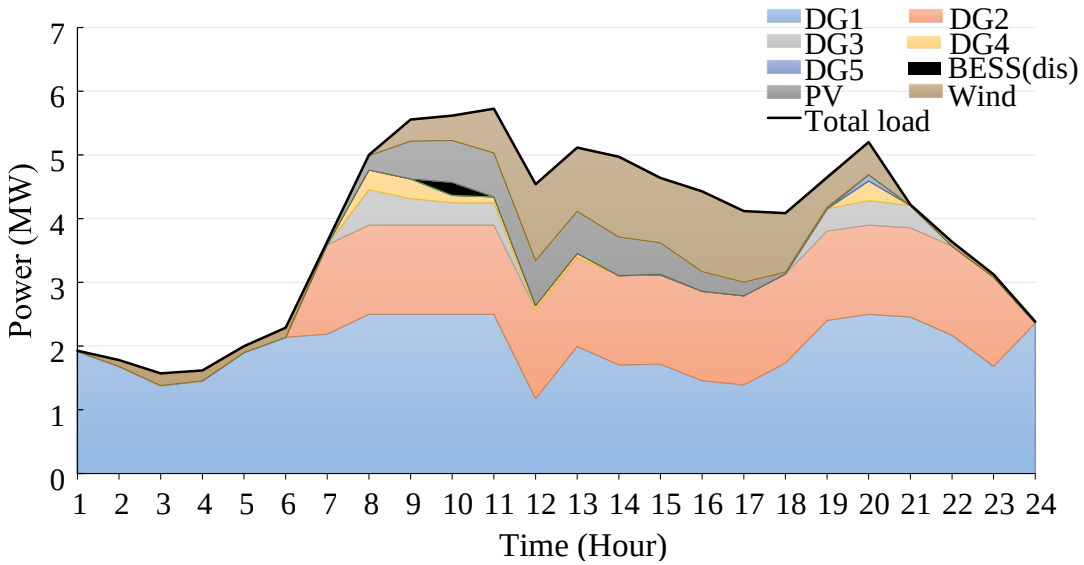

Figure 3.7: Supply and demand mix in Year-5 of Case-I, Scenario-a

$869,137 (compared to Case-I(a)) captures the BESS size accurately. The optimal scheduling and planning decisions indicate that the cost of isolated microgrid operation is higher when BESS degradation is considered, since the operation is more accurately modelled and the microgrid operator adjusts the energy allocation (reserve and discharging) of BESS accordingly. It should be noted that degradation due to cycling is only counted during discharging. Considering a flat rate of cycling degradation would lead to premature replacement and additional costs (overestimating BESS sizes) would be incurred since each system operator has different operating characteristics. However, when considering both cycling and calendar degradations accurately, the optimal sizes would be obtained and premature replacements are prevented.

Table 3.5: Optimal Battery Sizing Solutions (New BESS)

	Base Case	**Case-II**: with New BESS			
Scenario-	-	*a*	*b*	*c*	*d*
Deg./RY.*	-	**No/ Fixed**	**Yes/ Fixed**	**Yes/Variable**	**Yes/Variable**
J, \$	**82,097,474**	**61,534,080**	**62,556,243**	**61,885,146**	**61,873,402**
J_1, \$	82,097,474	58,465,019	58,927,916	58,476,460	58,155,742
J_2, \$	-	1,676,991	1,799,491	2,138,472	2,433,102
J_3, \$	-	53,852	49,078	58,049	62,469
J_4, \$	-	1,338,219	1,779,758	1,179,678	1,222,088
RY_y [year]	-	every 5 years		6	8
Pb_y [kW]	-	600	550	650	700
E_y [kWh]	-	750	950	1200	1450

*Deg./RY. denotes degradation and replacement year, respectively.

Case-1, Scenario-*c* considers both the optimal year of replacement and the impact of degradation; the total cost of the microgrid is reduced, and a saving of $806,800 is achieved, as compared to Case-I(b). Although the size of the REVB is greater than that in Case-I(b), *i.e.,* 1,200 kWh/ 650 kW, the optimal replacement year, which is year-7, ensures that the premature replacement observed in other Scenarios, is prevented. The replacement cost in Case-I(c) is decreased by $558,366 as the year of replacement is deferred to the seventh year, as opposed to that in Case-I(a) and Case-I(b), and most of the work reported in the literature, where replacement year is fixed, resulting in inaccurate BESS planning decisions. Moreover, implementing the optimal year of replacement prevents more replacements over the planning horizon, which reduces capital expenditure. If degradation and optimal replacement year are

ignored, the model's optimal decisions will be affected and hence reflected on the total cost of the microgrid, as well as its reliability during operation.

It is noted that in all scenarios of Case-II (Table 3.5), installing a new BESS increases the microgrid total cost. Comparing Case-I(c) with Case-II(c), it is seen that the microgrid achieves a saving of $1,321,514 over the planning horizon when an REVB is installed as the BESS instead of a new BESS. However, it should be noted that the battery management system of the REVB has to be as reliable as that of a new BESS. As in Case-I(c), when the model considers optimal replacement year in Case-II(c), a significant cost saving of $671,097 compared to Case-II(b), is achieved over the 10-year planning horizon.

Table 3.4 also shows that optimal investments in REVBs significantly reduces the microgrid cost over the planning horizon. The optimal planning model leads to further superior results after the replacement year is made a variable. When the replacement year was fixed, the system accrued additional costs since the BESS had not reached its EoL at the year of replacement. This premature replacement added more cost to the microgrid operator, as seen in Case-I(b) and Case-II(b).

Similarly, when the optimal planning model does not consider the BESS degradation (*Scenario-a in Case-I and Case-II*), the total cost of the microgrid, (J), is the lowest among the scenarios pertaining to that case, and it does not reflect the true cost of the microgrid. Optimal year of BESS replacement in Case-I(c) and Case-II(c) occurs when the battery capacity reaches 80% of its original rated capacity. Accordingly, in Table 3.4, Case-I(c) shows that the BESS is optimally replaced in year 7, while Case-II(c), in Table 3.5, shows that the BESS is optimally replaced in year 6; and not in year 5 as in Cases-I(a),(b), and Cases-II(a),(b).

The impact of BESS capacity degradation due to cycling and calendar aging is fully considered, given that BESS degrades when there is a discharging process. Most of the BESS sizing problems found in the literature consider a fixed degradation during cycling at each year irrespective of the operation, thereby obtaining a size and cost that are not quite accurate. When no degradation is considered, as in Scenario-a, the sizing of the REVB is lower than that when degradation model is implemented. The lower sizing is optimally chosen because the model sizes the REVB at the terminal year when the demand is the highest, assuming the REVB energy size will not degrade with time. This consideration is not valid even though it has the least cost among all scenarios.

The optimal replacement year would be most important when considering dis-

tributed BESS. Since each BESS operation would be different, the replacement year will also be different.

Most energy management and resource allocation studies for BESS sizing do not explicitly consider life-cycle degradation due to C2F or discharging. The latter leads to BESS size degradation which has a great impact on the operation of a system. In these case studies, since REVBs have lower number of C2F as compared to new BESS, the microgrid operator tends to allocate more reserve to the REVBs instead of discharging them, while the new BESS are scheduled for discharging operations much more. This is shown in Figure 3.8, which compares the reserve allocated to REVBs *vis*-à-*vis* new BESS. More discharging, understandably, leads to earlier replacement year for new BESS as compared to REVBs .

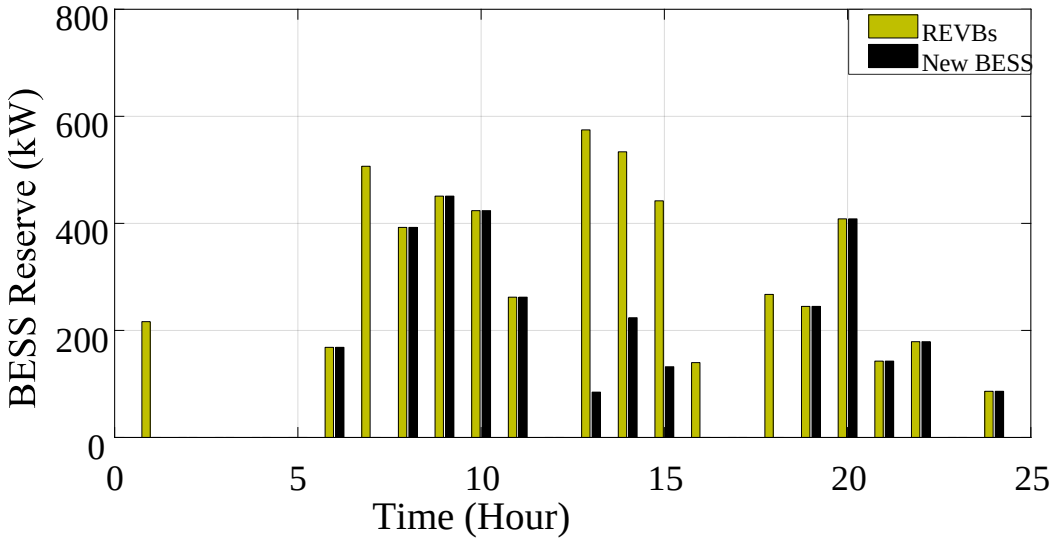

Figure 3.8: Reserves allocation of new BESS and REVBs in Year-9 of Case-I and Case-II, Scenario-a

Allocating more reserves is reflected as well, in the optimal replacement year to be year-7, in Case-I, Scenario-c, as against year-6 in Case-II, Scenario-c, as shown in Tables 3.4 and 3.5. However, in Case-II, the microgrid operator tends to discharge more energy since a new BESS has a higher number of C2F. Figures 3.9 and 3.10 depict the total microgrid reserve allocated by microgrid operator at year-10 to the thermal generators, REVBs , and new BESS to meet the reserve requirements.

It is noted from Figure 3.11 that the average reserve allocation is mostly higher

for REVBs as compared to new BESS. Also, it is clear from Figure 3.12 that new BESS units are involved more in energy buffering than REVBs . In the first and second year, both new BESS and REVBs are assigned only for reserve allocation so that the battery does not degrade while buffering. Also, the REVB is assigned for reserve allocation only, in year-4 and year-7, since it has fewer C2F as compared to new BESS.

In Case-I(d) and Case-II(d) presented in Tables 3.4 and 3.5, the C2F constraints are not considered. Due to the fact that the BESS does not have limits on C2F, the BESS tends to discharge more, which results in more degradation of the battery, that necessitates the system to have a larger size of BESS. Also, the replacement year of the BESS is shifted to, a later year. Even though the total microgrid operation cost is reduced, this reduction does not reflect the true operation cost of the microgrid. Case-I(d) demonstrates how the replacement year of REVBs is limited by the calendar degradation and REVBs have to be replaced at year-8, which is affected by Stage-I outputs, and demonstrates why it is important to consider Stage-I.

3.4.2.3 Stochastic Case Study of Stage-II and Stage-III

After the REVBs are clustered into three classes, the optimal decisions for different classes are obtained separately. The results obtained for each class are presented in Table 3.6; only Scenario-c of Case-I is considered. It is evident that the results of

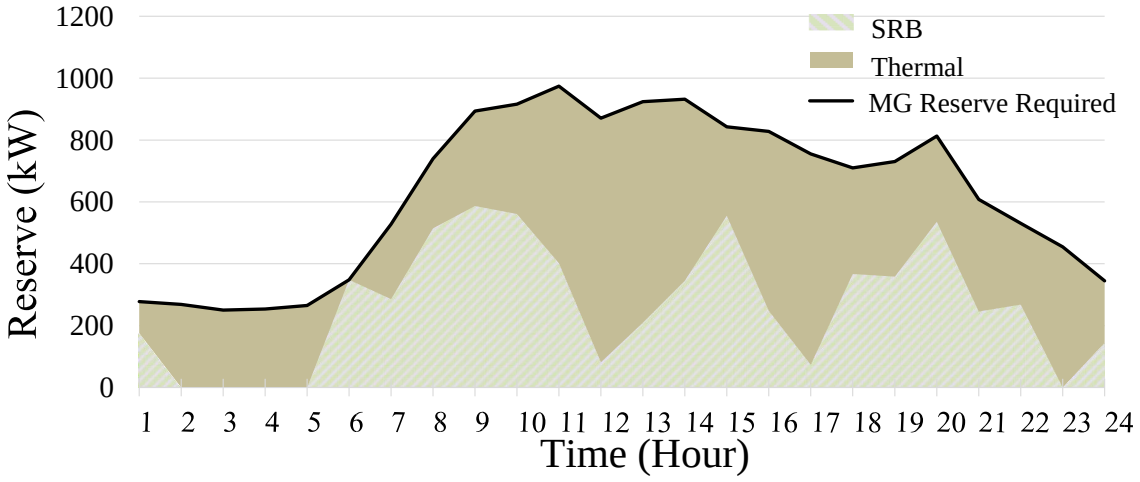

Figure 3.9: Reserve provisions in Year-10 of Case-I, Scenario-c

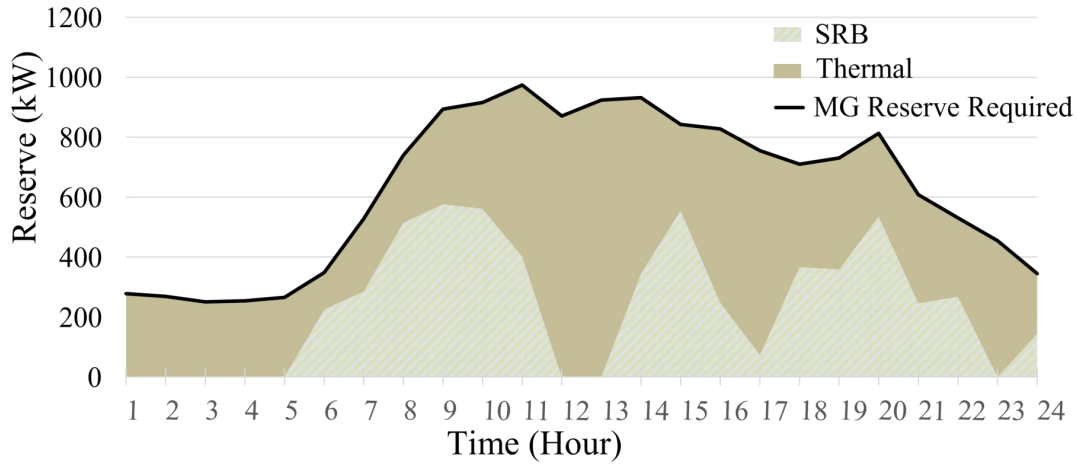

Figure 3.10: Reserve provisions in Year-10 of Case-II, Scenario-c

all the EV classes are quite similar. The installed REVB system based on EV1 class has a higher operation and planning cost than EV2 or EV3 because it has a higher Y2D, which was obtained in Stage-I, and lower number of C2F. EV2 and EV3 yield

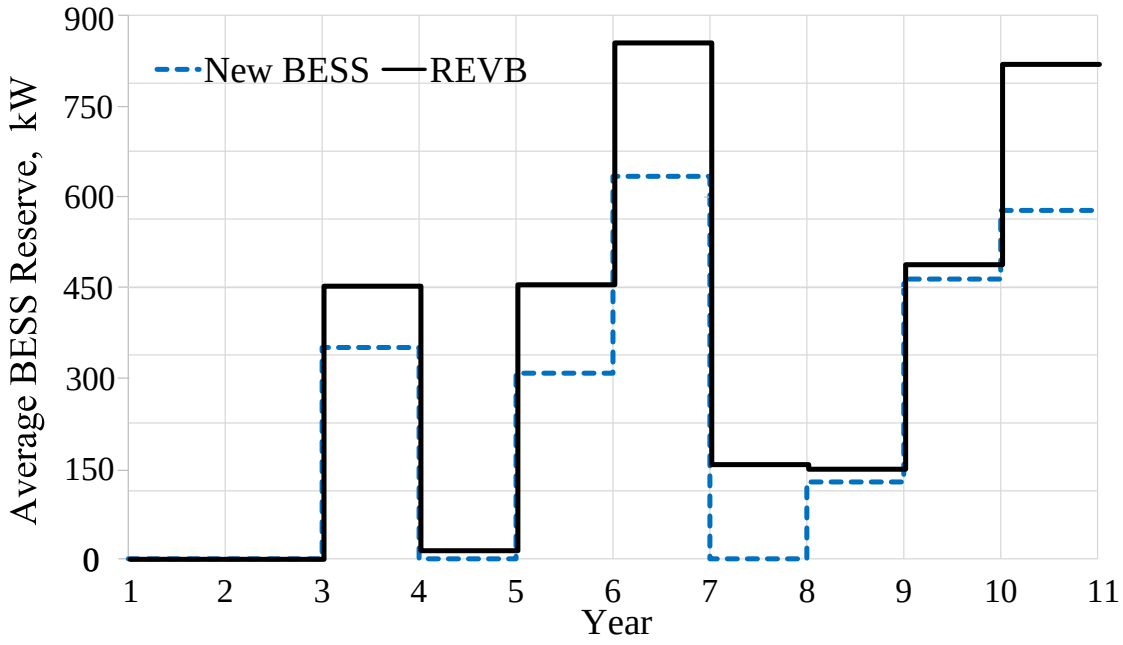

Figure 3.11: Average reserve over planning horizon

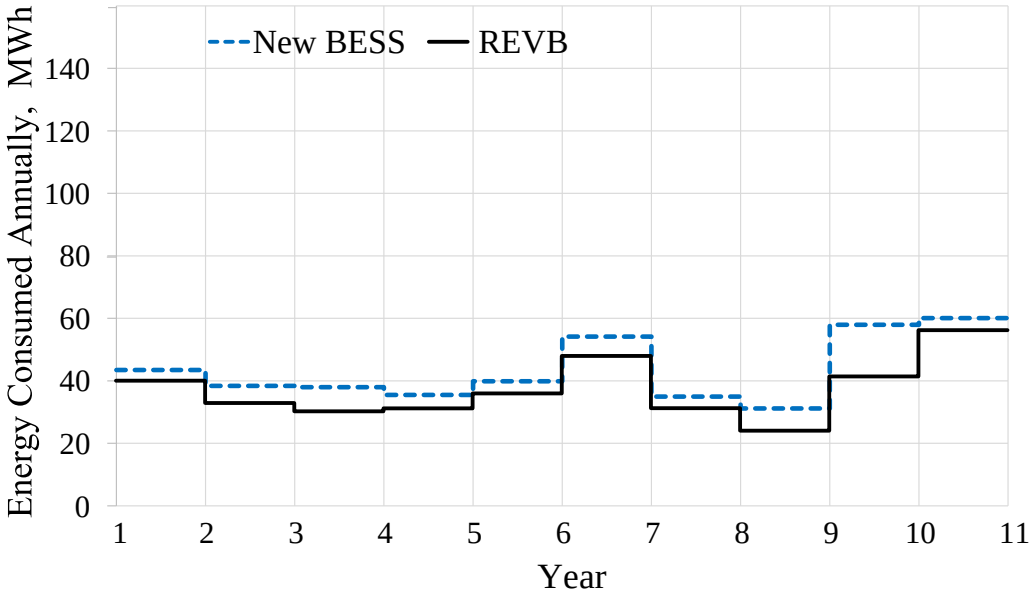

Figure 3.12: Annual energy consumption over planning horizon

the same optimal solutions because they have quite similar values of Y2D and C2F.

Table 3.6: Optimal Solutions with Different EV Classes

	Case-I-Scenario-C: with REVBs	
EV Class	**EV1**	**EV2 and EV3**
Deg./RY.*	**Yes/ Variable**	**Yes/ Variable**
J, \$	**60,339,949**	**60,171,400**
J_1, \$	58,172,088	58,000,046
J_2, \$	1,328,056	1,328,056
J_3, \$	59,095	62,588
J_4, \$	780,710	780,710
RY_y [year]	7	7
Pb_y [kW]	650	650
E_y [kWh]	1200	1200

*Deg./RY. denotes degradation and replacement year, respectively.

3.5 Algorithms and Computational Aspects

The Stage-I models -VLDM, VPM and BCDM- are programmed and simulated in Matlab/Simulink. The proposed microgrid planning model is programmed and executed in the GAMS environment on an IBM Server xSeries 460 with 8 Intel Xeon 2.8 GHz processors and 3 GB (effective) of RAM. The optimization model is an MILP model which is solved using the CPLEX solver, which provides an option to use either Benders decomposition algorithm, or by default, uses the conventional branch and bound (B&B) algorithm. In this work, the CPLEX was set to use the default B&B algorithm [112]. The MILP optimal solution is obtained by setting the optimality gap to 5%. The model and solver statistics for the chosen cases are given in Table 3.7.

Table 3.7: Model Statistics

	Base Case	Case-I(c)
Model Type	MILP	MILP
Solver Used	CPLEX	CPLEX
Number of Single Equations	5,541	12,434
Number of Single Variables	5,581	8,373
CPU time	0.182 (s)*	4 (h)*

*(s) and (h) denote second and hour, receptively.

3.5.1 Comments on Linearization

In mathematical programming, the concept of linearization involves approximating a given function using a linear function in an interval. In this work, three different linearization methods are used for different tasks. First, the PVF of (3.8) is linearized as an infinite series using binomial expression. By replacing the sum of higher-order terms of (3.9) with ε_y, a new representation of the PVF is derived. This linearization is only a transformation and does not impact the accuracy, as shown in Figure 3.2. The second type of linearization involves linearizing the product of a binary and a continuous variable, and is used at multiple instances, in the BESS operational and sizing constraints. This linearization uses the commonly used Big-M method where an additional set of linear constraints is used to represent the product of two variables. The linear set of constraints are effectively modeled to represent the

product of variables in an exact form. There is no approximation, and hence, no loss of accuracy. The third type of linearization is McCormick linearization [101], that is used to linearize the term associated with the replacement cost J_4 in (3.7). McCormick linearization is a convex relaxation approach used for bilinear variables (product of two continuous variables), wherein the lower and upper bounds of the two continuous variables are chosen in such a way that the search for the optimal solution is within practical limits of computation. It should be noted that the chosen boundaries of the two variables define the solution space.

In this work, the variables of concern in J_4 (3.7) are the replacement year (RY_y^v) and the BESS capacity (E_y^{ini}). As be noted from Table 3.8, the lower and upper

Table 3.8: Boundary Limits of Nonlinear Variables

	Lower Limits	Upper Limits
RY_y^v	1 year (new BESS)	10 years
RY_y^v	1 year (REVBs)	Depends on Y2D
E_y^{ini}	0 MWh	10 MWh

bounds of these variables are chosen based on realistic considerations of the microgrid planner; for example, maximum BESS capacity to be installed is chosen to be 10 MWh, which is governed by external factors such as budgetary limits or policy decisions. The replacement year for REVBs depends on the remaining life of the batteries. It should be noted that the accuracy of the planning model will not be impacted by the process of linearization.

3.6 Summary

The large-scale deployment of BESS within microgrids is constrained by their high investment cost barrier while the availability of used EVBs has created a less expensive option for the planners. Researchers have, thus far, not taken into account BESS degradation, in sizing and life-cycle assessment for microgrid long-term planning models. This work develops a systematic procedure to model the degradation of EVBs for different classes of EV during their first-life. This model is integrated into a novel microgrid planning model that determines the optimal decisions of new BESS and REVBs and their corresponding sizing and year of installation, taking into account a new set of mathematical relations of BESS degradation and optimal year of

replacement. REVBs are modeled considering their first-life drive cycles and degradation models, which impacts the microgrid planning decisions, if not considered. Stage-I and Stage-II of the proposed framework quantify the EV battery first-life and present a process to calculate the cost of REVB. The model in Stage-I can be used by researchers and EV manufacturers to develop a data set of EV batteries pertaining to their life. The mathematical model in Stage-III of the proposed framework is targeted to a microgrid or distribution system planner, wherein the planner accesses the data set from Stage-I and Stage-II, for the model in Stage-III. To have a robust operation of REVBs, they are assumed to be equipped with a BMS that controls the operation of the REVBs.

Chapter 4

A Backward-Forward Propagation Approach for REVB-Based Microgrid Planning Considering Adequacy*

4.1 Nomenclature

Indices

d	Time interval, days,	$d \in D$
g	Generation unit	$g \in G$
k	REVB unit	$k \in K$
t	Time interval, hours,	$t \in T$
y	Planning horizon, years,	$y \in Y$

Parameters

CND	Chosen number of days in a single year	
C^{UNS}	Cost of unserved demand	[\$/kW]
C^{v}_{E}	REVB annual installation cost of energy capacity	[\$/kWh]
C^{v}_{pb}	REVB annual installation cost of power capacity	[\$/kW]
C^{fx}	Annual fixed installation cost of REVB	[\$]

*Parts of this chapter have been submitted as a paper in: T. Alharbi, K. Bhattacharya and M. Kazerani, "A New Approach for Repurposed EV Battery-Based Microgrid Planning Considering Adequacy," in IEEE Transactions on Power System, 2020

$\overline{DoD}$	Maximum DoD of the REVB	[%]
$\underline{DoD}$	Minimum DoD of the REVB	[%]
$\overline{(E/P)}$	Maximum energy to power ratio of the REVB	
$\underline{(E/P)}$	Minimum energy to power ratio of the REVB	
$\overline{\mathrm{M}}$	Large number	
OMC^{fx}	Annual fixed O&M cost of the REVB	[$/kW]
OMC^{v}	Annual variable O&M cost of REVB	[$/kW]
$P_{d,t}^{Solar}$	Isolated microgrid solar power output forecast	[kW]
$P_{d,t}^{Wind}$	Isolated microgrid wind power output forecast	[kW]
$Pd_{d,t}$	Isolated microgrid demand	[kW]
RC	REVB replacement cost	[$/kWh]
SDN_g	Shut-down cost of generator	[$/h]
SUP_g	Start-up cost of generator	[$/h]
TD	Total number of days in a year	
η_{ch}	REVB charging efficiency	[%]
η_{dch}	REVB discharging efficiency	[%]
σ_k	Lower threshold of SoH for the REVB	
α_k	REVB degradation factor	[%]
Λ_E	Market standard for REVB energy capacity sizes	[kWh]
Λ_P	Market standard for REVB power capacity sizes	[kW]
β	Energy sharing based degradation factor	[%]

Variables

AC_k	Energy capacity of REVB added in replacement year	[kWh]
B_k	Binary decision for REVB installation [1 or 0]	
CRB_k	REVB remaining energy capacity	[kWh]
CF_k	Binary decision for CRB_k	[kWh]
CF_k^+	Binary decision for REVB when CRB_k is [+]	
CF_k^-	Binary decision for REVB when CRB_k is [0 or -]	
E_k	REVB energy capacity	[kWh]
E_k^{ini}	REVB nominal energy capacity at time of installation	[kWh]
$Edeg_k^{\mathrm{Cyc}}$	REVB capacity degradation due to cycling effect	[kWh]
$Edeg_k^{\mathrm{Cal}}$	REVB capacity degradation due to calendar effect	[kWh]
$\overline{E_k}$	REVB total installed nominal energy capacity	[kWh]
$\overline{E_k^{de}}$	REVB total energy capacity after degradation	[kWh]
$\overline{E_k^{de}}/\overline{Pb_k}$	REVB energy to power ratio at current capacity	
$\underline{E_k}$	Minimum REVB energy capacity	[kWh]
$\overline{n1}_k$	Integer variables for REVB energy capacity size	
$n2_k$	Integer variables for REVB power capacity size	
ord_y	Relative position of the REVB replacement year	
$P_{d,t}^{\mathrm{UNS}}$	Isolated microgrid unserved demand	[kW]
Pb_k	REVB power capacity	[kW]

$\underline{Pb_k^{ini}}$	REVB nominal power capacity at time of installation	[kW]
$\overline{Pb_k}$	REVB total installed power capacity	[kW]
$Pba_{k,d,t}$	REVB charging (-)/discharging (+) power	[kW]
$Pg_{g,d,t}$	Generator power output	[kW]
RY_k^v	REVB replacement year	
$SRB_{k,d,t}$	Reserve provided to the microgrid by REVB	[kW]
$SOC_{k,d,t}$	SoC of the REVB	[kWh]
$U_{g,d,t}$	Generator shut-down binary decision [1 or 0]	
$V_{g,d,t}$	Generator start-up binary decision [1 or 0]	
$W_{g,d,t}$	Generator commitment binary decision[1: ON, 0: OFF]	
$X_{k,d,t}^{ch}$	Binary decision for REVB charging	
$X_{k,d,t}^{dch}$	Binary decision for REVB discharging	
Z_k^{RY}	Binary decision on REVB replacement	
γ_k	REVB weighing factor for energy sharing	
$\Delta_{k,d,t}^{+}$	Binary decision for REVB $\Delta SOC_{k,d,t}^{+}$	
$\Delta_{k,d,t}^{-}$	Binary decision for REVB $\Delta SOC_{k,d,t}^{-}$	
$\Delta SOC_{k,d,t}$	Change in SoC of the REVB	[kWh]
$\Delta SOC_{k,d,t}^{+}$	Change in SoC of the REVB when charging	[kWh]
$\Delta SOC_{k,d,t}^{-}$	Change in SoC of the REVB when discharging	[kWh]

4.2 Introduction

Chapter 3 presented a systematic procedure to model the degradation of EVBs for different classes of EVs during their first-life. This model was integrated into a novel microgrid planning framework to determine the optimal investment plan for new BESS and REVBs. However, the planning model did not take into consideration system adequacy aspects, which are very important for isolated microgrids.

Moreover in Chapter 3, the REVBs were considered as single unit systems, for simplicity in modeling. However, in real systems, that is not the case. For example, a 450 kW/450 kWh REVB would in real-life, is typically comprised of three 150 kW/150 kWh batteries. Therefore, a multiple unit REVB installation plan is now considered and a new energy sharing strategy is proposed in this chapter.

Ideally a single comprehensive MILP model would solve the REVB-based microgrid planning problem, as was considered in the previous chapter. However, such a formulation is computationally very intensive and after the introduction of adequacy constraints and multi-unit REVBs, the problem dimension is significantly increased and fails to arrive at a feasible optimal solution. To circumvent these issues, a new

heuristic backward-forward propagation approach is proposed in this chapter to arrive at the sub-optimal microgrid plan decisions.

In view of the above discussions, the main objectives of this chapter are as follows:

- To extend the previously proposed microgrid planning model to include multi-unit REVBs to simultaneously determine their optimal installations, power and energy sizing, as well as replacement and investment timelines.
- To accommodate multiple installations and replacements of REVBs over the planning horizon, a novel power sharing strategy among various installed REVB units is proposed to enhance the battery useful life and delay their replacements so as to minimize the total cost.
- A novel, heuristic, adequacy check module is introduced starting from the terminal year of the planning horizon, and backwords propagating to the initial year, to ensure that the microgrid's capacity adequacy requirements are met at all years. The investment plan is revised appropriately, if at any year the adequacy constraint is not satisfied.
- A novel forward-propagation approach, based on the operation of the REVB units is introduced to take into account their degradation, and hence to appropriately select their replacement year, which may also require revising the installed energy capacity of the REVBs.

The structure of the chapter is as follows: The proposed backward-forward propagation approach is presented in Section 4.4. The mathematical model for multi-year, multi-unit REVB-based microgrid planning is presented in Section 4.4 as well. In Section 4.5, the system under study and its parameters are introduced. Thereafter, the results of the case study using the proposed approach are presented and discussed in detail in Section 4.6 to demonstrate the effectiveness of the approach. The work is summarized in Section 4.7.

4.3 Proposed Concept for Adequacy Check using Battery E/P Ratio

The installed REVB units will experience both cycle and calendar degradations over the years because of operation and idling, which will reduce their E/P ratio below unity, as given in Figure 4.1. Therefore, a degraded REVB unit will not be able to supply the rated power P for the entire one hour interval.

In order for the microgrid to maintain the required adequacy level after installing REVB units, the total microgrid capacity (including REVBs) need be maintained by ensuring that the E/P ratio of the installed REVBs is always above unity.

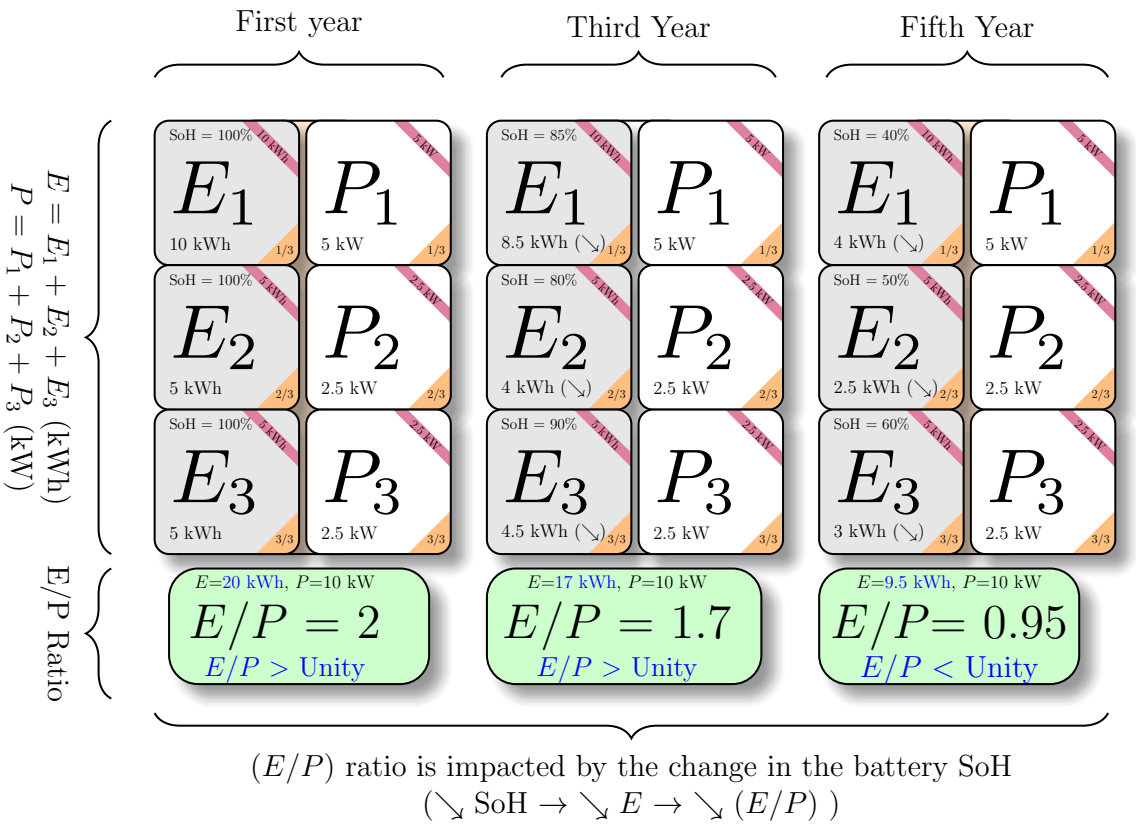

Figure 4.1: Proposed Energy to Power ratio adequacy check

As an example shown in Figure 4.1, in the first year, three battery units are installed, of sizes 10 kWh /5 kW, 5 kWh / 2.5 kW, and 5 kWh / 2.5 kW, respectively. Battery units experience degradation over time, their energy capacity permanently reduces thus reducing the amount of energy a battery unit can store during operation. As seen in the third year, the first unit energy capacity is reduced to 8.5 kWh (85% SoH) and by the fifth year it is 4 kWh (40% SoH). The other battery units also experience similar degradation in their SoH.

The degradation of the battery will impact the E/P ratio. As previously mentioned, the E/P ratio is the total energy capacity of all battery units divided by their

total power capacity. In the first and the third year, the E/P ratio is greater than unity, being 2 and 1.7 respectively. The E/P ratio being greater than unity indicates that the battery can supply power at its rated capacity P for one hour, or more, and is hence satisfying the adequacy constraint. On the other hand, in the fifth year, the E/P ratio falls below unity which means the battery is not able to provide P kW power for one hour, and hence the E/P ratio represents a lack of adequacy. In conclusion, if the E/P ratio is above unity, the battery is fully available, while if not, then it is on partial outage and impacts system adequacy and needs to be replaced by new battery units.

4.4 Backward-Forward Propagation Approach for Multi-year, Multi-Unit REVB-based Microgrid Planning Considering Adequacy

In this section, a comprehensive multi-year, multi-unit REVB-based microgrid planning framework is proposed to determine the optimal power and energy sizes, year of installation, and year of replacements of the REVB units. Also, a power sharing strategy is proposed to enhance the battery useful life and delay the replacements of the REVB units to minimize the total investment cost while ensuring the adequacy is not compromised. A three-stage approach is proposed, as outlined below.

Stage-I: determines the optimal power, energy size and number of REVB units required to be in place, at the plan terminal year while ensuring the microgrid adequacy is met.

Stage-II: includes the backward-propagation approach which determines the optimal year of installation of all REVB units, for the decisions obtained in Stage-I.

Stage-III is a forward-propagation approach that determines the optimal year of replacements, and the weighing decision variables for REVB-discharging that accounts for battery degradation. The decisions obtained in Stage-I and Stage-II will be revised if the degradation of REVB units violate the allowable adequacy limit of the microgrid.

The backward propagation of the model starts from the plan terminal year Y and ends at the first year. The forward propagation follows, where the model is executed from the first year and ending at the terminal year. Within the forward propagation process, a power sharing strategy is incorporated and an iterative adequacy check is introduced that involves post-processing evaluation of the plan decisions such as power and energy capacities. This adequacy check ensures that the target plan adequacy level is met for every year and that degradation is minimized. The details of the proposed framework are discussed next.

4.4.1 Stage-I: Terminal Year Optimal Sizing of REVB Based on Adequacy Check

In this stage, the microgrid optimal plan decisions include the power and energy sizes of the REVB units for the terminal year Figure 4.2. The number of REVB units needed to be installed are divided into clusters, each with a set of REVB units. The step-by-step procedure is discussed in detail as follows.

S1.1 Read input data for the test system to be input to the microgrid planning model for terminal year (Y).

S1.2 Solve the planning model to determine the optimal REVB power (${Pb_k}^{ini}$) and energy (${E_k}^{ini}$) sizes, along with other optimal plan decisions.

S1.3 Using the plan outcomes, microgrid generating unit data (including reliability data), and terminal year demand, execute the LOLP Convolution Algorithm to construct the COPT for terminal year.

S1.4 Using the COPT, evaluate the microgrid's LOLP and check if it satisfies adequacy standards.

S1.5 If YES, select the optimal REVB sizes obtained, and go to next step. If NO, reject the optimal REVB decisions and increase ${Pb_k}^{ini}$, following the available capacity standards. Go to Step **S1.2** , re-execute the microgrid planning model again.

S1.6 Final plan decisions for terminal year (Y) are obtained, which satisfy target adequacy standard of the microgrid,

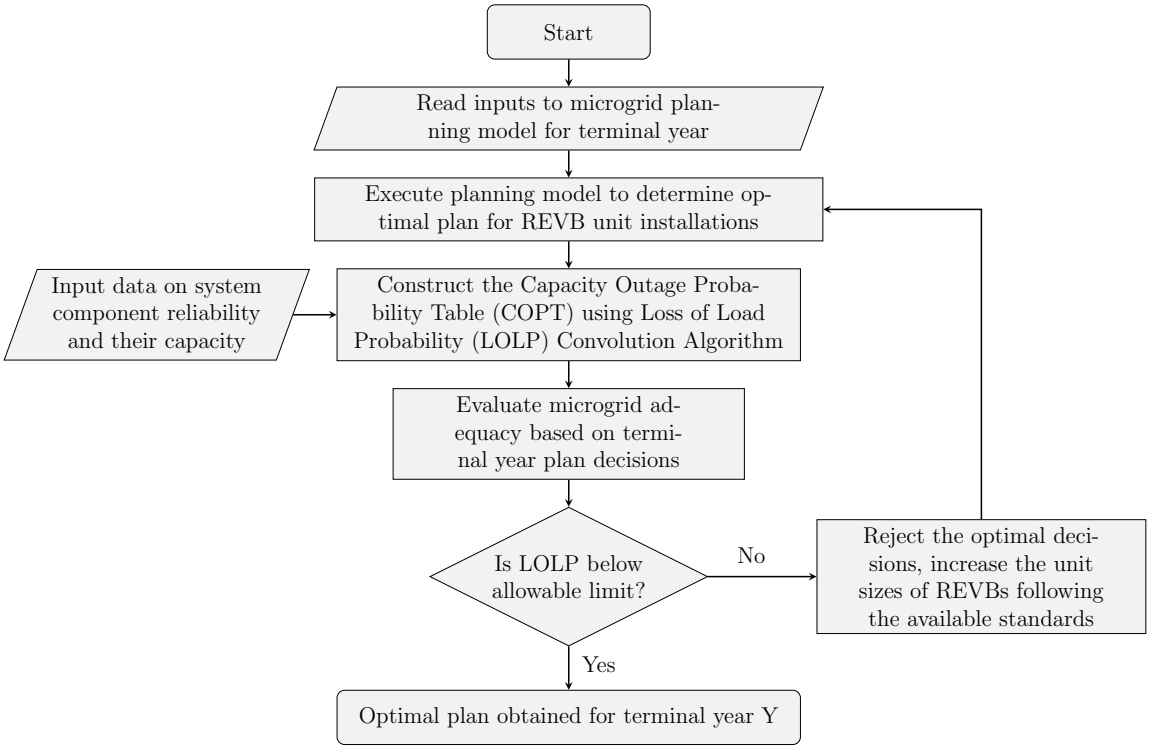

Figure 4.2: Flowchart for Stage-I

In the next stage, a backward-propagation approach, which starts from year $Y-1$ and terminated at the initial year, is used to obtain the optimal installation year of each REVB unit belonging to a given cluster of REVBs.

4.4.2 Stage-II: REVBs Optimal Sizing and Year of Installation

After the optimal power and energy sizes are obtained for year Y in Stage-I and the allocation of number of battery units in each REVB cluster is laid out, the optimal REVB sizes required in the earlier years of the plan, along with the installation year of the REVB units are now determined in Stage-II, starting from year Y-1, as shown in Figure 4.3. The adequacy check used in Stage-I has been used in Stage-II, as well.

The obtained REVB power size ${Pb_k}^{ini}$ of year y is fixed, as a starting point for year y-1. Since ${Pb_k}^{ini}$ for year y satisfies the target adequacy standard, its value is

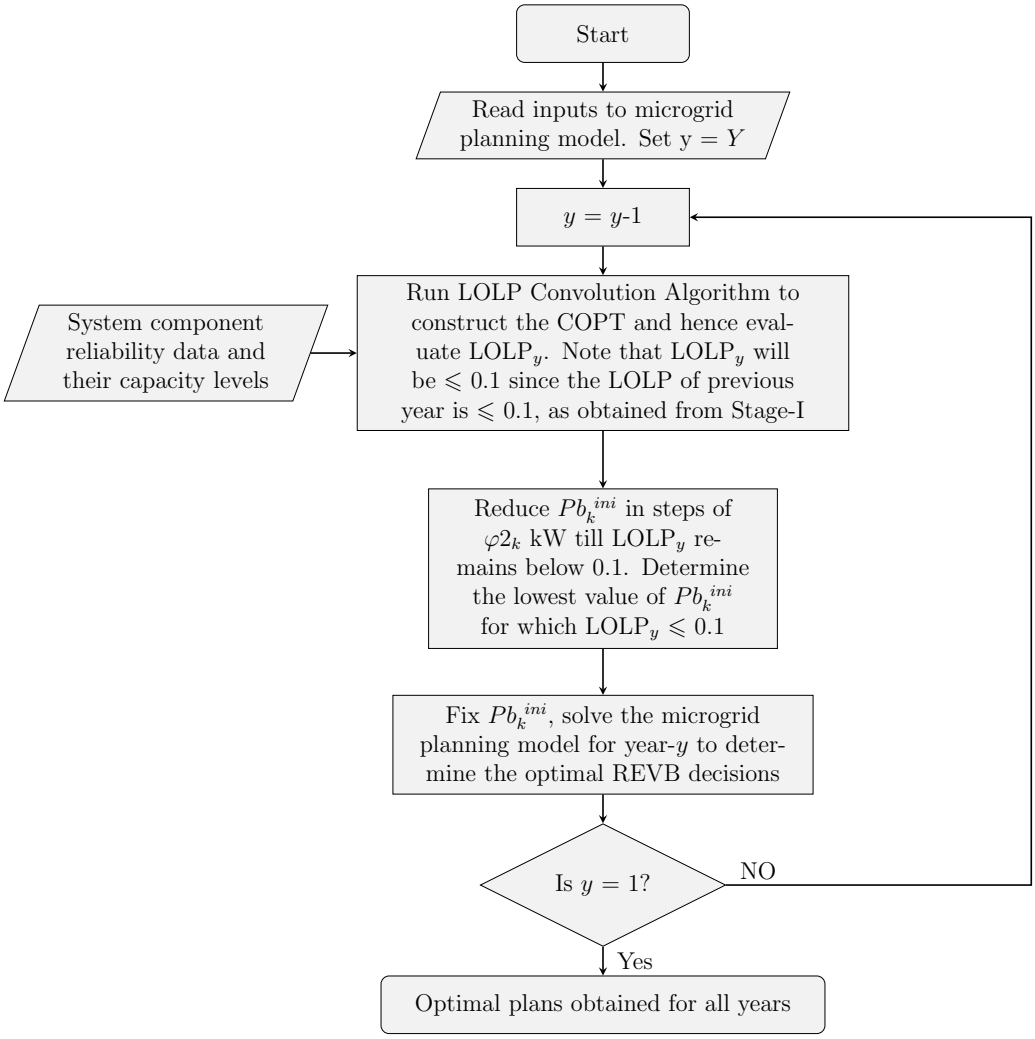

Figure 4.3: Flowchart for Stage-II

reduced in steps to obtain the minimum Pb_k^{ini} while satisfying the target adequacy at year y-1. The planning model is then solved for year $y-1$, fixing the obtained value of Pb_k^{ini} to determine the optimal E_k^{ini} decisions. This is repeated until the power and energy sizes of the REVBs are determined for all years.

The optimal installation years are obtained directly from solving the planning model in the final iteration.

4.4.3 Stage-III: Optimal Year of Replacement of REVB

In the previous stages, the optimal sizing and year of installation of REVBs are determined based on the backward-propagation approach. In Stage-III, a forward-propagation process, starting from the initial year and terminating at year Y is proposed, to determine the optimal replacement year of each REVB unit, as shown in Figure 4.4.

When an REVB is installed in year y, and continuously operated, it will experience both cycle and calendar degradations over the years. Because of this, although its Pb_k will remain the same, its E_k will decrease, thereby reducing the E_k/P_k ratio below unity and hence not allowing the REVB to supply the Pb_k power for one hour, which means the microgrid adequacy is violated. Therefore, if the $LOLP$ target level is violated the optimal decisions of Stage-II, i.e., the optimal REVB sizes, may have to be revised by the new proposed approach, forward propagation, implemented in Stage III, as REVB operations are taken into consideration. The new proposed approach, forward-propagation, is essential since the REVB cumulative energy degradation can make the E_k/P_k ratio less than unity, which will violate the adequacy limit. In this stage, the microgrid planning model is solved after the proposed energy sharing constraints of the REVBs have been introduced by fixing ${Pb_k}^{ini}$, ${E_k}^{ini}$ and the installation year, that are obtained in earlier stages.

In the microgrid planning model, the energy sharing strategy is based on new weighing decision variables that are optimally chosen by the microgrid planning model to allocate the discharging power needed by the microgrid among the installed multiple of REVBs.

4.4.4 Microgrid Planning Model for Horizon Year

The objective function J of the horizon year planning model of the microgrid seeks to minimize its total annualized investment and operating cost at the horizon year, which is given as follows:

$$J = \sum_{y} J_1 + J_2 + J_3 + J_4. \tag{4.1}$$

In (4.1), J_1 represents the total operating cost of the microgrid and is comprised

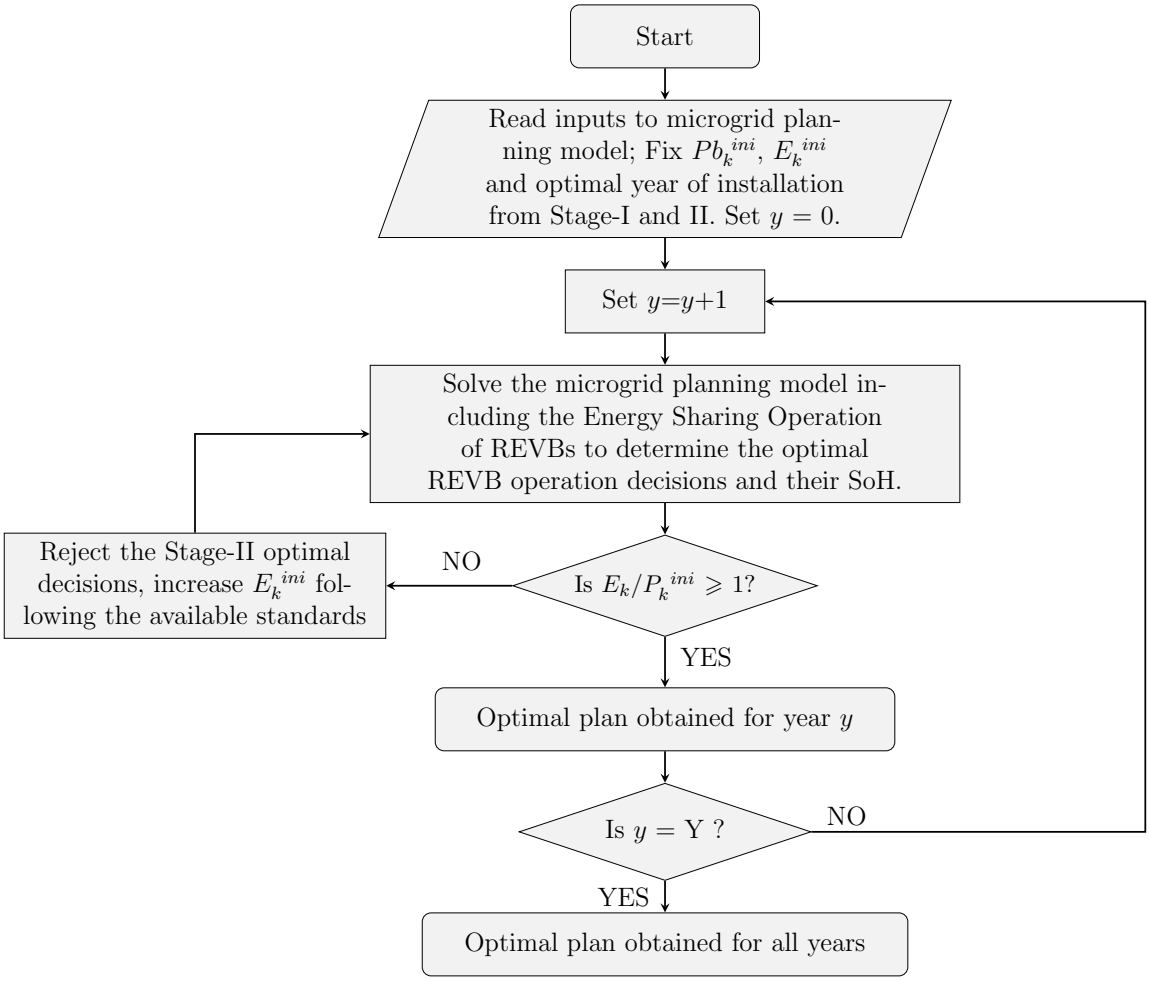

Figure 4.4: Flowchart for Stage-III

of the generation cost of each unit, and cost of unserved demand, given as follows:

$$J_1 = (\text{TD/CND}) \sum_{g \in G} \sum_{d \in D} \sum_{t \in T} \Bigg[(Pg_{g,d,t}\ b_g + c_g W_{g,d,t}) + \text{SUP}_g U_{g,d,t} + \text{SDN}_g V_{g,d,t} + P_{d,t}^{\text{UNS}}\ C_{d,t}^{\text{UNS}} + \Bigg]. \quad (4.2)$$

In (4.1), J_2 represents the installation cost of multiple REVB units and includes their power capacity cost, energy capacity cost, and a fixed installation cost, given

as follows:

$$J_2 = \sum_{k \in K} \left[\left(Pb_k^{ini} C_{pb}^v + E_k^{ini} C_E^v + B_k C^{fx} \right) \right]. \tag{4.3}$$

In (4.1), J_3 represents the Operating and Maintenance (O&M) cost and comprises the fixed and variable O&M costs of the REVB.

$$J_3 = \underbrace{\sum_{k \in K} \left[OMC^{fx} \left(Pb_k \right) \right]}_{\text{Fixed O\&M Cost of the Battery}} + \underbrace{(\text{TD/CND}) \sum_{k \in K} \sum_{d \in D} \sum_{t \in T} \left[OMC^v \left(\frac{\eta_{ch}}{1 - \eta_{dch} \cdot \eta_{ch}} (-Pba_{k,d,t}) \right) \right]}_{\text{Variable O\&M Cost of the Battery}}. \tag{4.4}$$

In (4.1), J_4 represents the REVB replacement cost and is applied only when the REVB reaches its specified EoL, as given below.

$$J_4 = \sum_{k=1}^{K} \left[\left(E_k^{ini} - R \cdot LRY_k \right) \cdot RC + \varepsilon_k \cdot \left(E_k^{ini} \cdot RC \right) \right]. \tag{4.5}$$

It should be noted that J_4 is only considered in Stage-III of the planning framework when determining the optimal replacement decisions, and (4.5) is adopted from Eq. (3.11) [54] . The McCormick method [101] has been applied to replace the bilinear term, obtained from multiplication of the two variables RY_k^v and E_k^{ini}, by replacing $(RY_k^v \cdot E_k^{ini})$ with a new variable, LRY_k, which is linked with the two variables [54]. An in depth explanation can be found in (3.38)−(3.43).

Model Sizing Constraints

• *Capital Budget of REVB:* This constraint imposes an upper limit on the capital spending/ investment on the microgrid towards multiple installations and replacements of REVBs in the plan horizon year.

$$\sum_{k=1}^{K} \left[\left(Pb_k^{ini} C_{pb}^v + E_k^{ini} C_E^v + B_k C^{fx} \right) \right] \leqslant BL. \tag{4.6}$$

The first and second terms in (4.6) represents the costs associated with the installed power and energy capacities of each unit, respectively, and the third term represents the fixed installation cost of REVB units. These costs altogether must be below the assigned budget limit.

• *REVB Power Sizing:* These constraints pertain to the limits on REVB power capacity to be installed.

$$B_k \cdot Pb^{it} \leqslant Pb_k^{ini} \leqslant M \cdot B_k \qquad \forall k \in K \qquad (4.7)$$
$$Pb_k = Pb_k^{ini} \qquad \forall k \in K \qquad (4.8)$$
$$Pb_k^{ini} = \varphi 2_k \cdot \Lambda_P \qquad \forall k \in K \qquad (4.9)$$

Note from Eq. (4.8) that the power size remains constant throughout the planning horizon. The installed power capacity is restricted to follow available market standards as given (4.9); $\varphi 2_k$ is an integer variable. Also note that Pb_k^{ini} is only active in the year of installation, and Pb^{it} is a power capacity setting used as lower limit when the adequacy check is not satisfied in the previous iteration.

• *REVB Energy Sizing:* The binary variables B_k take the value of unity if there is an installation during the plan interval.

$$B_k \cdot E^{it} \leqslant E_k^{ini} \leqslant M \cdot B_k \qquad \forall k \in K \qquad (4.10)$$
$$E_k^{ini} = \varphi 1_k \cdot \Lambda_E \qquad \forall k \in K \qquad (4.11)$$
$$\underline{(E/P)}\ Pb_k^{ini} \leqslant E_k^{ini} \leqslant Pb_k^{ini}\ \overline{(E/P)} \qquad \forall k \in K \qquad (4.12)$$
$$E_k = E_k^{ini} - Edeg_k^{\mathrm{Cyc}} - Edeg_k^{\mathrm{Cal}} + AC_k \qquad \forall k \in K \qquad (4.13)$$
$$Edeg_k^{\mathrm{Cyc}} = (\mathrm{TD/CND}) \cdot \sum_{d \in D} \sum_{t \in T} \left(\alpha_k \cdot \Delta SOC_{k,d,t}^{-}\right) \qquad \forall k \in K \qquad (4.14)$$

Once the REVB unit is installed, the energy capacity of each unit k is restricted between its lower and upper bounds, as in (4.10). The E_k^{ini} sizes should adhere to energy ratings available in the market, Λ_E, as given in (4.11). Moreover, the E_k^{ini} value has to be within the upper and lower limits of E/P ratio, as given in (4.12). Note that once Stage-I and Stage-II decisions are final, the B_k vector for a given year y is created.

The REVB capacity lost due to cycling and calendar degradations, ($Edeg_k^{\mathrm{Cyc}}$, $Edeg_k^{\mathrm{Cal}}$), respectively, during operation (discharging only, $\Delta SOC_{k,d,t}^{-}$) and idling modes are accounted for, as given in (4.13) and (4.14). The last term in (4.13) is only active when there is replacement of REVB unit which is optimally selected based on the REVB operation. Note that, E^{it} is an energy capacity setting used

as lower limit when the adequacy check is not satisfied in the previous iteration of Stage-III, i.e., the $E_k/{P_k}^{ini}$ ratio after degradation is less than unity. In (4.11) the $\varphi 1_k$ is an integer variable. It should be noted that in Stage-III, at the end of year y, the value of E_k will be E_k^{ini} for next year. The variables denoting REVB capacity lost due to cycling degradation, $Edeg_k^{\text{Cyc}}$, and replacement capacity, AC_k, are operational-planning dependent variables, as they will be discussed later.

• *REVB Operational Constraints:* Once the REVB unit is installed, the operational constraints that define the discharging and charging process and balancing the energy level of the battery are given as follows [107]:

$$SoC_{k,d,t} = SoC_{k,d,t-1} + Pba_{k,d,t}\left[\frac{(X^{dch}_{k,d,t})}{\eta_{dch}} + (X^{ch}_{k,d,t})\eta_{ch}\right] \quad \forall k \in K \in d \in D, t \in T \tag{4.15}$$

The energy balance equation of REVB given in (4.15) dictates the SoC level of each unit, which must be within the capacity limit of the battery as given in (4.16). The lower limits depends on how much DoD is allowed each time, $\overline{DoD}$. It should be noted that (4.15) is a non-linear equation and the detailed linearization using "Big-M" method can be found in [35, 54].

$$E_k \cdot \left(1 - \overline{DoD}\right) \leqslant SoC_{k,d,t} \leqslant E_k \qquad \forall k \in K \in d \in D, t \in T \tag{4.16}$$
$$-M\ X^{ch}_{k,d,t} \leqslant Pba_{k,d,t} \leqslant M\ X^{dch}_{k,d,t} \qquad \forall k \in K \in d \in D, t \in T \tag{4.17}$$
$$-Pb_k \leq Pba_{k,d,t} \leq Pb_k \qquad \forall k \in K \in d \in D, t \in T \tag{4.18}$$
$$X^{dch}_{k,d,t} + X^{ch}_{k,d,t} \leqslant B_k \qquad \forall k \in K \in d \in D, t \in T \tag{4.19}$$
$$(\text{TD/CND}) \cdot \sum_{d \in D}\sum_{t \in T} X^{dch}_{k,d,t} + X^{ch}_{k,d,t} \leqslant N_{C2F_k} \qquad \forall k \in K \in d \in D, t \in T \tag{4.20}$$

To activate the charging and discharging process, binary variables $X^{ch}_{k,d,t}$, $X^{dch}_{k,d,t}$, respectively, are introduced in (4.17). The charging/discharging power, $Pba_{k,d,t}$, is limited by the installed power size of the REVB unit (4.18). The binary variables are forced to act as a switch between the charging and discharging processes, as shown in (4.19). In order to count how many operational cycles the REVB has gone through, (4.20) is introduced which is limited by the manufacturer stated C2F, N_{C2F_k} [34, 35]. It should be noted that N_{C2F_k} for a certain year is carried over to the following year until the battery unit is replaced.

– *Energy Sharing Operation of REVBs Included in Stage-III:* The proposed energy sharing operation strategy among the multiple installed REVB units is based on

weighing factors (γ_k), optimally determined by the model in Stage-III. These factors represent the magnitude of degradation of each REVB unit on a yearly basis and depends on the REVB discharging power which is a function of $Edeg_k^{\text{Cyc}}$. The SoH of the battery is impacted by the values of γ_k, as given below,

$$\sum_{k \in K} \gamma_k = 1 \tag{4.21}$$

$$\sum_{k \in K} \gamma_k \cdot Edeg_k^{\text{Cyc}} \leq \ \beta \ \sum_{k \in K} E_k^{ini}. \tag{4.22}$$

Note that the γ_k of each unit is between zero and unity. The parameter β in (4.22) represents the upper limit of cycling degradation of each REVB unit. This parameter is a decision of the microgrid planner, and has a significant influence on the battery EoL and discharging schedules.

• *REVB Replacement Constraints:* Once the energy capacity of REVBs, E_k, reaches the lower SoH threshold, given by (4.23), the associated variables and constraints below will be active. Note that, σ_k is a percentage of the rated capacity recommended by the manufacturer at which the battery should be replaced.

$$\underline{E_k} = \sigma_k \ E_k^{ini} \qquad \forall k \in K \tag{4.23}$$

$$CRB_k = \ E_k - \underline{E_k} \qquad \forall k \in K \tag{4.24}$$

$$CF_k = \begin{cases} CF_k^+ & \text{if } CRB_k \text{ is a positive value} \\ CF_k^- & \text{otherwise} \end{cases} \qquad \forall k \in K \tag{4.25}$$

$$Z_{k+1}^{RY} = \ CF_{k+1}^- - CF_k^- \qquad \forall k \in K \tag{4.26}$$

$$RY_k^v = Z_k^{RY} \times ord_y \qquad \forall k \in K \tag{4.27}$$

$$AC_k = E_k^{ini} - E_k \quad \Rightarrow \exists \text{ if } Z_k^{RY} = 1 \qquad \forall k \in K \tag{4.28}$$

The CF_k takes a binary variable, as given in (4.25). If REVB energy capacity reaches the lower SoH threshold, then there is a replacement and CF_k^- will be unity while CF_k^+ is zero. The binary variable Z_{k+1}^{RY} is an indicator variable that marks the replacement year, as explained mathematically in (4.26) and (4.27). Finally when Z_{k+1}^{RY} is unity, the variable AC_k, ensures that the REVB energy capacity is equal to E_k^{ini} as mentioned earlier in (4.13).

• *System Operational Constraints:* The microgrid supply-demand balance is given below where the total discharge and charge power from all the installed REVB units

are included, given as follows :

$$\sum_{g\in G} P_{g,d,t} + \sum_{k\in K} Pba_{k,d,t} + P^{PV}_{d,t} + P^{W}_{d,t} + P^{UNS}_{d,t} = Pd_{d,t} \qquad \forall d \in D, t \in T. \quad (4.29)$$

Reserve constraints ensure that enough capacity is committed from generators and all installed REVB units, in order to meet the system peak demand and maintain a capacity margin, given as follows [35].

$$\sum_{g\in G} \left(\overline{P_g} W_{g,d,t} - P_{g,d,t}\right) + \sum_{k\in K} SRB_{k,d,t} \geq \chi\big[(Pd_{d,t} - P^{UNS}_{d,t}) + P^{Solar}_{d,t} + P^{Wind}_{d,t}\big] \qquad \forall d \in D, t \in T. \quad (4.30)$$

In (4.30), χ is a reserve allocation factor to be maintained, taking into account the uncertainty of RESs. Similar to the supply-demand balance constraint, the total reserve from all the installed REVB units are summed up to arrive at an overall reserve capacity, $SRB_{k,d,t}$, given as follows:

$$SRB_{k,d,t} \leq -Pba_{k,d,t} + \min\left\{ \left[SOC_{k,d,t} - E_{k,d,t}(1 - \overline{DoD})\right] \eta_{dch}, Pb_k \right\} \qquad \forall d \in D, t \in T. \quad (4.31)$$

The $SRB_{k,d,t}$ value of each installed REVB unit takes the higher capacity from either the available energy or the installed power of REVB unit and it also subtracts or adds the discharging/charging power, as mathematically given in (4.31).

All standard unit commitment constraints are considered for generating units, such as ramp-up/ramp-down constraints, minimum-up/minimum-down time constraints, and binary coordination constraints, which are discussed in [70].

• *LOLP Convolution Algorithm:* The Forced Outage Rate (FOR) is defined as the probability of the generating unit or the installed REVB clusters being in an outage state. In order to determine the LOLP of the microgrid, the COPT has to be constructed, which will include the capacities and associated FOR. The COPT can be derived from the conditional probability relationship, given as follows:

$$Cprb^{new}(X) = Cprb^{old}(X) \cdot (1 - FOR) + Cprb^{old}(X - C) \cdot FOR \quad \forall X < C \quad (4.32)$$

$$Cprb(X) = 1 \quad \forall X \geqslant C \quad (4.33)$$

where x represents the demand of the system and c represents the capacity of the

next unit to be convolved. $Cprb^{new}$ denotes the cumulative probability of *x kW or more* on outage for a system after convolving the next unit, while $Cprb^{old}$ represents the probability of *x kW or more* on outage for the system before c is added [71].

4.5 System Under Study

The test system under study is the CIGRE isolated microgrid benchmark which houses three diesel generators with ratings of 2,500 kW, 1,400 kW, and 800 kW, respectively, a CHP-diesel unit with a capacity of 310 kW; a 500 kW gas-fired micro-turbine; and eight solar PV units for a total of 840 kW, and four wind turbine units with a total capacity of 1,450 kW [67, 113].

As mentioned earlier, the generators and the REVBs supply three days of demand, each representing a season with the associated peak in first year being 5.54, 5.40 and 5.03 MW, respectively, which increases by 2% annually over a 10-year planning horizon [67]. The target LOLP for the microgrid is assumed to be 0.1 or lower. The market standard for power and energy capacities of REVBs, Λ_P and Λ_E respectively, are assumed to be 50 kW and 50 kWh.

The annual increase in the fuel cost is assumed 3%. The total capital expenditures on REVB installations and replacements, made by the microgrid operator, is limited by an annual budget limit of $2.5 million. The parameter α_k in (4.14) is a degradation factor equal to 0.0003 which accounts for cycling degradation and is based on lab measurements [105]. The FOR of all generating units and REVBs are assumed to vary between 0.07 to 0.1.

Li-Ion batteries are considered for REVBs, whose costs are given in Table 4.1 [54, 108]. The maximum and the minimum DoD are assumed to be 80% and 20%, respectively, whereas the E/P ratio is between 1 and 4 [108]. The degradation of a battery unit is defined and limited is this work by the parameter $\beta = 8\%$, in (4.22).

Table 4.1: REVB Cost Parameters

	C^v_{Pb}	C^v_E	OMC^{fx}	OMC^v	RC	Energy Capacity	Power Capacity
	$\$/kW$	$\$/kWh$	$\$/kWh$	$\$/kWh$	$\$/kWh$	$\$/kWh$	$\$/kW$
REVB	1,334	456	13.2	0.018	1,115	200	236

The operating reserve requirement of the isolated microgrid is 13% of the hourly demand. The fixed installation for REVB cost is $\$20,000$, which is incurred only at

the year of installation. The discount rate (R) of the planning problem is assumed to be 8%. It should be noted that the Big-M value is set to be 10,000 which is similar to the maximum REVB energy capacity.

4.6 Results and Discussions

The proposed framework discussed in Section 4.4.1 is used to determine the optimal power and energy sizes for the terminal year, as shown in Table 4.2, iteration-1. Although this is the lowest cost plan, note that it does not meet the microgrid's adequacy level. Hence, this solution is revised by increasing Pb_k^{ini} to satisfy the condition that $\text{LOLP}_Y \leqslant 0.1$. The optimal solution with REVBs satisfying the adequacy constraint is obtained in the ninth iteration (as highlighted). The total power capacity required to meet the adequacy constraint is 1,350 kW, for which the corresponding optimal energy capacity is 1,450 kWh. The resulting LOLP of 0.071 meets the target adequacy level of the microgrid.

Table 4.2: Stage-I Optimal REVB Power Sizing and LOLP

Iteration	Power Size	**REVB Clusters**			LOLP
		C_1	C_2	C_3	
	kW	kW	kW	kW	
1	950	500	450	-	0.1318
2	1000	500	450	50	0.1308
3	1050	500	450	100	0.1273
4	1100	500	450	150	0.1201
5	1150	500	450	200	0.1162
6	1200	500	450	250	0.1155
7	1250	500	450	300	0.1143
8	1300	500	450	350	0.1139
9	1350	500	450	400	0.0711

The installed REVBs are grouped into three clusters, C_1, C_2 and C_3, each with multiple battery units. Cluster C_1 has 3 battery units for a total of 500 kW/ 550 kWh, cluster C_2 has 4 units for a total of 450 kW/550 kWh and cluster C_3 has 3

battery units for a total of 400 kW/400 kWh. Table 4.3 presents the cluster-wise REVBs power and energy sizes for the plan terminal year.

Table 4.3: Stage-I Optimal REVB Power and Energy Sizes in Year-10

Total Capacity	**Clusters**	**Units**			
		1	**2**	**3**	**4**
1450 kWh/ 1350 kW	C1	250 kWh	150 kWh	150 kWh	-
	550 kWh/500 kW	250 kW	100 kW	150 kW	-
	C2	100 kWh	100 kWh	150 kWh	150 kWh
	500 kWh/450 kW	100 kW	100 kW	150 kW	100 kW
	C3	150 kWh	100 kWh	150 kWh	-
	400 kWh/400 kW	150 kW	100 kW	150 kW	-

In Stage-II, starting from year Y-1 and fixing the terminal year plan obtained from Stage-I, the LOLP is determined as seen from the first iteration of year-9 in Table 4.4, to have met the target, i.e., $\text{LOLP}_Y \leqslant 0.1$. However, installing this amount of REVB power capacity is costly and not needed. Therefore, ${Pb_k}^{ini}$ is reduced in steps until the LOLP is not violated. At the fifth iteration, when ${Pb_k}^{ini} = 1150\ kW$, the LOLP exceeds 0.1; hence the previous iteration value of ${Pb_k}^{ini} = 1200\ kW$ is selected. The corresponding optimal ${E_k}^{ini}$ at year-9 is obtained to be 1,300 kWh.

This approach is repeated for the previous year by fixing the optimal ${Pb_k}^{ini}$ and ${E_k}^{ini}$ obtained for the current year, until year-1 is reached. The detailed iteration results for Stage-II are given in Table 4.4, and the summary plan is given in Table 4.5.

Table 4.4: Stage-II Optimal REVB Power Sizing Capacity and LOLP

Iteration	Power Size	**REVB Clusters**			LOLP
		C_1	C_2	C_3	
	kW	kW	kW	kW	
Year-10 (obtained from Stage-I)					
9	1350	500	450	400	0.0711
Year-9					
1	1350	500	450	400	0.0686
2	1300	500	450	350	0.0689
3	1250	500	450	300	0.0696

Continued on next page

Table 4.4 – *Continued from previous page*

Iteration	Power Size	REVB Clusters			LOLP
		C_1	C_2	C_3	
	kW	kW	kW	kW	
4	1200	500	450	250	0.0702
5	1150	500	450	200	0.1127
Year-8					
1	1200	500	450	250	0.0686
2	1150	500	450	200	0.0687
3	1100	500	450	150	0.0693
4	1050	500	450	100	0.1121
Year-7					
1	1100	500	450	150	0.0630
2	1050	500	450	100	0.0634
3	1000	500	450	50	0.0638
4	950	500	450	-	0.0644
5	900	500	400	-	0.11189
Year-6					
1	950	500	450	-	0.0632
2	900	500	400	-	0.0636
3	850	500	350	-	0.0643
4	800	500	300	-	0.11180
Year-5					
1	850	500	350	-	0.0615
2	800	500	300	-	0.0615
3	750	500	250	-	0.0623
4	700	500	200	-	0.0628
5	650	500	150	-	0.11006
Year-4					
1	700	500	200	-	0.0615
2	650	500	150	-	0.0619
3	600	500	100	-	0.0625
4	600	500	100	-	0.11003
Year-3					
1	600	500	100	-	0.0561
2	550	500	50	-	0.0565
3	500	500	0	-	0.0572

Continued on next page

Table 4.4 – *Continued from previous page*

Iteration	Power Size	REVB Clusters			LOLP
		C_1	C_2	C_3	
	kW	kW	kW	kW	
4	450	450	0	-	0.10997
Year-2					
1	500	500	-	-	0.0560
2	450	450	-	-	0.0560
3	400	400	-	-	0.0568
4	350	350	-	-	0.0574
5	300	300	-	-	0.10993
Year-1					
1	350	350	-	-	0.0547
2	300	300	-	-	0.0551
3	250	250	-	-	0.0558
4	200	200	-	-	0.1086

From Table 4.4 the highlighted rows, which denote the optimal REVB sizes for the given year, are collected and presented in Table 4.5. Note that Table 4.5a presents the yearly cumulative REVB sizes from the terminal year to the first year, with the binary numbers denoting the cumulative presence of battery units in the three clusters of the REVBs. For example, in year-8, the cumulative REVB size required for the microgrid is 1100 kW/1200 kWh and this capacity will be distributed over the three clusters, C_1, C_2, C_3, with three, four and one battery units respectively, whose sizes are given in Table 4.3. In Table 4.5b, the actual unit sizes to be installed in each year of the plan horizon are hence presented, along with the exact cluster in which that unit will belong, and the year of commissioning, denoted by the B_k matrix.

After the final sizes of the REVBs and their corresponding years of installations were determined in Stage-I and Stage-II, the microgrid planning model is again executed, this time for year-1 onward, proceeding forward over the plan horizon, and including the Energy Sharing Constraints of the REVBs, given by (4.21) and (4.22). The optimal values of γ and hence the REVB units' cycling degradation are obtained.

Table 4.5: Stage-II: Summary Microgrid Plan for REVB

Year	$\overline{Pb_k}$	$\overline{E_k}$	C_1	C_2	C_3
	kW	kWh			
10	1350	1450	1 1 1	1 1 1 1	1 1 1
9	1200	1300	1 1 1	1 1 1 1	1 1 0
8	1100	1200	1 1 1	1 1 1 1	1 0 0
7	950	1050	1 1 1	1 1 1 1	0 0 0
6	850	900	1 1 1	1 1 1	0 0 0 0
5	700	750	1 1 1	1 1	0 0 0 0 0
4	600	650	1 1 1	1	0 0 0 0 0 0
3	500	550	1 1 1	0	0 0 0 0 0 0
2	350	400	1 1	0 0	0 0 0 0 0 0
1	250	250	1	0 0 0	0 0 0 0 0 0

(a)

Year	Pb_k/E_k	C_1	C_2	C_3
	kW/kWh	B_k Matrix		
1	250/250	1	0 0 0	0 0 0 0 0 0 0
2	100/150	0	1 0 0	0 0 0 0 0 0 0
3	150/150	0 0	1 0 0	0 0 0 0 0 0 0
4	100/100	0 0 0	1 0 0	0 0 0 0 0 0
5	100/100	0 0 0 0	1 0 0	0 0 0 0 0
6	150/150	0 0 0 0 0	1 0 0	0 0 0 0
7	100/150	0 0 0 0 0 0	1 0 0	0 0 0
8	150/150	0 0 0 0 0 0 0	1 0 0	
9	100/100	0 0 0 0 0 0 0 0	1 0	
10	150/150	0 0 0 0 0 0 0 0 0	1	

(b)

Table 4.6 shows the replacement decisions of the REVB units when they reach their EoL. It is seen that there are a total of ten new installations in the 10-year plan horizon while only five replacements are planned for.

As can be seen in Table 4.6, in the first year, only one REVB unit was installed and from Figure 4.5 it is noted that the optimal schedule of the microgrid did not require any REVB discharge; hence the REVB capacity was only kept as reserve Figure 4.6. Therefore, only calendar degradation was accounted for in year-1, and the 250 kWh REVB at the start of year-1 was degraded to 247.5 kWh at the start of year-2 (Table 4.6). Moving-forward, as more REVB units are installed, the optimal energy sharing decision variables γ_k for each unit are determined from the microgrid planning model, and the energy discharged from each REVB unit is known, and hence the cycling degradation comes into play.

In year-2, when the second REVB unit in C_1 is installed, $\gamma_{C_1,1} = 0.6$ and $\gamma_{C_1,2} = 0.4$ are obtained, and the total discharge energy split between the two units are determined. Note from Table 4.6, the total REVB energy capacity after degradation at the start of year-2 is 397.5 kWh, which is greater than the total microgrid installed power capacity of 350 kW; hence the $E_k/{P_k}^{ini}$ ratio is greater than unity and thus meets the targeted adequacy level. Therefore, the REVB microgrid plan for year-2 is considered final.

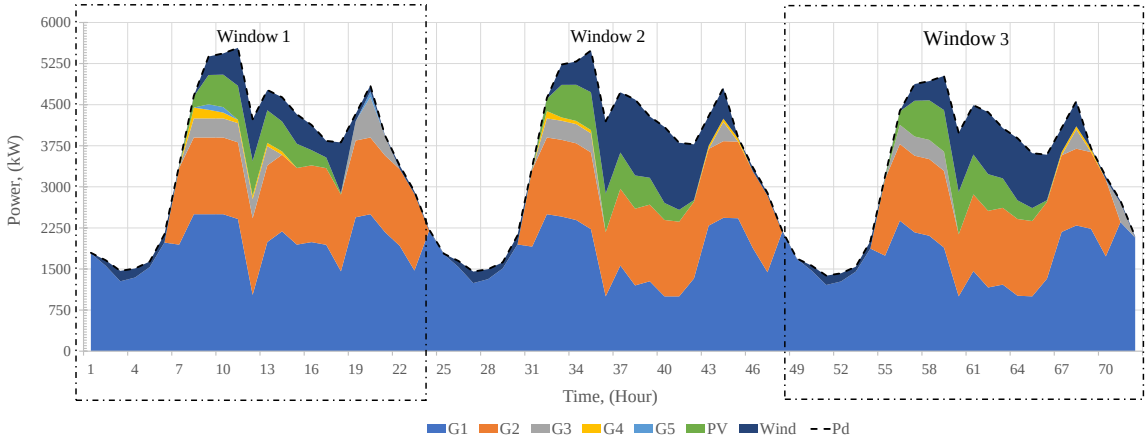

Figure 4.5: Dispatch of microgrid generators in year-1

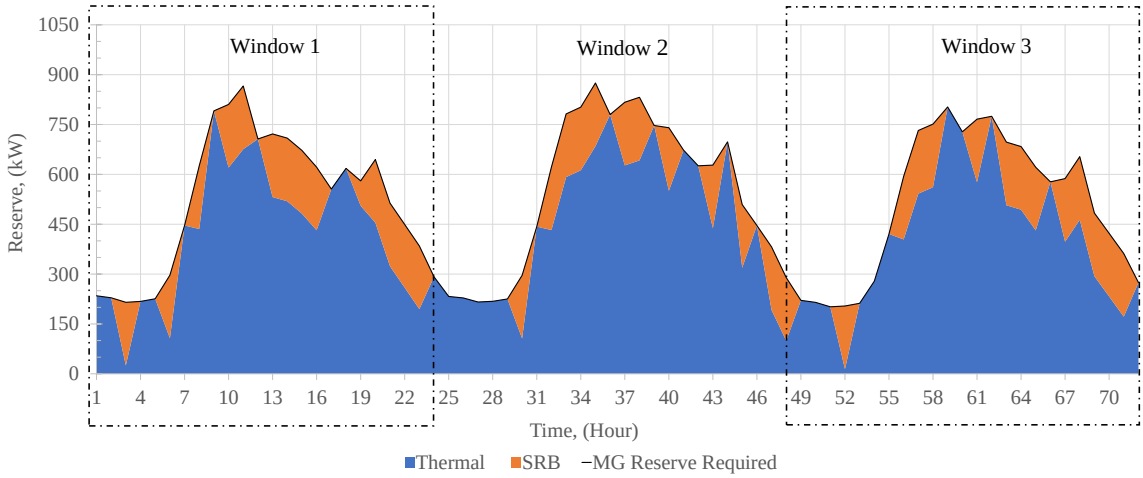

Figure 4.6: Isolated microgrid reserve provisions in Year-1

Furthermore, note from Table 4.6 that in year-4, there are four REVB units, three of which belong to C_1 (217.5 kWh, 137.3 kWh, 145.2 kWh) installed in previous years, while the fourth in C_2 of 100 kW/100 KWh installed in year-4. The cumulative sum of the energy capacities after degradation and the new unit at the beginning of year-4 is 600 kWh, and its $E_k/{P_k}^{ini}$ ratio is unity. Therefore, the final plan for year-4 is achieved.

Table 4.6: Stage-III Results based on Stage-I and -II Outputs

Year	$\overline{Pb_k}$	$\overline{E_k}$	Degraded Energy Capacity of REVB units										$\overline{E_k^{de}}$	$\overline{E_k^{de}}/\overline{Pb_k}$
	kW	kWh	C_1 (550 kWh)			C_2 (500 kWh)			C_3 (400 kWh)				kWh	
1	**250**	250	250										250	1
2	**350**	400	247.50	150									397.5	1.14
3	**500**	550	235.40	142.10	150								527.4	1.06
4	**600**	650	217.50	137.30	145.20	100							600	1
5	**700**	750	250	132.55	133.95	95.75	100						712.3	1.02
6	**850**	900	241.88	150	123.08	91	95.25	150					851.2	1.001
7	**950**	1,050	235.49	144.61	150	86.11	90.36	144.61	150				1,001.2	1.054
8	**1100**	1,200	222.49	137.86	140.63	100	84.11	137.86	143.25	150			1,116.2	1.015
9	**1200**	1,300	209.99	131.36	131.63	94	100	131.36	136.75	143.50	100		1,178.6	0.982
10	**1350**	1,450	200.27	122.64	122.90	85.78	91.78	122.64	128.03	134.78	91.78	150	1,250.6	0.926

$\overline{E_k^{de}}$ denotes total energy capacity after degradation.

The corresponding values of γ_k are 50%, 10%, 30% and 10%, respectively, which determines the energy sharing of these units during year-4 operation, and it is noted that the energy discharged by Unit-2 of C_1 is the same as that by Unit-1 of C_2 since their γ_k values are the same.

Unit-1 of C_1 reached its EoL at the end of year-4 and is replaced by a new REVB unit of the same size at the start of year-5 (shown by the "black" box in Table 4.6). If the energy sharing strategy (4.22) was not included in Stage-III, more energy would have been scheduled for discharge from REVB units installed earlier as compared to the newer units because the microgrid planning model seeks to minimize the installation and replacement cost. In the present work, the proposed energy sharing strategy is able to reduce the degradation of the battery unit which was installed earliest, and hence maintain the $E_k/{P_k}^{ini}$ ratio above unity to ensure microgrid adequacy.

It is also noted from Table 4.6 that the $E_k/{P_k}^{ini}$ ratio at the start of year-9 falls below unity, which means that the targeted adequacy level of the microgrid is not met. Therefore, the energy capacity installed in year-9 (Unit-2 of C_3), as obtained from Stage-II, is rejected and needs to be revised. Table 4.7 presents the revised results of Stage-III for year-9 and year-10, wherein it is noted that the energy capacity

of REVB Unit-2 of C_3 is increased by 100 kW, in year-9, to satisfy the E_k/P_k^{ini} ratio of that year, and it satisfies for year-10 as well.

Table 4.7: Stage-III Revised Energy Capacities

Year	$\overline{Pb_k}$	$\overline{E_k}$	REVB C_1			REVB C_2				REVB C_3			$\overline{E_k^{de}}$	$\overline{E_k^{de}}/\overline{Pb_k}$
	kW	kWh	(550 kWh)			(500 kWh)				(500 kWh)			kWh	
1	**250**	250	250										250	1
2	**350**	400	247.5	150									397.5	1.14
3	**500**	550	235.4	142.100	150								527.5	1.06
4	**600**	650	217.5	137.3	145.2	100							600	1
5	**700**	750	250	132.55	133.95	95.750	100						712.3	1.02
6	**850**	900	241.875	150	123.075	91	95.25	150					851.2	1.001
7	**950**	1050	235.487	144.612	150	86.112	90.362	144.612	150				1001.2	1.054
8	**1,100**	1200	222.487	137.862	140.625	100	84.112	137.862	143.25	150			1116.2	1.015
9	**1,200**	1400	209.987	131.362	131.625	94	100	131.362	136.75	143.5	200		1,278.6	1.066
10	**1,350**	1,550	204.237	123.362	123.625	86.5	94.45	123.362	126.8	132.25	189.25	150	1,353.8	1.003

$\overline{E_k^{de}}$ denotes total energy capacity after degradation.

Table 4.8 presents the SoH of each REVB unit of the three clusters after the Stage-III final solution is obtained (Table 4.7). Note that, the battery is replaced when the SoH is below 80%. Also note that both cycling and calendar degradations contribute to the drop in SoH of the battery unit. The SoH of each unit starts to degrade as the Stage-III algorithm progresses to the terminal year. Once the SoH reaches its threshold limit of 80%, as Unit-1 in C_1 at year-5 (highlighted in green), there will be a replacement of the unit according to the optimization model described earlier. For example, in year-5 the said unit was replaced by an unit of the same size (250 kWh).

The year-wise costs to the microgrid, after the optimal plan is obtained, are determined, and presented in Table 4.9 which includes the yearly total operation cost, the REVBs installation cost, the REVBs O&M cost, and the REVBs replacement cost.

It is noted that the operating cost of the microgrid increases over the plan horizon, as shown in Table 4.9. The installation cost in the first year is the highest because of the sizes of Pb_k^{ini} and E_k^{ini} installed that year. The yearly O&M cost also increases

Table 4.8: REVB State of Health

Year	$\overline{E_k}$	REVB C_1			REVB C_2				REVB C_3		
	kWh	**550 kWh**			**500 kWh**				**500 kWh**		
1	**250**	1.000	0.000	0.000	0.000	0.000	0.000	0.000	0.000	0.000	0.000
2	**400**	0.990	1.000	0.000	0.000	0.000	0.000	0.000	0.000	0.000	0.000
3	**550**	0.942	0.947	1.000	0.000	0.000	0.000	0.000	0.000	0.000	0.000
4	**650**	0.870	0.915	0.968	1.000	0.000	0.000	0.000	0.000	0.000	0.000
5	**750**	1.000	0.884	0.893	0.958	1.000	0.000	0.000	0.000	0.000	0.000
6	**900**	0.968	1.000	0.821	0.910	0.953	1.000	0.000	0.000	0.000	0.000
7	**1,050**	0.942	0.964	1.000	0.861	0.904	0.964	1.000	0.000	0.000	0.000
8	**1,200**	0.890	0.919	0.938	1.000	0.841	0.919	0.955	1.000	0.000	0.000
9	**1,400**	0.840	0.876	0.878	0.940	1.000	0.876	0.912	0.957	1.000	0.000
10	**1,550**	0.817	0.822	0.824	0.865	0.945	0.822	0.845	0.882	0.946	1.000

Install Replace

significantly over the plan horizon as there are more installations and hence more cost associated with it. There are only five replacements over the plan horizon. As can be seen, year-6 and year-7 have the same replacement cost as they have the same energy capacity. The same thing goes for year-8 and year-9.

Table 4.9: Microgrid Costs Considering Optimal REVB Plan Decisions

	UC	**Install**	**OMC**	**RC**	**TC**
	J_1,\$	J_2,\$	J_3,\$	J_4,\$	J,\$
Year 1	6,997,568	467,500	3,300	-	7,468,368
Year 2	7,383,571	221,800	5,444	-	7,610,816
Year 3	7,783,709	288,500	7,733	-	8,079,942
Year 4	8,205,454	199,000	9,266	-	8,413,720
Year 5	8,676,094	199,000	10,793	278,750	9,164,637
Year 6	9,149,587	288,500	13,077	167,250	9,618,415
Year 7	9,670,584	221,800	14,714	167,250	10,074,348
Year 8	10,339,533	288,500	16,993	111,500	10,756,526
Year 9	11,001,071	244,600	18,734	111,500	11,375,905
Year 10	11,835,598	288,500	21,024	-	12,145,122
MGTC (J), \$			**94,707,798**		

4.6.1 Computational Details

The MILP optimization model for the test system was programmed and executed in the General Algebraic Modeling Systems (GAMS) environment [112]. The solver used was CPLEX [114] which was executed on four Intel® Xeon® L7555 1.87-GHz processors and 256 GB of RAM. The CPLEX solver utilizes the Branch and Cut-based algorithm to solve the MILP model, which is a hybrid between Branch-and-Bound and the cutting plane methods that are extensively used for solving such programs [114]. In this model, CPLEX uses Symmetric Multi Processing (SMP), also called *threads*, to control the number of processors to be used in parallel. The model and solver statistics, including the resource usage and the relative optimality gap are given in Table 4.10. Note that the relative optimality gap is defined as the difference between the obtained solution and the minimum bound.

4.7 Summary

The chapter presented a novel backward-forward propagation approach with an embedded power sharing strategy for REVB units to develop a microgrid planning

Table 4.10: Model Statistics

Model Type	MILP
Solver Used	CPLEX
Blocks of Equations	108
Blocks of Variables	46
Number of Single Equations	3,605
Number of Single Variables	2,455
Non-Zero Elements	12,814
Discrete Variables	1,461
Generation Time	0.015 (s)*
CPU time	4.070 (s)*
Relative Gap (%)	0.00299
Threads	10

*(s) denotes time is second.

model taking into consideration its adequacy aspects. A novel concept of measuring the adequacy level of the microgrid in terms of REVB energy to power E_k/P_k^{ini} ratio was presented. A sequential 3-stage scheme along with an associated mathematical model for isolated microgrid planning and operation, and the adequacy check criteria, were presented in detail. The successful operation of REVBs was ensured by the power sharing strategy that is directly related to its degradation and hence its replacement cost. The proposed power sharing strategy was capable of allocating the power needed by the microgrid among different REVB units.

The results obtained from Stage-I and Stage-II were shown to be generally in close agreement with those of Stage-III, although some improvements could be made by using a more detailed battery model which would, however, render the planning model to be computationally very challenging, even for small-sized microgrids. The proposed framework is generic in nature, and can be used by both the microgrid operator or third party investor to set up long-term plans.

Chapter 5

Control and Hardware-in-the-Loop Simulation of Community Energy Storage Systems Based on Repurposed Electric Vehicle Batteries [‡]

5.1 Nomenclature

Indices

$CESS$	CESS index
Cal	Calculated
$cont$	Controller
d	Direct-axis
ref	Reference
lo	Lower
$load$	Total system load

[‡]Parts of this chapter have been submitted for review for possible publication: T. Alharbi, M. Restrepo, M. Kazerani and K. Bhattacharya,"Control and Hardware-in-the-Loop Simulation of Community Energy Storage Systems Based on Repurposed Electric Vehicle Batteries," Electric Power Systems Research, 2020.

max	Maximum
min	Minimum
P	Active Power index
Q	Reactive Power index
q	Quadrature-axis
sys	System
R	Node index
thr	Threshold
up	Upper

Variables

P	Active Power	[kW]
Q	Reactive Power	[kVAR]
S	Apparent Power	[kVA]
V	Voltage	[V]
θ	Angle	[rad]
m	Rule-based controller slope	
SoC	SoC of the REVB battery unit	[%]
SoH	SoH of the REVB battery unit	[%]
χ	Percentage of the converter rating	

5.2 Introduction

Chapter 3 and Chapter 4 presented investment planning frameworks and models for installing single or multiple REVB units in an isolated microgrid. Another application of REVBs is their role as CESS to help distribution networks.

With the increasing adoption of EVs, their charging loads can lead to under-voltages at distribution system nodes, and over-loading of feeders and transformers [50]. These impacts can be alleviated by upgrading the transformers and feeders or implementing coordinated charging of EVs [51–53]. Given that upgrading the transformers and feeders is not a cost-effective solution, and since regulatory policies and communication infrastructure for coordinated charging are not available yet, installing CESSs in LV distribution systems [46] particularly with REVBs, is a viable alternative, because of the increasing availability of these batteries in the market. Once CESS is adopted, there are challenges that have to be overcome in controlling the active and reactive powers using CEMS, while seeking to reduce the adverse impact on the battery SoH. A CEMS equipped with an effective controller for the CESS is capable of improving the flexibility of the distribution system in a cost-

effective manner, while extending the life of the REVBs and the LV distribution transformer.

To realize the operational benefits of a CESS employing REVBs with a properly-designed CEMS, it should be tested in an HIL simulation environment under different conditions. The CEMS should monitor the condition of the LV distribution system and set limits for the P and Q controller of the CESS. The controller determines the battery charging and discharging decisions based on the intended application, considering battery degradation. Thus, the controller should be so designed that the required output power is delivered while slowing down the battery degradation process.

This chapter presents the utilization and control of CESS in LV distribution networks. A real-time CEMS is proposed for the control of the CESS, which uses REVBs and a power electronic interface comprised of a four-quadrant ac/dc converter and a bidirectional dc/dc converter together with the corresponding controllers. To assess the capability of the controller in providing CESS services in the form of active and reactive power control in an LV residential distribution network, four case studies are carried out using HIL simulations. The HIL simulations use an actual battery pack and a four-quadrant converter system. The impact of the proposed controller on the REVB cycling performance is evaluated using an RCA. The distribution transformer LoL is also estimated. The HIL simulation results demonstrate the effectiveness of the proposed real-time CEMS in slowing down the degradation of the battery and LoL of the distribution transformer, while improving the LV distribution voltage profile.

In view of the above, this chapter presents a novel real-time CEMS to control an REVB-based CESS and studies its interactions with a practical LV distribution system using an HIL simulation environment. Therefore, the main objectives of this chapter are as follows:

- Introducing an interactive real-time CEMS for an REVB-based CESS in an LV distribution system. This is an extension (in terms of operation and control) to the work reported in Chapter 3, where economic viability of installing REVBs was proved.
- Developing a rule-based control strategy for the four-quadrant CESS charger, which is embedded in the real-time CEMS, to reduce the loading of the distribution transformer and battery degradation.
- Experimental verification of operation of the proposed real-time CEMS and its

rule-based controller thorough HIL simulation.

The rest of the chapter is structured as follows: Section 5.3 describes the proposed real-time CEMS, as well as the detailed model of the proposed rule-based controller. In Section 5.4, the effectiveness of the proposed CEMS is verified through HIL simulation, followed by discussion of the results in Section 5.5. Finally, some conclusions are presented in Section 5.6.

5.3 The Proposed Real-Time CEMS and Rule-Based CESS Controller

The main objectives of the real-time CEMS are improving the distribution system voltage profile and reducing the adverse impact of EV charging load on the lifespan of LV distribution transformer due to overloading. The process starts with generating detailed daily household load profiles and processing real EV charging data. An LV distribution system is modeled and power flow simulations are carried out. Then, the distribution system is coupled with the real-time HIL simulation setup. The real-time HIL simulation connects an actual battery, a four-quadrant converter, and associated circuits for protection against over voltage/current with the LV distribution system via the Real-Time Target (RTT), as discussed later in this section. The CEMS is then modeled and connected to the LV distribution system and the real-time HIL simulation in order to receive and store feedback signals. The CEMS houses the proposed rule-based controller to control the repurposed EVB-based CESS. Once the real-time CEMS is simulated and experimentally verified, the degradation of repurposed-EVBs is estimated by applying the RCA on the obtained SoC profiles of the CESS battery pack. Finally, the impact of the repurposed EVBs-based CESS operation on LoL of the distribution transformer is estimated.

5.3.1 Real-Time CEMS for HIL Simulation Architecture

The real-time CEMS uses a practical model of the battery, for off-line simulation, and an actual Li-ion battery pack, for HIL simulation, together with a four-quadrant charger, acting as an active and reactive power source/sink. Figure 5.1 shows the proposed architecture for the HIL simulation of the real-time CEMS, which is built

upon an effective exchange of information between the CESS and the LV distribution system. The CEMS or the so-called aggregator (entity (c) in Figure 5.1) is the controller that receives feedback signals from the LV transformer and the CESS (entities (a) and (b), respectively, in Figure 5.1) through the RTT, and sends active and reactive power control signals to the CESS, based on the embedded rule-based controller. The CEMS seeks to reduce the transformer overloading, thus decelerating the transformer LoL, regulate the voltage at CESS node, and slow down the degradation of the battery.

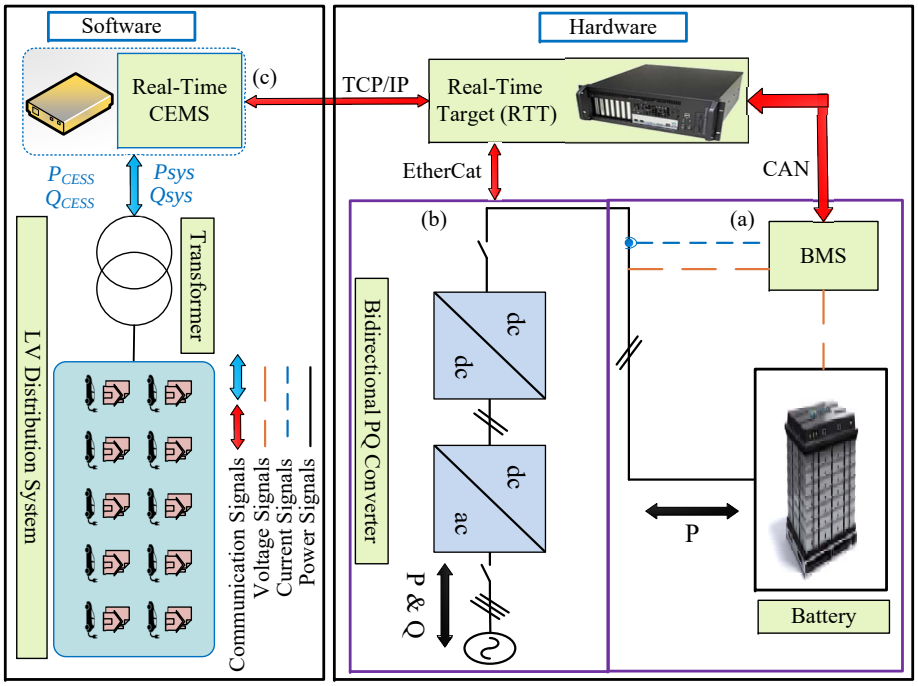

Figure 5.1: Detailed architecture of HIL simulation of the proposed real-time CEMS

The proposed real-time CEMS, with the structure shown in Figure 5.2, is comprised of the rule-based controller for CESS, Phase-Locked Loop (PLL), dq transformations, P and Q controller, and BMS measurements. The proposed rule-based controller for CESS determines the P_{ref} and Q_{ref} as set-points, based on which the d- and q-axis components of CESS currents, I_d and I_q, respectively, are calculated,

as follows:

$$I_d = \ 2 \cdot P_{ref}/V_d \tag{5.1}$$
$$I_q = -2 \cdot Q_{ref}/V_d \tag{5.2}$$

Note that, to facilitate the decoupled active and reactive power control with I_d and I_q, the PLL circuit sets the q-axis component of the CESS terminal voltage, V_q, to zero.

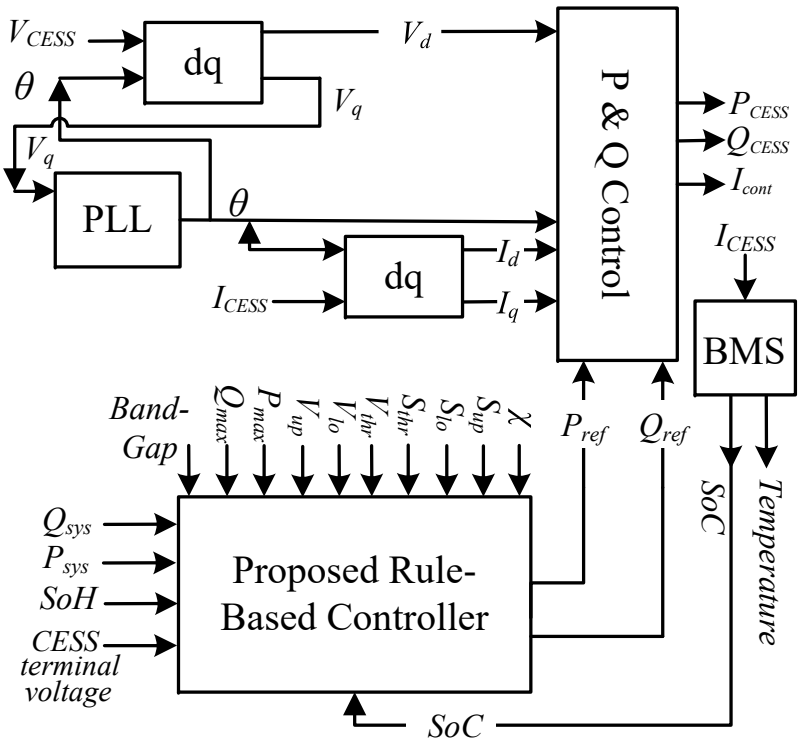

Figure 5.2: Architecture of the proposed real-time CEMS

It is assumed that the rule-based controller is an embedded controller in the CEMS located at the distribution transformer, receiving real-time measurements of active and reactive power consumption of all residential loads and the voltage at the CESS connection point. It should be noted that the CESS is located at the end of the LV feeder.

5.3.2 Proposed Rule-Based Controller for CESS

The bidirectional P–Q converter of the CESS (entity (b) in Figure 5.1) receives control signals from the aggregator (CEMS) to either inject or absorb active power P and reactive power Q within the limits of CESS based on the BMS measurements.

The CESS rule-based controller is governed by a set of rules that are defined by the CEMS and aim to:

- Reduce voltage deviations by sending reactive power control signals;
- Reduce transformer loading and distribution transformer LoL by sending active power control signals;
- Reduce the CESS repurposed EVB degradation by cycling the battery at a proper DoD.

The set points P_{ref} and Q_{ref} of the CESS are the outputs of the controller, as shown in Figure 5.2, that are determined using the following set of rules, illustrated by Figure 5.3.

$$P_{ref} = \begin{cases} -P_{max} \quad \text{(discharge)} & S_{sys} > S_{up} \\ m_p \left(S_{sys} - S_{thr}\right) & S_{lo} \leq S_{sys} \leq S_{up} \\ P_{max} \quad \text{(charge)} & S_{sys} < S_{lo} \end{cases} \tag{5.3}$$

where

$$m_p = \frac{0 - P_{max}}{S_{thr} - S_{lo}} \quad ; \quad P_{max} = S_{max} \tag{5.4}$$

The value of P_{ref} is constrained by the maximum and minimum values of the battery SoC and voltage, converter rating S_{max}, and battery pack temperature, and is derived based on the distribution transformer loading (S_{sys}) and BMS measurements.

As stated by IEEE Standard C57.91-2011 [93], the aging of the distribution transformer will increase exponentially as loading increases. Therefore, the limits of the P-compensation function (S_{up}, S_{lo}) are chosen, based on their impact on the transformer LoL, ensuring that the transformer loading is below 100%, while the operating limits of the battery are respected and the battery degradation is reduced.

Since there is a close relationship between deep battery cycling and battery degradation, an appropriate droop region for the rule-based controller is selected based on

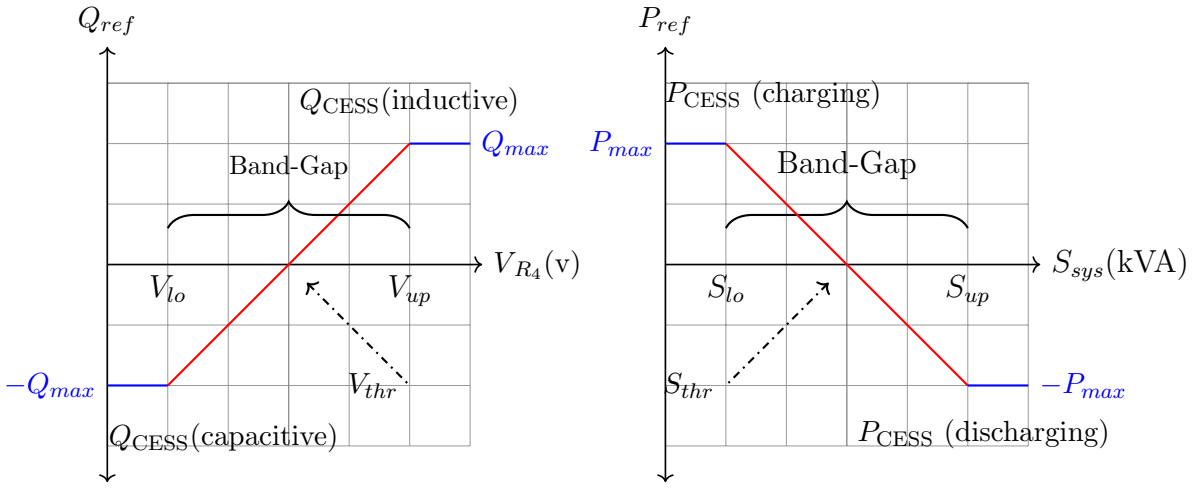

(a) Q-compensation (b) P-compensation

Figure 5.3: Proposed rule-based controller of CESS

the SoH of the battery, so that rapid degradation of the battery, due to deep battery cycling in attempt to prevent overloading of distribution transformer, are avoided.

The value of Q_{ref}, constrained by the apparent power capability of CESS inverter, S_{max}, is determined using the proposed Q-compensation controller function based on the magnitude of the voltage at the CESS connection node (R_4), as follows (see Figure 5.3(b)):

$$Q_{ref} = \begin{cases} Q_{max}(\text{CESS inductive}) & V_{\text{CESS}} > V_{up} \\ m_Q\,(V_{\text{CESS}} - V_{thr}) & V_{lo} \leq V_{\text{CESS}} \leq V_{up} \\ -Q_{max}(\text{CESS capacitive}) & V_{\text{CESS}} < V_{lo} \end{cases} \tag{5.5}$$

where

$$m_Q = \frac{0 - Q_{max}}{V_{thr} - V_{up}} \quad ; \quad Q_{max} = \chi\, S_{max} \tag{5.6}$$

According to ANSI C84.1-2011 standard [115], the voltage at residential nodes must be maintained within Range A, based on the nominal voltage of 120 V (Vmin = 114 V (0.95 pu),Vmax = 126 V (1.05 pu)). Therefore, the limits of the Q-compensation function, V_{up}, V_{lo}, are chosen to satisfy Range A specification. The reactive power compensation from the CESS seeks to improve the voltage at the

end of the feeder and keep it always above the minimum service voltage. Note that the value of χ in (5.6) is assumed to be half the rating of the converter so that the CESS converter does not wear out due to excessive use of the dc-link capacitor, as the provision of reactive currents tends to increase the dc voltage ripple, and thus, has adverse impact on the lifespan of this component.

The reactive power reference Q_{ref} generated by the proposed rule-based controller is sent to the CESS bidirectional charger which is constrained by the charger's apparent power capability, as follows [116]:

$$P_{ref}^2 + Q_{ref}^2 \leqslant S_{max}^2 \tag{5.7}$$

$$Q_{ref} = \frac{\mid Q_{ref} \mid}{Q_{ref}} \sqrt{S_{max}^2 - P_{ref}^2} \tag{5.8}$$

$$\mid Q_{ref} \mid \leqslant Q_{max} = \chi \, S_{max} \tag{5.9}$$

Equations (5.8) and (5.9) are only used to limit the reactive power reference when the apparent power limit is reached.

It should be noted that the proposed rule based controller has some similarities to the IEEE 1547-2018 standard which provides the technical specifications and requirements for distributed energy resources (DERs) in LV in general. However, IEEE 1547-2018 standard does not take into account the degradation of the battery and its SoH during operation.

5.4 Experimental Setup for HIL Simulation

The CEMS, including the proposed rule-based controller (Section 5.3), is validated using the HIL simulation setup shown in Figure 5.4. The setup is comprised of a power module which includes the CESS bidirectional converter, an RTT, the CEMS work-station equipped with Matlab, and a battery pack whose BMS communicates with the RTT through a Controller Area Network (CAN) bus to allow HIL simulations.

The CEMS receives/sends the control signals from/to the RTT through a Transmission Control Protocol/Internet Protocol (TCP/IP) link. At the same time, the

RTT communicates with the four-quadrant converter and the battery BMS through EtherCat and CAN links. This connection allows an external agent such as the CEMS to control the CESS.

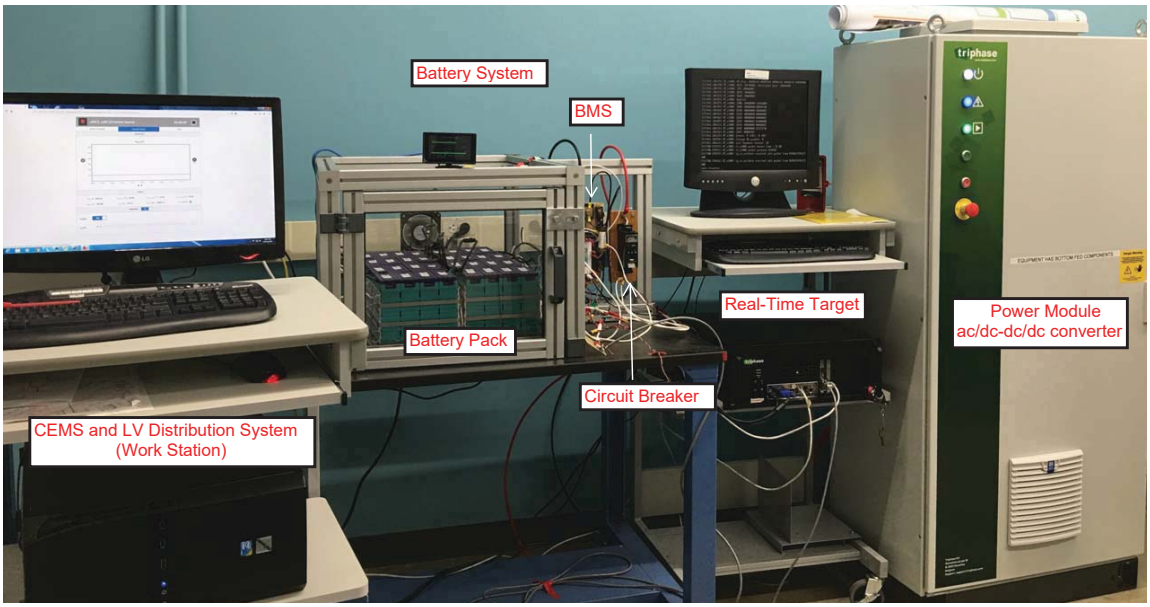

Figure 5.4: Experimental setup for HIL simulation

In the following, the main system components are explained in detail.

• Power Module: This is the part of CESS that interfaces the battery pack with the grid. It is comprised of a filter, an ac/dc converter, and a dc/dc converter with three independent channels. The power module is equipped with sensor of measurements line voltage and current to monitor the state of the equipment during tests. The power module parameters and its schematic diagram used in thesis are reported in Table B1 and Figure B1 in Appendix B. Please refer to [117] for more system parameters.

• RTT: This is a high-performance computer based on Linux that runs the HIL simulation model and communicates the measurements and control signals from the converter and the BMS to the CEMS in real-time, using an industrial ethernet link (EtherCat) and CAN bus. Please refer to [117] RTT specifications.

• Battery Pack: This is a part of the CESS that is connected to the dc/dc converter - with its three dc channels connected in parallel - through a circuit breaker. A BMS is also included for monitoring the performance of the battery pack. Since

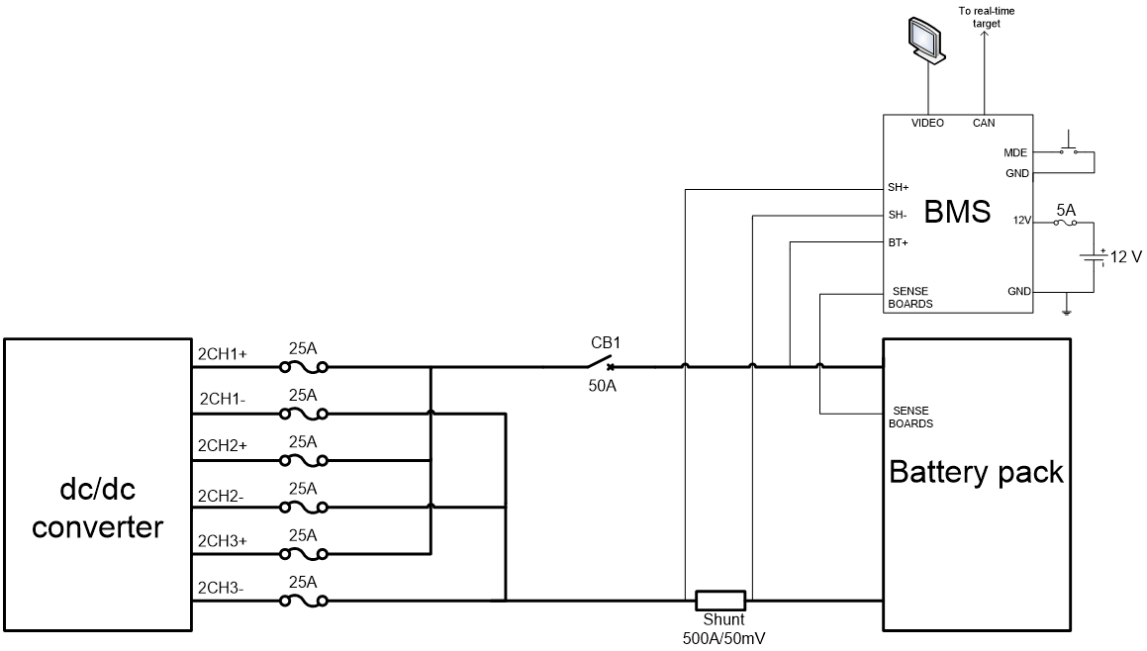

Figure 5.5: Power module hardware and battery pack set up

the interface with the grid is a three-phase ac/dc converter, and the simulated CESS operates in a single-phase distribution network, only the current and voltage signals corresponding to phase A are used in the simulation, considering a scaling factor to make the power level of the simulated system the same as that of the actual hardware. The power module and battery pack set up used in this thesis is shown in Figure 5.5.

• CEMS and LV Distribution System Work-station: This is a computer that runs Matlab and is connected to the RTT through a TCP/IP link, and serves to build and compile the distribution system simulation model, control the operation of the power module in real-time, and visualize the simulation signals.

• CAN bus: The RTT is connected to the CEMS and BMS to allow them to exchange information. The BMS is connected to the RTT via CAN bus to read and log the battery data, such as SoC, over-current and over-voltage signals, cell voltages, pack voltage, and pack temperature, during HIL simulation. It should be noted that the actual signals of the converter and battery pack are used in the LV distribution system model to evaluate the performance of the CEMS, in compliance with the standard levels of voltage and transformer load.

Table 5.1: Rule-Based Controller Parameters

$S_{up} = 50$	$S_{lo} = 40$	$S_{thr} = 45$	(kVA)
$V_{up} = 1.03$	$V_{lo} = 0.96$	$V_{thr} = 1$	(p.u.)

5.5 Results and Discussions

5.5.1 Test System, Input Data and Assumptions

5.5.1.1 LV Distribution System

The developed real-time CEMS framework is used to perform HIL simulations on the CIGRÉ North American 10-bus LV distribution system with a household load at each bus, served by 50 kVA transformer with single-phase (12.47 kV) primary and split-phase (240 V-120V) secondary [118]. The data for the LV distribution system, extracted from [113], corresponds to a North-American LV residential feeder, shown in Figure 5.6 .

The battery pack used in HIL simulation is a 4.1 kWh, 115 V Li-ion battery pack, while the repurposed EVB considered for off-line simulation is a Toyota RV4 battery pack, with an initial capacity of 42 kWh. It is assumed that the EVB capacity had degraded to 33.6 kWh, i.e., 80% of its initial capacity, when it was removed from the EV [54]. Since it was not possible to use a large-capacity EVB in the HIL simulations, a 4.1 kWh battery was used instead and the simulation parameters and signals were scaled down, accordingly.

The CESS is connected at the end of the LV distribution system feeder, at node R_4. The simulated model of the CESS charger in the distribution system imitates the actual current and voltage signals measured directly on the CESS converter and received via the RTT. The parameters of the proposed rule-based controller are given in Table 5.1. Note that the controller band-gap in Figure 5.3(a) is set at 10 kVA for P_{max} by trial and error and P_{min} of a $\pm$10 kW.

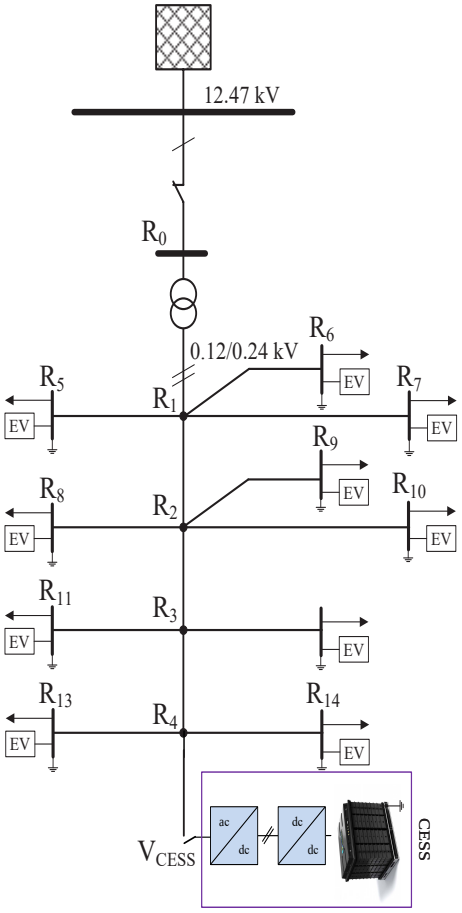

Figure 5.6: CIGRE Secondary distribution system model

5.5.1.2 EV Charging Load Profiles

A large volume of data is collected from the Dataloggers installed on several EVs operating in Waterloo Region of Ontario, Canada, through the Drive4Data Program [119]. The data includes initial battery SoC, EV arrival and departure times, drive cycle, charging current and voltage. The EV charging load profiles are calculated from the corresponding voltage and current data available.

5.5.1.3 Residential Load Profiles

The load profiles of the residential customers at each of the 10 LV distribution system nodes are created using the method presented in [120]. A sample stacked load profile of a high-demand house in Summer is shown in Figure 5.7. Each load profile consists of 5,760 data-points representing the demand of a house every 5 minutes, for 24 hours. The summer average demand of a household is 2 kVA higher than its annual average demand. The residential loads are modeled as constant impedance loads, which are therefore, voltage dependent. Some of the residential loads have a peak demand of 12 kVA which results in a total system peak demand of 51 kVA at 9 PM; however, because of the voltage dependency of loads, and voltage drop due to heavy consumption, the actual load tends to be lower.

5.5.2 Test Results and Discussions

To investigate and illustrate the benefits of the proposed CEMS and the rule-based CESS controller, the following four cases are simulated.

1) Case 0: no EV, no CESS, off-line simulation.
2) Case I: with EV, no CESS, off-line simulation.
3) Case II: with EV, CESS, and CEMS, off-line simulation.

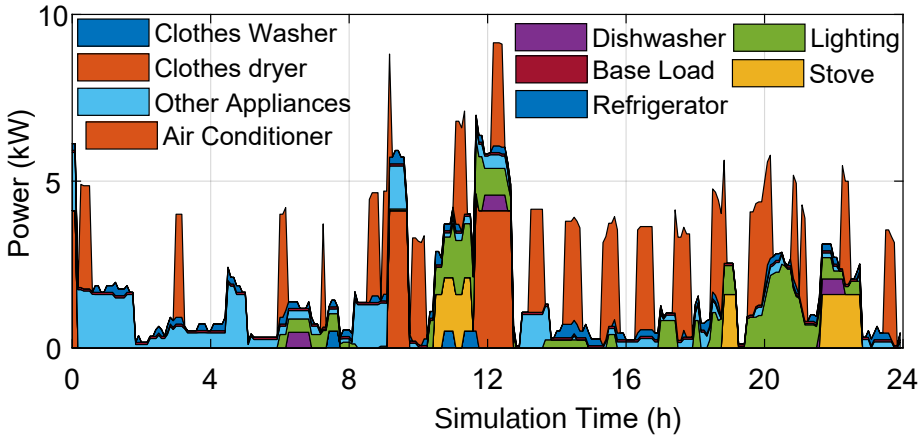

Figure 5.7: A stacked daily load profile of a sample house in Summer

4) Case III: with EV, CESS, and CEMS, HIL simulation.

Note that the baseline (Case I) refers to no CESS is installed.

5.5.2.1 Case I

Figures 5.8(a)-(c) present Case I results for the total active, reactive, and apparent power loading on the distribution transformer, as well as the system node voltages in the presence of EV charging. It is noted that new peaks appear during early morning and evening due to simultaneous charging of EVs, with total apparent power, S_{sys}, surpassing the transformer rated capacity of 50 KVA, contributing to distribution transformer's LoL. The node voltages have clearly dropped during these periods, violating the Range A limits (V_{min} = 0.95 p.u., or 228 V). In this work, the thermal model of distribution transformers, proposed by IEEE C57.91-2011 [93], has been adopted to estimate the LoL of the transformer based on its loading. As Table 5.2 shows, in Case I, the annual LoL is 7.7% of the nominal life of 180,000 h, that is beyond the specified 5% limit. Note also that the annual LoL of the distribution transformer is approximately 0.3% in the Case 0, when neither EV load nor CESS was considered. These results show that EV charging is detrimental to the life span of the transformer. This impact would be even greater with larger EVBs with greater charging capacities.

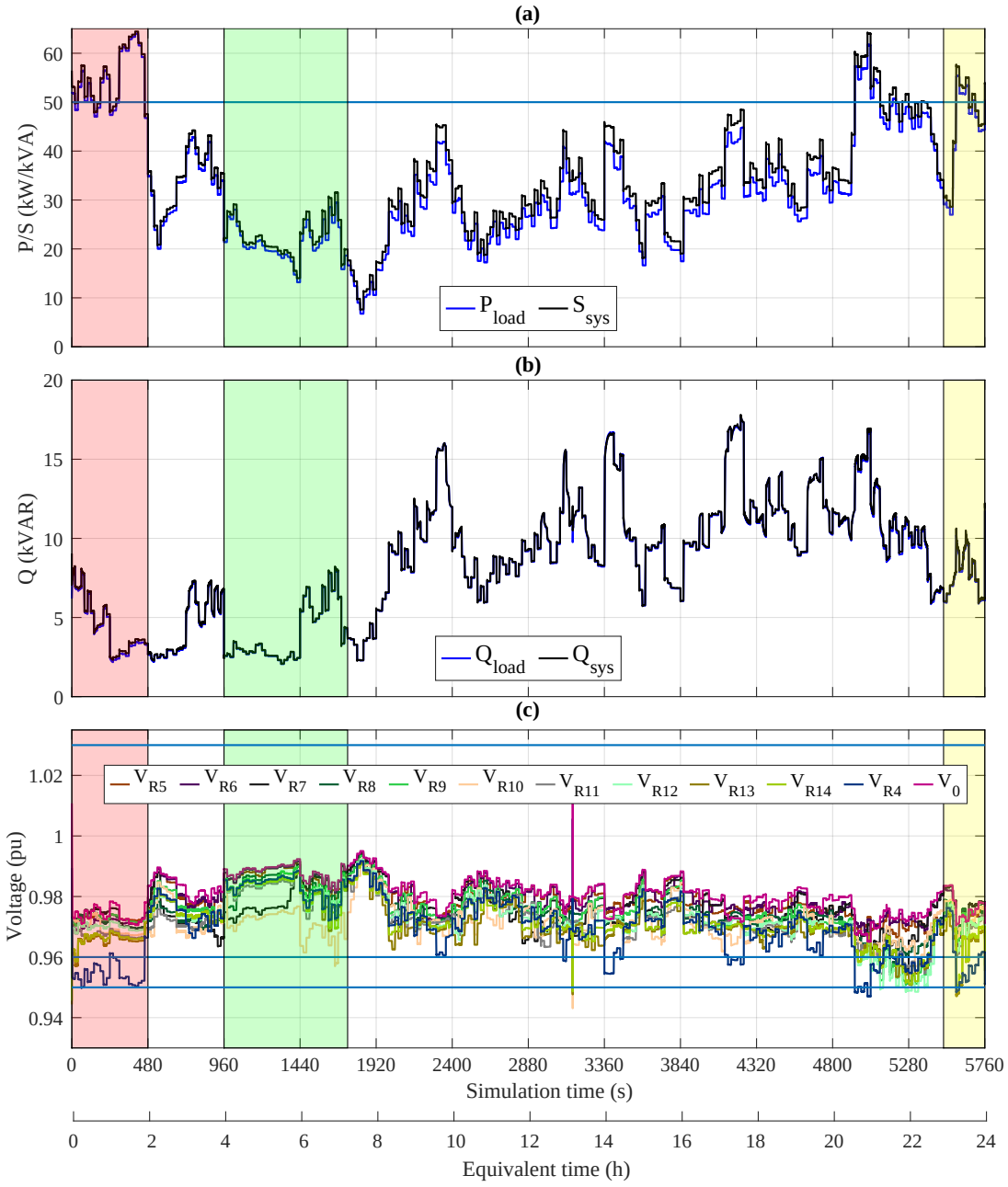

Figure 5.8: Case I (a) Load active power and transformer apparent power and capacity limit; (b) Load and transformer reactive power; (c) LV distribution system bus voltages and voltage limits.

5.5.2.2 Case II

In Case II, with CESS and real-time CEMS under the proposed rule-based control, the distribution transformer load (S_{sys}) is shaved to a point below the rated capacity of 50 kVA, for most of the time. The loading in this case is 110%, lasting less than 20 minutes. According to [121], the rated overloading of the transformer depends on the transformer's previous loading. In the case under study, since the transformer is previously loaded to approximately 94% of its rated capacity, it can be loaded to 110%, for 60 minutes, at 78℃ [121]. Also, as can be noted from Figure 5.9(a), the total active power loading on the transformer, P_{sys}, is reduced by virtue of the P-compensation of the CESS during peak hours. The system voltages are also improved and are now within the acceptable range specified by ANSI [115] (Figure 5.9(c)), when compared to the voltages in Figure 5.8(c). This is due to the fact that less current is drawn from the distribution transformer, as a result of the active and reactive power compensation provided by CESS. It should be noted that the spikes seen in Fig. 5.8(c) are due to merging of data from consecutive HIL simulations.

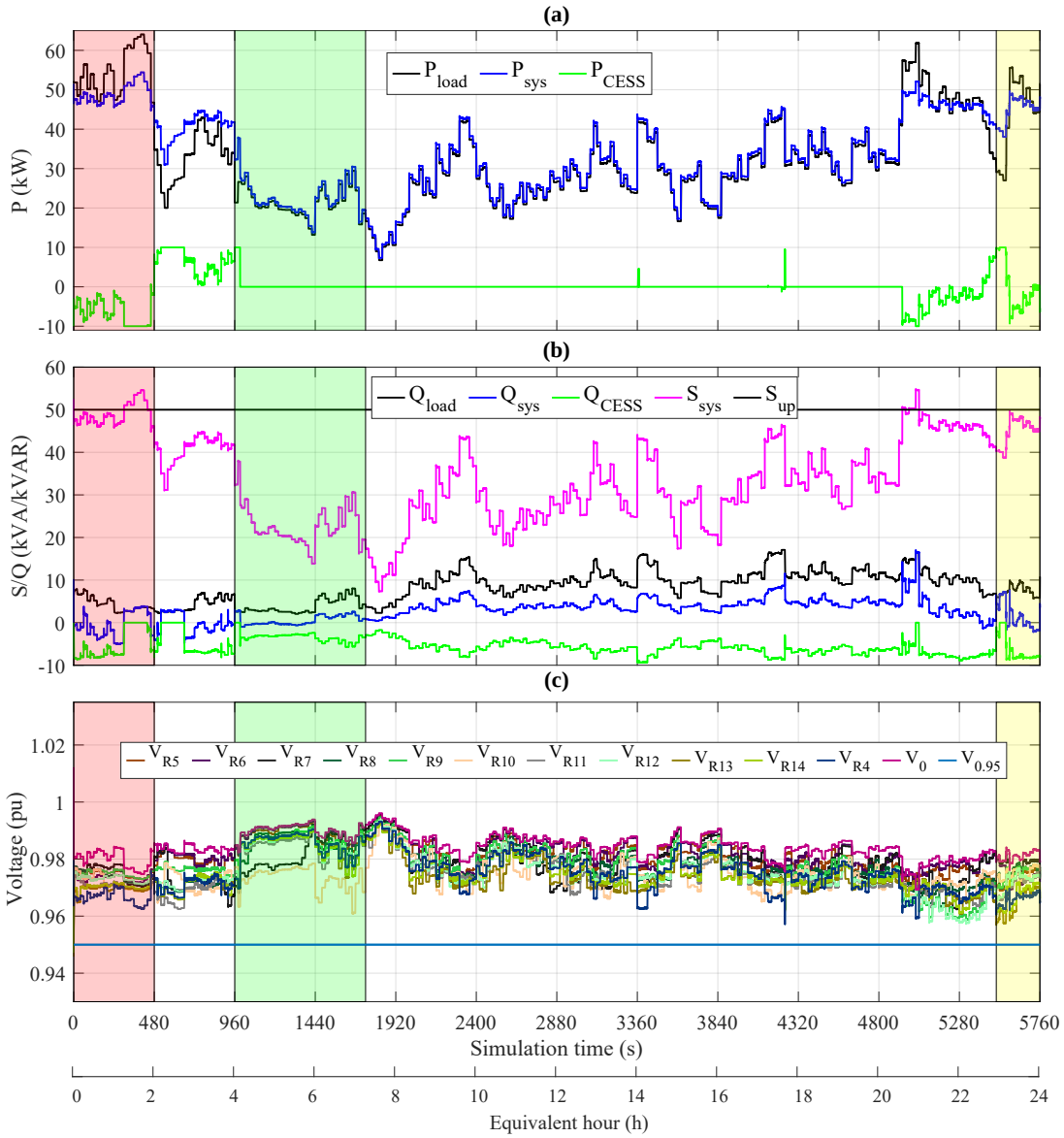

Figure 5.9: Case II (a) Active powers of load, transformer, and CESS; (b) Apparent and reactive powers of load, transformer, and CESS; (c) LV system bus voltages.

It can be observed that the real-time simulation time-scale of 5,760 seconds used in this work, corresponds to a 24-hour equivalent time-scale.

Table 5.2: Distribution Transformer's LoL

	Case 0	**Case I**	**Case II**	**Case III**
Daily LoL (%)	0.00083	0.0211	0.0065	0.0065
Annual LoL (%)	0.30290	7.7	2.37	2.37

For Case-II, Figure 5.10 presents the P_{CESS} and Q_{CESS} delivered to the LV distribution system, which are following closely the P_{ref} and Q_{ref} set-points, issued by the controller. Note that in the first window in Figure 5.10, between 0 and 480s, there is a need for more active power from the CESS.

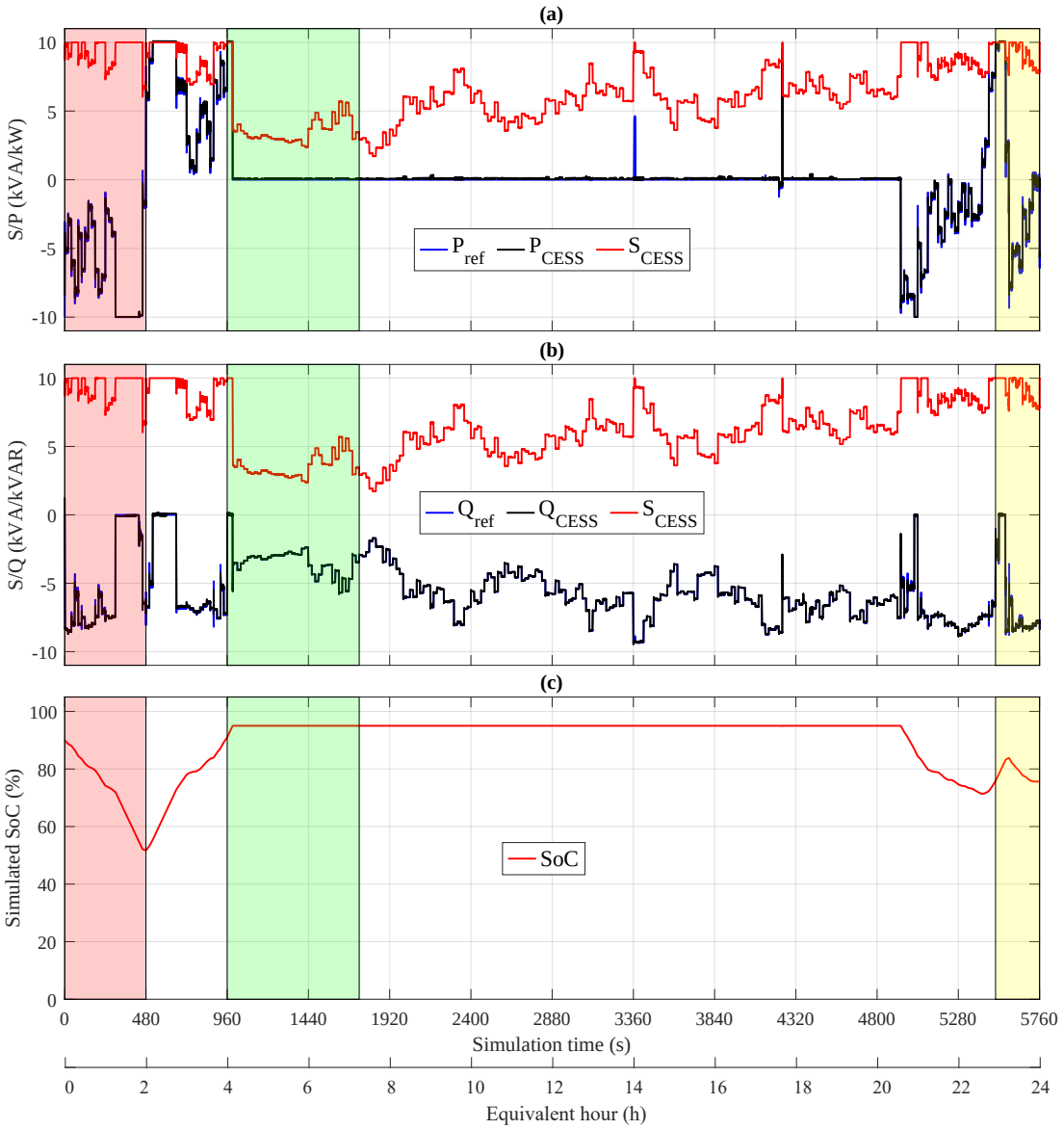

Figure 5.10: Case II (a) CESS apparent, active power and its reference; (b) CESS apparent, reactive power and its reference; (c) SoC of CESS battery pack

Also note that, in some instances, the CESS bidirectional charger provides more Q-compensation to the LV distribution system than what the system needs, which can be transferred to the MV side of the distribution transformer. The P_{CESS} profile

is reflected on the SoC profile of the battery, as shown in Figure 5.10(c). The annual LoL of the distribution transformer in Case II is reduced to approximately 2.4% of nominal life, which is below the specified limit (see Table 5.2). This demonstrates the benefit of CESS in reducing the detrimental impact of EV charging on the life of the transformer.

5.5.2.3 Case III

To validate the off-line CEMS simulation results and illustrate successful operation under the embedded rule-based controller in following the set-points in the four quadrants of the P-Q plane, Case III, *i.e.*, HIL simulation is performed and results are presented in Figures 5.11 to 5.12. It can be observed that the P, Q, and voltage plots of Figure 5.11 are very similar to those of Figure 5.9, upon down-scaling.

Figures 5.11 (a)-(c) show the actions of the CEMS in setting the CESS battery discharging at the maximum capacity of the charger when the transformer loading is higher than its rated capacity, S_{up}, and charging at the maximum capacity where transformer loading is below S_{lo}. The charging and discharging are governed by the S_{max} of the CESS bidirectional charger, shown in Figs. 5.11(a) and (b).

The voltage and current profiles of the CESS monitored by the BMS, are shown in Figure 5.12, and are within their respective limits. Also, the SoC profile of the battery pack in Case III is very similar to that obtained from the off-line simulations in Case II. The SoC of the CESS battery was re-calculated based on its real-time voltage and current to compare it with the SoC signal from the BMS. Figure 5.12 (c) shows that the SoC profiles agree closely.

It is evident from Figure 5.12 that the rule-based controller of the CEMS respects the SoH of the repurposed EVB by discharging only when needed and with fewer number of cycles and smaller DoD, so that battery degradation is minimal. This was accomplished by implementing a properly-sized band-gap.

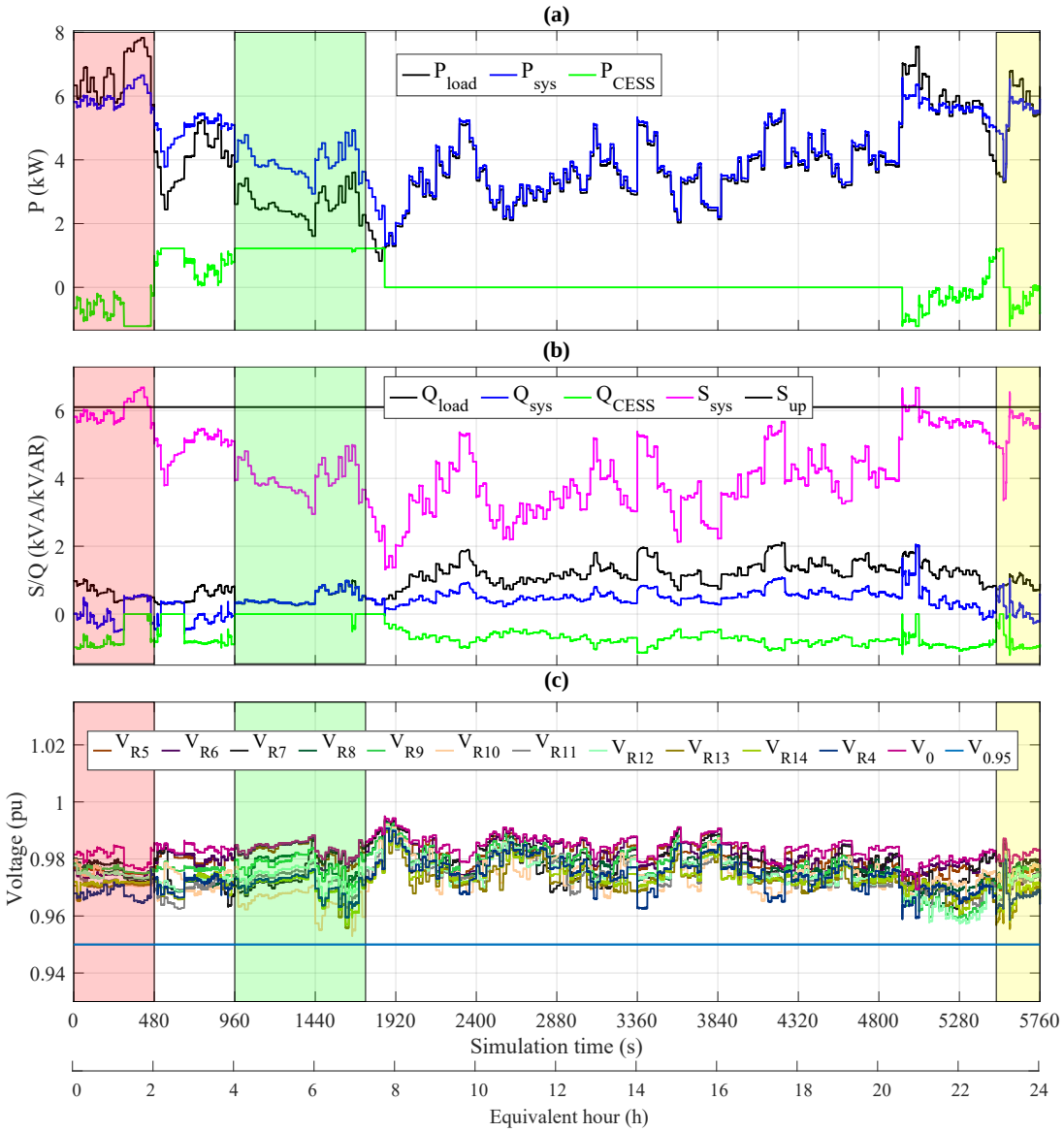

Figure 5.11: Case III (a) Active powers of load, transformer, and CESS; (b) Reactive powers of load, transformer, and CESS and apparent power of transformer; (c) LV system bus voltages and voltage limits

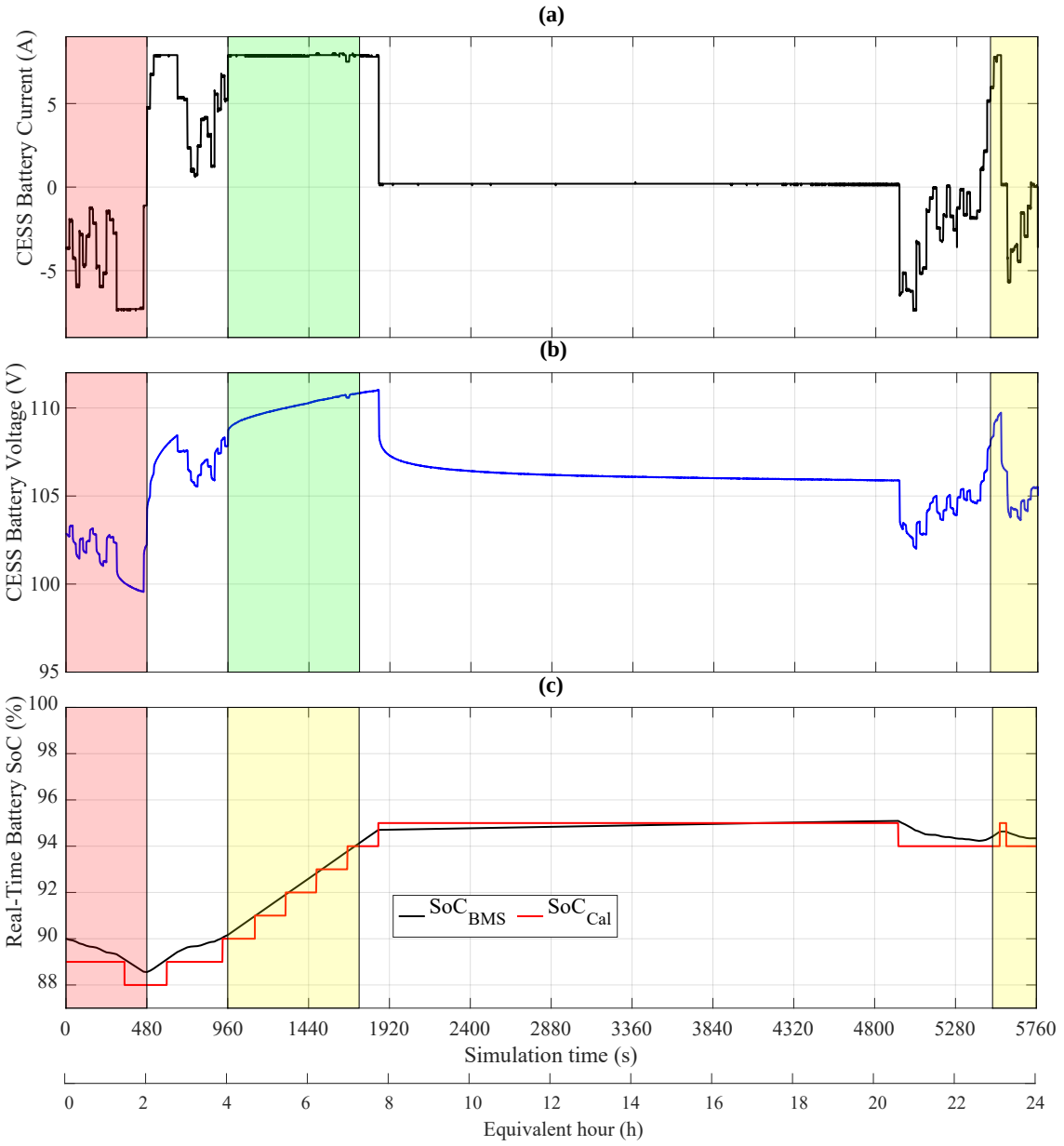

Figure 5.12: Case III (a) CESS battery current; (b) CESS battery voltage; (c) CESS battery pack SoC

In order to measure how the CEMS would minimize battery degradation by cycling the battery at lower DoD, the RCA which is a lifetime estimation method

based on counting the charge and discharge cycles for different ranges of DoD [95], is used in this work. Each DoD range corresponds to a specific number of cycles to failure. This information is provided by the battery manufacturer and is used to quantify the cumulative degradation impact of the cycles. The RCA decomposes the SoC profile obtained from Case II into a combination of cycles based on the counts of charging and discharging and their corresponding DoD, also referred to as, *cycle range or cycle amplitude*. Figure 5.13 shows the inputs and outputs of the RCA.

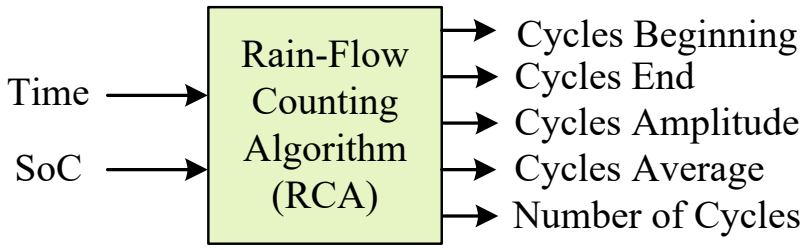

Figure 5.13: Inputs and outputs of RCA

The histogram of the SoC cycles, shown in Figure 5.14, depicts the number of SoC cycles and the corresponding cycle average and DoD, where the cycle average of each counted cycle is the mean of SoC at the beginning and end of each cycle. The RCA counts only one cycle from the SoC (Figure 5.10(c)) with high DoD, while the remaining counted cycles have low DoD, as shown in Figure 5.14.

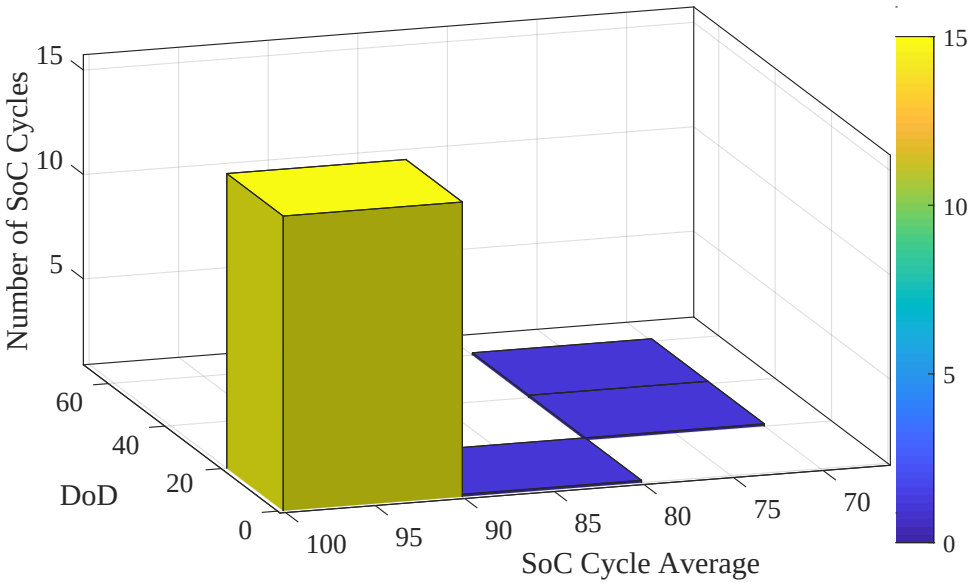

Figure 5.14: RCA histogram based on simulated SoC

The options for voltage control in LV distribution systems are limited; however, a CESS with REVBs, bidirectional converters and the proposed real-time CEMS can accomplish this task effectively with a reliable communication. The idea is to integrate several REVBs to create an energy hub for the LV distribution system. From the utility's perspective, the objective of employing REVBs as CESS is to minimize the impact of EV charging load on the grid and prolong the life span of the transformer. Alternatively, from the EV owners' perspective, the objective of adopting REVBs as residential BESS is to minimize the energy cost of EV charging and arbitrage the remaining BESS capacity with the utility, through proper control of the REVB charging and discharging.

Network upgrade deferral, improvement of voltage and system reliability, and participation in active and reactive power services are all benefits that can be accrued by REVB-based CESS and its associated proposed controller. To elaborate on the first benefit, the total NPV is calculated without and with CESS, as one of the most commonly used criteria for calculating the saving on investment. In this work, in order to calculate the total NPV, the installation cost of the utilized REVB is assumed to be \$9,080 with a replacement cost of \$6,720 (taken from Chapter 3), and the replacement cost of transformer is assumed to be a \$27,886 [121]. The total NPV for a planning period of 24-year, with 8% discount rate, would yield a

benefit of $6,257 (14% savings with respect to the case where no CESS is installed), considering the obtained LoL of Case I and Case II. The savings would be much higher considering that there are a large number of LV distribution systems within the jurisdiction of each LDC.

With proper sizing of the repurposed EVB-based CESS in the LV distribution system, and effective coordination of operation with possible battery energy storage systems in the households, it is possible to fully eliminate overloading of the distribution transformer according to the industry code.

5.6 Summary

This chapter proposed a CEMS equipped with a rule-based controller for REVB-based CESS. Since the degradation of the batteries should be taken into account whether the battery is new or used, the adopted controller structure can be modified based on the specific characteristics of the battery. An HIL simulation was used to validate the simulation results and illustrate the effectiveness of the proposed CEMS and its rule-based control algorithms, using actual signals from the BMS and the bidirectional charger setup. The performance of the controller and its compliance with system voltage and transformer loading standards in an LV distribution system were studied and analyzed. The results obtained from the HIL simulation were satisfactory and showed improvement in operation of the LV distribution system in terms of reducing LoL of distribution of transformer and system voltage regulation as well as slowing down the CESS battery pack degradation.

Chapter 6

Conclusions

6.1 Summary

The research presented in this thesis focused on planning, operation and control of BESSs and REVBs.

Chapter 1 laid out the motivation of the research, emphasising the need for comprehensive models and strategies for planning, operation and control considering REVBs in isolated microgrid or as CESS in an LV distribution system. A literature review of related works, particularly on planning and operation of BESS in microgrids as well as the control of CESS utilizing HIL simulation, was presented. This chapter also presented an overview of the research objectives.

Chapter 2 presented a brief background on the topics related to the research including microgrids and basic UC model in such systems, BESSs and some basic definitions, EVs and EVB models and their degradation. Furthermore, REVBs for second-use applications, bi-directional converters and transformer LoL were presented. Also, the well-known RCA was introduced and a brief overview of mathematical programming was presented.

Chapter 3 discussed how the retired EVBs, after repurposing, can serve as an alternative to new batteries in a BESS. The chapter proposed a comprehensive and novel framework for planning and operation of a BESS based on REVBs. The first stage of the framework presented a systematic procedure to model EVB degradation during first life to capture their impact on the SoH and hence the number of years

to their EoL. Taking into account the cost information from the second stage, a novel microgrid planning model for optimal BESS sizing was proposed considering the impact of degradation due to calendar and cycling effects. The proposed model introduced a novel set of mathematical relations for BESS degradation and their optimal year of replacement. The first stage was tested on a real EV drive cycle database and the microgrid planning model was verified using the CIGRE isolated microgrid test system benchmark.

Chapter 4 presented a novel backward-forward propagation approach with an embedded energy sharing strategy for REVB units, which was incorporated within an extended formulation of the previously developed microgrid planning model taking into consideration its reliability aspects. The novel concept of measuring microgrid adequacy in terms of REVB E/P ratio was presented. A sequential 3-stage scheme along with the associated mathematical model for isolated microgrid planning including the adequacy check criteria were presented in detail. The optimal operation of REVBs was determined by the energy sharing strategy which was capable of distributing the power needed by the microgrid among different REVB units. The results obtained from Stage-I and Stage-II were shown to be generally in close agreement with those of Stage-III.

Chapter 5 proposed a novel CEMS equipped with a rule-based controller for REVB-based CESS. Since degradation of batteries should be taken into account, the proposed controller structure can be modified to suit the specific characteristics of the battery. An HIL simulation was used to validate the simulation results and illustrate the effectiveness of the proposed CEMS and its rule-based control algorithm, using actual signals from the BMS and the bidirectional charger setup. The performance of the controller and its compliance with system voltage and transformer loading standards in an LV distribution system were studied and analyzed. The results obtained from the HIL simulation were satisfactory and showed improvement in operation of the LV distribution system in terms of reducing LoL of distribution transformers and system voltage regulation as well as slowing down the CESS battery pack degradation.

The main conclusions drawn from the presented research are as follows:

- The inclusion of BESS degradation models in the planning and operations framework helps in avoiding under-/over-estimating the system regulation reserve requirements, and hence reduces the investment cost.
- If degradation and optimal replacement years are ignored, the optimal decisions

will be affected and hence reflected on the total cost and reliability of the microgrid.
- Including the feature of determining the optimal year of replacement prevents excessive replacements over the planning horizon, which reduces capital expenditure.
- Since REVBs have lower number of C2F as compared to new BESS, the microgrid operator tends to keep REVBs in reserve instead of discharging them, while the new BESS are scheduled for discharging operations significantly more.
- Including the REVB energy sharing strategy in the proposed planning model helps reduce the degradation of the installed battery, and hence maintain the E/P ratio above unity to ensure microgrid reliability.

6.2 Contributions

The main contributions of the research presented in this thesis can be summarized as follows:

- The degradation characteristics and SoH of EVBs are captured and modeled in detail, considering cycling and calendar degradations using real EV drive cycle data.
- A novel microgrid planning model is proposed that determines the optimal decisions on new BESS or REVBs, and their corresponding size and year of installation, taking into account a new set of mathematical constraints relating to BESS degradation and optimal year of replacement. The REVBs are modeled considering their first-life degradation, which impacts the microgrid planning decisions.
- The extended microgrid planning model considering reliability allows including multiple REVB units and simultaneous determination of their optimal sizing and replacement timeline using a new energy sharing strategy among various installed REVB units. Furthermore, the proposed heuristic algorithm is computationally efficient and does not involve any additional complexity, beyond that of the planning model proposed earlier, while enabling the inclusion of the reliability constraint.
- The proposed rule-based control strategy embedded in an interactive real-time CEMS ensures that the controller structure can be maneuvered to suit the adopted battery's characteristics and hence slow down its degradation and

reduce loading of the distribution transformer.

The main contents and contributions of Chapter 3 have been published in IEEE Transactions on Industrial Informatics [54]. The main contents of Chapter 4 is submitted for review and possible publication in IEEE Transactions on Power System [122], and the main contents of Chapter 5 is submitted for review and possible publication in Electric Power Systems Research Journal [123].

6.3 Scope for Future Work

Further research can be conducted based on the work presented in this thesis. Some ideas are presented below:

- To ease the computational burden and to be able to include dynamic decision variables and non-linearities in BESS; decomposition based optimization methods are appealing options which may be considered for future studies.
- Inclusion of uncertainties in RES and demand and their impact on the microgrid plan decisions need to be investigated.
- The currently available microgrid planning models do not consider degradation costs. There is a need to develop an appropriate degradation cost function for REVBs based on their operating and physical characteristics for inclusion in the microgrid planning models.
- The proposed rule-based controller can be further improved by introducing an optimized dead-band around the threshold to avoid frequent controller switching between injecting/absorbing active and reactive power actions.
- Further improvements can be made by optimally sizing the CESS and including distributed REVBs instead of one CESS unit owned by the utility. The CEMS presented, is designed for a single REVB unit. This configuration can be made more generic so that individual EV owners may connect their REVBs and converters and respond with different degrees of flexibility to the control signals from the CEMS. This will yield greater benefits than what can be realized with a single REVB owner.

References

[1] NASA, "NASA, NOAA analyses reveal record-shattering global warm temperatures in 2015," 2016. [Online]. Available: https://www.nasa.gov/press-release/nasa-noaa-analyses-reveal-record-shattering-global-warm-temperatures-in-2015

[2] Environment and Climate Change Canada, "Greenhouse gas emissions by canadian economic sector," 2017. [Online]. Available: https://www.ec.gc.ca/indicateurs-indicators/default.asp?lang=en&n=F60DB708-1

[3] Ministry of the Environment and Climate Change, "Ontario's five year climate change action plan 2016-2020," 2016. [Online]. Available: http://www.applications.ene.gov.on.ca/ccap/products/CCAPENGLISH.pdf

[4] Sandia National Labs, "Canadian environmental sustainability indicators: Progress towards canada's greenhouse gas emission reduction target," Sandia National Labs., USA, Tech. Rep., 2018. [Online]. Available: https://www.canada.ca/content/dam/eccc/documents/pdf/cesindicators/progress-towards-canada-greenhouse-gas-reduction-target/2019/progress-towards-ghg-emissions-target-en.pdf

[5] Clean Energy Ministerial, "Electric vehicles initiative (EVI)," 2016. [Online]. Available: http://www.cleanenergyministerial.org/Portals/2/pdfs/factsheets/EVI-CEM7-FS.pdf

[6] International Energy Agency, "Outlook 2017: Two million and counting," 2017. [Online]. Available: https://www.iea.org/publications/freepublications/publication/GlobalEVOutlook2017.pdf

[7] Electric Mobility Canada, "Electric vehicle sales in canada in 2018," 2020. [Online]. Available: https://emc-mec.ca/new/electric-vehicle-sales-in-canada-in-2018/

[8] Ministry of the Environment and Climate Change, "Paris declaration on electro-mobility and climate change & call to action," 2015. [Online]. Available: http://newsroom.unfccc.int/media/521376/paris-electro-mobility-declaration.pdf

[9] J. Neubauer, K. Smith, E. Wood, and A. Pesaran, "Identifying and overcoming critical barriers to widespread second use of PEV batteries," National Renewable Energy Lab., Golden, CO, USA, Tech. Rep., 2015.

[10] S. X. Chen and H. B. Gooi, "Sizing of energy storage system for microgrids," in *2010 IEEE 11th International Conference on Probabilistic Methods Applied to Power Systems*, June 2010, pp. 6–11.

[11] H. Wang and J. Huang, "Joint investment and operation of microgrid," *IEEE Transactions on Smart Grid*, vol. 8, no. 2, pp. 833–845, March 2017.

[12] E. Hajipour, M. Bozorg, and M. Fotuhi-Firuzabad, "Stochastic capacity expansion planning of remote microgrids with wind farms and energy storage," *IEEE Transactions on Sustainable Energy*, vol. 6, no. 2, pp. 491–498, April 2015.

[13] H. Xie, S. Zheng, and M. Ni, "Microgrid development in China: A method for renewable energy and energy storage capacity configuration in a megawatt-level isolated microgrid." *IEEE Electrification Magazine*, vol. 5, no. 2, pp. 28–35, June 2017.

[14] T. Alharbi and K. Bhattacharya, "Optimal scheduling of energy resources and management of loads in isolated/islanded microgrids," *Canadian Journal of Electrical and Computer Engineering*, vol. 40, no. 4, pp. 284–294, 2017.

[15] M. C. E. Center, C. E. Solutions, S. E. Advantage, D. E. Advisors, A. Analytics *et al.*, "State of charge: Massachusetts energy storage initiative," Massachusetts Department of Energy Resources, Tech. Rep., 2016. [Online]. Available: http://www.mass.gov/eea/docs/doer/state-of-charge-report.pdf

[16] "Fuels technical report- module 2: Demand outlook," Ministry of Energy, Tech. Rep., Sep 2016. [Online]. Available: http://www.energy.gov.on.ca/en/archive/fuels-technical-report/module-2/

[17] P. Plötz, T. Gnann, and M. Wietschel, "Modelling market diffusion of electric vehicles with real world driving data. Part I: Model structure and validation," Karlsruhe, Working Paper Sustainability and Innovation S4/2014, 2014. [Online]. Available: http://hdl.handle.net/10419/96521

[18] A. Bandivadekar, *On the Road in 2035: Reducing Transportation's Petroleum Consumption and GHG Emissions*. Massachusetts Institute of Technology, 2008. [Online]. Available: https://books.google.ca/books?id=EN0sQwAACAAJ

[19] B. M. Al-Alawi and T. H. Bradley, "Review of hybrid, plug-in hybrid, and electric vehicle market modeling studies," *Renewable and Sustainable Energy Reviews*, vol. 21, no. Supplement C, pp. 190 – 203, 2013.

[20] Bloomberg, "Electric vehicle outlook 2017: Bloomberg new energy finance's annual long-term forecast of the world's electric vehicle market," 2017. [Online]. Available: https://data.bloomberglp.com/bnef/sites/14/2017/07/BNEF_EVO_2017_ExecutiveSummary.pdf

[21] A. Millner, "Modeling Lithium-Ion battery degradation in electric vehicles," in *2010 IEEE Conference on Innovative Technologies for an Efficient and Reliable Electricity Supply*, Sept 2010, pp. 349–356.

[22] L. Lam and P. Bauer, "Practical capacity fading model for Li-Ion battery cells in electric vehicles," *IEEE Transactions on Power Electronics*, vol. 28, no. 12, pp. 5910–5918, 2013.

[23] M. Broussely, *Aging Mechanisms and Calendar-Life Predictions in Lithium-Ion Batteries*. Boston, MA: Springer US, 2002, pp. 393–432. [Online]. Available: https://doi.org/10.1007/0-306-47508-1_14

[24] A. Keeli and R. K. Sharma, "Optimal use of second life battery for peak load management and improving the life of the battery," in *2012 IEEE International Electric Vehicle Conference*, March 2012, pp. 1–6.

[25] E. Cready, J. Lippert, J. Pihl, I. Weinstock, and P. Symons, "Technical and economic feasibility of applying used EV batteries in stationary applications," Sandia National Labs., Albuquerque, NM (US); Sandia National Labs., Livermore, CA (US), Tech. Rep., 2003.

[26] C. White, B. Thompson, and L. G. Swan, "Repurposed electric vehicle battery performance in second-life electricity grid frequency regulation service," *Journal of Energy Storage*, vol. 28, p. 101278, 2020.

[27] D. Strickland, L. Chittock, D. A. Stone, M. P. Foster, and B. Price, "Estimation of transportation battery second life for use in electricity grid systems," *IEEE Transactions on Sustainable Energy*, vol. 5, no. 3, pp. 795–803, July 2014.

[28] L. Canals Casals, B. Amante García, and M. González Benítez, "A cost analysis of electric vehicle batteries second life businesses," in *18th International Congress on Project Management and Engineering. Alcañiz*, 2014.

[29] J. S. Neubauer, A. Pesaran, B. Williams, M. Ferry, and J. Eyer, "A techno-economic analysis of PEV battery second use: Repurposed-battery selling price and commercial and industrial end-user value," in *SAE 2012 World Congress and Exhibition*. SAE International, April 2012.

[30] C. K. Narula, R. Martinez, O. Onar, M. Starke, and G. Andrews, "Final report economic analysis of deploying used batteries in power systems," *Oak Ridge National Laboratory, Oak Ridge, TN*, 2011.

[31] J. Neubauer, K. Smith, E. Wood, and A. Pesaran, "Identifying and overcoming critical barriers to widespread second use of PEV batteries," National Renewable Energy Lab.(NREL), Golden, CO (United States), Tech. Rep., 2015.

[32] N. Mukherjee and D. Strickland, "Control of second-life hybrid battery energy storage system based on modular boost-multilevel buck converter," *IEEE Transactions on Industrial Electronics*, vol. 62, no. 2, pp. 1034–1046, 2015.

[33] I. Miranda, N. Silva, and H. Leite, "A holistic approach to the integration of battery energy storage systems in island electric grids with high wind penetration," *IEEE Transactions on Sustainable Energy*, vol. 7, no. 2, pp. 775–785, 2016.

[34] I. Alsaidan, A. Khodaei, and W. Gao, "A comprehensive battery energy storage optimal sizing model for microgrid applications," *IEEE Transactions on Power Systems*, vol. 33, no. 4, pp. 3968–3980, 2018.

[35] H. Alharbi and K. Bhattacharya, "Stochastic optimal planning of battery energy storage systems for isolated microgrids," *IEEE Transactions on Sustainable Energy*, vol. 9, no. 1, pp. 211–227, 2018.

[36] W. Zhong, L. Wang, Z. Liu, and S. Hou, "Reliability evaluation and improvement of islanded microgrid considering operation failures of power electronic equipment," *Journal of Modern Power Systems and Clean Energy*, vol. 8, no. 1, pp. 111–123, 2020.

[37] J. Dong, L. Zhu, Y. Su, Y. Ma, Y. Liu, F. Wang, L. M. Tolbert, J. Glass, and L. Bruce, "Battery and backup generator sizing for a resilient microgrid under stochastic extreme events," *IET Generation, Transmission Distribution*, vol. 12, no. 20, pp. 4443–4450, 2018.

[38] S. Bahramirad, W. Reder, and A. Khodaei, "Reliability-constrained optimal sizing of energy storage system in a microgrid," *IEEE Transactions on Smart Grid*, vol. 3, no. 4, pp. 2056–2062, 2012.

[39] A. S. Bin Humayd and K. Bhattacharya, "Distribution system planning to accommodate distributed energy resources and PEVs," *Electric Power Systems Research*, vol. 145, pp. 1 – 11, 2017.

[40] T. Ding, Y. Hu, and Z. Bie, "Multi-stage stochastic programming with nonanticipativity constraints for expansion of combined power and natural gas systems," *IEEE Transactions on Power Systems*, vol. 33, no. 1, pp. 317–328, 2018.

[41] K. Baker, G. Hug, and X. Li, "Energy storage sizing taking into account forecast uncertainties and receding horizon operation," *IEEE Transactions on Sustainable Energy*, vol. 8, no. 1, pp. 331–340, 2017.

[42] M. Petrollese, L. Valverde, D. Cocco, G. Cau, and J. Guerra, "Real-time integration of optimal generation scheduling with MPC for the energy management of a renewable hydrogen-based microgrid," *Applied Energy*, vol. 166, pp. 96 – 106, 2016.

[43] A. Hoke, A. Brissette, K. Smith, A. Pratt, and D. Maksimovic, "Accounting for Lithium-Ion battery degradation in electric vehicle charging optimization," *IEEE Journal of Emerging and Selected Topics in Power Electronics*, vol. 2, no. 3, pp. 691–700, 2014.

[44] eCamion, "Communitiy energy storage (CES)/ 250kwh," 2017. [Online]. Available: http://www.ecamion.com/portfolio/ces/

[45] B. P. Koirala, E. van Oost, and H. van der Windt, "Community energy storage: A responsible innovation towards a sustainable energy system?" *Applied Energy*, vol. 231, pp. 570 – 585, 2018.

[46] S. A. El-Batawy and W. G. Morsi, "Optimal design of community battery energy storage systems with prosumers owning electric vehicles," *IEEE Transactions on Industrial Informatics*, vol. 14, no. 5, pp. 1920–1931, 2018.

[47] S. Hashemi, Guangya Yang, J. Østergaard, Shi You, and Seung-Tae Cha, "Storage application in smart grid with high PV and EV penetration," in *IEEE PES ISGT Europe 2013*, 2013, pp. 1–5.

[48] R. Arghandeh, J. Woyak, A. Onen, J. Jung, and R. Broadwater, "Economic optimal operation of community energy storage systems in competitive energy markets," *Applied Energy*, vol. 135, pp. 71 – 80, 2014.

[49] S. Van der Stelt, T. AlSkaif, and W. Van Sark, "Techno-economic analysis of household and community energy storage for residential prosumers with smart appliances," *Applied Energy*, vol. 209, pp. 266 – 276, 2018.

[50] J. A. P. Lopes, F. J. Soares, and P. M. R. Almeida, "Integration of electric vehicles in the electric power system," *Proceedings of the IEEE*, vol. 99, no. 1, pp. 168–183, 2011.

[51] N. Mehboob, M. Restrepo, C. A. Cañizares, C. Rosenberg, and M. Kazerani, "Smart operation of electric vehicles with four-quadrant chargers considering uncertainties," *IEEE Transactions on Smart Grid*, vol. 10, no. 3, pp. 2999–3009, 2019.

[52] M. C. Kisacikoglu, B. Ozpineci, and L. M. Tolbert, "EV/PHEV bidirectional charger assessment for V2G reactive power operation," *IEEE Transactions on Power Electronics*, vol. 28, no. 12, pp. 5717–5727, 2013.

[53] M. Yilmaz and P. T. Krein, "Review of the impact of vehicle-to-grid technologies on distribution systems and utility interfaces," *IEEE Transactions on Power Electronics*, vol. 28, no. 12, pp. 5673–5689, 2013.

[54] T. Alharbi, K. Bhattacharya, and M. Kazerani, "Planning and operation of isolated microgrids based on repurposed electric vehicle batteries," *IEEE Transactions on Industrial Informatics*, vol. 15, no. 7, pp. 4319–4331, 2019.

[55] F. Zhang, F. Luo, Z. Dong, Y. Liu, and G. Ranzi, "Hierarchical energy management scheme for residential communities under grid outage event," *IET Smart Grid*, vol. 3, no. 2, pp. 174–181, 2020.

[56] C. Liu, K. T. Chau, D. Wu, and S. Gao, "Opportunities and challenges of vehicle-to-home, vehicle-to-vehicle, and vehicle-to-grid technologies," *Proceedings of the IEEE*, vol. 101, no. 11, pp. 2409–2427, 2013.

[57] M. N. Mojdehi, M. Fardad, and P. Ghosh, "Technical and economical evaluation of reactive power service from aggregated EVs," *Electric Power System Research*, vol. 133, pp. 132 – 141, 2016.

[58] A. S. Vijay, S. Doolla, and M. C. Chandorkar, "Real-time testing approaches for microgrids," *IEEE Journal of Emerging and Selected Topics in Power Electronics*, vol. 5, no. 3, pp. 1356–1376, 2017.

[59] M. A. Awadallah and B. Venkatesh, "Energy storage in distribution system planning and operation: Current status and outstanding challenges," *Canadian Journal of Electrical and Computer Engineering*, vol. 42, no. 1, pp. 10–19, 2019.

[60] Z. R. Ivanović, E. M. Adžić, M. S. Vekić, S. U. Grabić, N. L. Čelanović, and V. A. Katić, "HIL evaluation of power flow control strategies for energy storage connected to smart grid under unbalanced conditions," *IEEE Transactions on Power Electronics*, vol. 27, no. 11, pp. 4699–4710, 2012.

[61] A. Nourai, R. Sastry, and T. Walker, "A vision amp; strategy for deployment of energy storage in electric utilities," in *IEEE PES General Meeting*, July 2010, pp. 1–4.

[62] L. Wang, D. H. Liang, A. F. Crossland, P. C. Taylor, D. Jones, and N. S. Wade, "Coordination of multiple energy storage units in a low-voltage distribution network," *IEEE Transactions on Smart Grid*, vol. 6, no. 6, pp. 2906–2918, 2015.

[63] Y. Yang, H. Li, A. Aichhorn, J. Zheng, and M. Greenleaf, "Sizing strategy of distributed battery storage system with high penetration of photovoltaic for

voltage regulation and peak load shaving," *IEEE Transactions on Smart Grid*, vol. 5, no. 2, pp. 982–991, 2014.

[64] D. B. Wickramasinghe Abeywardana, B. Hredzak, and V. G. Agelidis, "A fixed-frequency sliding mode controller for a boost-inverter-based battery-supercapacitor hybrid energy storage system," *IEEE Transactions on Power Electronics*, vol. 32, no. 1, pp. 668–680, 2017.

[65] M. Restrepo, J. Morris, M. Kazerani, and C. A. Cañizares, "Modeling and testing of a bidirectional smart charger for distribution system EV integration," *IEEE Transactions on Smart Grid*, vol. 9, no. 1, pp. 152–162, 2018.

[66] S. Chowdhury and P. Crossley, *Microgrids and Active Distribution Networks*, ser. Energy Engineering. Institution of Engineering and Technology, 2009. [Online]. Available: https://digital-library.theiet.org/content/books/po/pbrn006e

[67] D. E. Olivares, C. A. Cañizares, and M. Kazerani, "A centralized energy management system for isolated microgrids," *IEEE Transactions on Smart Grid*, vol. 5, no. 4, pp. 1864–1875, 2014.

[68] J. Royer, "Status of remote/off-grid communities in Canada," Natural Resources Canada, Standard, August 2011. [Online]. Available: https://www.nrcan.gc.ca/sites/www.nrcan.gc.ca/files/canmetenergy/files/pubs/2013-118_en.pdf

[69] H. Pandžić, Ting Qiu, and D. S. Kirschen, "Comparison of state-of-the-art transmission constrained unit commitment formulations," in *2013 IEEE Power Energy Society General Meeting*, 2013, pp. 1–5.

[70] M. Carrion and J. M. Arroyo, "A computationally efficient mixed-integer linear formulation for the thermal unit commitment problem," *IEEE Transactions on Power Systems*, vol. 21, no. 3, pp. 1371–1378, 2006.

[71] R. Billinton and R. Allan, *Reliability evaluation of power systems*. Springer Science & Business Media, 2013.

[72] X. Xu, M. Bishop, D. G. Oikarinen, and C. Hao, "Application and modeling of battery energy storage in power systems," *CSEE Journal of Power and Energy Systems*, vol. 2, no. 3, pp. 82–90, 2016.

[73] Q. Fu, A. Hamidi, A. Nasiri, V. Bhavaraju, S. B. Krstic, and P. Theisen, "The role of energy storage in a microgrid concept: Examining the opportunities and promise of microgrids." *IEEE Electrification Magazine*, vol. 1, no. 2, pp. 21–29, 2013.

[74] DTE Energy, "DTE energy advanced implementation of energy storage technologies," DTE Energy, Detroit,MI, Tech. Rep., 2015.

[75] H. Rudnick and L. Barroso, "Flexibility needed: Challenges for future energy storage systems [guest editorial]," *IEEE Power and Energy Magazine*, vol. 15, no. 5, pp. 12–19, 2017.

[76] M. Arriaga, C. A. Cañizares, and M. Kazerani, "Renewable energy alternatives for remote communities in northern ontario, canada," *IEEE Transactions on Sustainable Energy*, vol. 4, no. 3, pp. 661–670, 2013.

[77] R. H. Byrne, T. A. Nguyen, D. A. Copp, B. R. Chalamala, and I. Gyuk, "Energy management and optimization methods for grid energy storage systems," *IEEE Access*, vol. 6, pp. 13 231–13 260, 2018.

[78] M. Broussely, *Lithium-Ion Batteries for EV, HEV and other Industrial Applications*. Boston, MA: Springer US, 2003, pp. 645–685. [Online]. Available: https://doi.org/10.1007/978-0-387-92675-9_21

[79] M. Ehsani, Y. Gao, and A. Emadi, *Modern electric, hybrid electric, and fuel cell vehicles: fundamentals, theory, and design*. CRC press, 2009.

[80] A. Ostadi and M. Kazerani, "Optimal sizing of the battery unit in a plug-in electric vehicle," *IEEE Transactions on Vehicular Technology*, vol. 63, no. 7, pp. 3077–3084, 2014.

[81] A. Khaligh and Z. Li, "Battery, ultracapacitor, fuel cell, and hybrid energy storage systems for electric, hybrid electric, fuel cell, and plug-in hybrid electric vehicles: State of the art," *IEEE Transactions on Vehicular Technology*, vol. 59, no. 6, pp. 2806–2814, 2010.

[82] F. Conte, "Battery and battery management for hybrid electric vehicles: a review," *e & i Elektrotechnik und Informationstechnik*, vol. 123, no. 10, pp. 424–431, 2006.

[83] R. Garcia-Valle and J. A. P. Lopes, *Electric vehicle integration into modern power networks*. Springer Science & Business Media, 2012.

[84] A123 Systems, "High power lithium ion battery products, apr18650 m1a," 2017. [Online]. Available: http://www.a123systems.com/lithium-battery.htm

[85] Electric cars available in Canada, "Plug'n Drive," 2017. [Online]. Available: https://www.plugndrive.ca/electric-cars-available-in-canada

[86] Min Chen and G. A. Rincon-Mora, "Accurate electrical battery model capable of predicting runtime and I-V performance," *IEEE Transactions on Energy Conversion*, vol. 21, no. 2, pp. 504–511, 2006.

[87] Lijun Gao, Shengyi Liu, and R. A. Dougal, "Dynamic lithium-ion battery model for system simulation," *IEEE Transactions on Components and Packaging Technologies*, vol. 25, no. 3, pp. 495–505, 2002.

[88] S. Buller, M. Thele, R. W. A. A. De Doncker, and E. Karden, "Impedance-based simulation models of supercapacitors and Li-ion batteries for power electronic applications," *IEEE Transactions on Industry Applications*, vol. 41, no. 3, pp. 742–747, 2005.

[89] S. C. Hageman, "Simple pspice models let you simulate common battery types," 1993.

[90] X. Lin, H. E. Perez, J. B. Siegel, A. G. Stefanopoulou, Y. Li, R. D. Anderson, Y. Ding, and M. P. Castanier, "Online parameterization of lumped thermal dynamics in cylindrical lithium ion batteries for core temperature estimation and health monitoring," *IEEE Transactions on Control Systems Technology*, vol. 21, no. 5, pp. 1745–1755, 2013.

[91] Q. Badey, G. Cherouvrier, Y. Reynier, J.-M. Duffault, and S. Franger, *Ageing forecast of lithium-ion batteries for electric and hybrid vehicles*, January 2011, pp. 65–79.

[92] M. Foster, P. Isely, C. Standridge, and M. Hasan, "Feasibility assessment of remanufacturing, repurposing, and recycling of end of vehicle application lithium-ion batteries," *Journal of Industrial Engineering and Management*, vol. 7, no. 3, pp. 698–715, 2014.

[93] "IEEE guide for loading mineral-oil-immersed transformers and step-voltage regulators," *IEEE Std 1547-2018 (Revision of IEEE Std 1547-2003)*, pp. 1–138, March 2012.

[94] Y. Assolami, "Probabilistic impact of charging plug-in electric vehicles on the electric energy distribution systems," Master's thesis, University of Ontario Institute of Technology, 2016.

[95] C. Amzallag, J. Gerey, J. L. Robert, and J. Bahuaud, "Standardization of the rainflow counting method for fatigue analysis," *International Journal of Fatigue*, vol. 16, no. 4, pp. 287–293, 1994.

[96] S. D. Downing and D. Socie, "Simple rainflow counting algorithms," *International Journal of Fatigue*, vol. 4, no. 1, pp. 31–40, 1982.

[97] R. Dufo-López and J. Bernal-Agustín, "Multi-objective design of PV–wind–diesel–hydrogen–battery systems," *Renewable Energy*, vol. 33, no. 12, pp. 2559 – 2572, 2008.

[98] V. Herrera, A. S. de Ibarra, A. Milo, H. Gaztañaga, and H. Camblong, "Optimal energy management of a hybrid electric bus with a battery-supercapacitor storage system using genetic algorithm," in *2015 International Conference on Electrical Systems for Aircraft, Railway, Ship Propulsion and Road Vehicles (ESARS)*, March 2015, pp. 1–6.

[99] S. S. Rao, *Engineering optimization: theory and practice*. John Wiley & Sons, 2009.

[100] W. L. Winston, M. Venkataramanan, and J. B. Goldberg, *Introduction to mathematical programming*. Thomson/Brooks/Cole Duxbury; Pacific Grove, CA, 2003, vol. 1.

[101] P. M. Castro, "Tightening piecewise McCormick relaxations for bilinear problems." *Computers & Chemical Engineering*, vol. 72, pp. 300–311, 2015.

[102] CNET. (2017, June) ABB & GM . [Online]. Available: http://www.cnet.com/uk/news/nissan-leafbatteries-seek-second-life-as-home-storage

[103] S. Saxena, C. L. Floch, J. MacDonald, and S. Moura, "Quantifying EV battery end-of-life through analysis of travel needs with vehicle powertrain models," *Journal of Power Sources*, vol. 282, pp. 265–276, 2015.

[104] National Renewable Energy Laboratory. NREL battery second-use repurposing cost calculator for electric vehicles (EVs). [Online]. Available: https://www.nrel.gov/transportation/b2u-calculator.html

[105] Y. Riffonneau, S. Bacha, F. Barruel, and S. Ploix, "Optimal power flow management for grid connected PV systems with batteries," *IEEE Transactions on Sustainable Energy*, vol. 2, no. 3, pp. 309–320, 2011.

[106] E. M. Krieger, J. Cannarella, and C. B. Arnold, "A comparison of lead-acid and lithium-based battery behavior and capacity fade in off-grid renewable charging applications," *Energy*, vol. 60, pp. 492–500, 2013.

[107] F. Ramos, C. Cañizares, and K. Bhattacharya, "Effect of price responsive demand on the operation of microgrids," in *2014 Power Systems Computation Conference*, 2014, pp. 1–7.

[108] A. Akhil, G. Huff, A. Currier, B. Kaun, D. Rastler, S. Chen, A. Cotter, D. Bradshaw, and W. Gauntlett, *DOE/EPRI 2013 electricity storage handbook in collaboration with NRECA*. Sandia National Laboratories Albuquerque, NM, 2013.

[109] United States Environmental Protection Agency (EPA), "Vehicle and Fuel Emissions Testing," 2017. [Online]. Available: https://www.epa.gov/vehicle-and-fuel-emissions-testing/dynamometer-drive-schedules

[110] C. Robert and G. Casella, *Monte Carlo statistical methods*. Springer Science & Business Media, 2013.

[111] U. S. C. for Automotive Research (USCAR), "FreedomCAR and USABC energy storage goals for power-assist HEVs," 2002. [Online]. Available: http://www.uscar.org/commands/files_download.php?files_id=83

[112] GAMS Development Corporation, General Algebraic Modeling System (GAMS), software. [Online]. Available: http://www.gams.com.

[113] K. Strunz *et al.*, "Benchmark systems for network integration of renewable and distributed energy resources," CIGRE Task Force C6.04.02, Tech. Rep., 2014.

[114] CPLEX 12 Solver, General Algebraic Modeling System (GAMS), software. [Online]. Available: https://www.gams.com/latest/docs/S_CPLEX.html

[115] Standerd, ANSI, "For electric power systems and equipment-voltage ratings (60 Hz)," *ANSI C84*, pp. 1–2006, 2006.

[116] K. Turitsyn, P. Sulc, S. Backhaus, and M. Chertkov, "Options for control of reactive power by distributed photovoltaic generators," *Proceedings of the IEEE*, vol. 99, no. 6, pp. 1063–1073, 2011.

[117] "Triphase NV, PM15A30F03 - Power Modules," https://triphase.com/products/power-modules/PM15/A30F03/, January 2019.

[118] Hydro One Networks Inc. (2013) Distribution Customers Conditions of Service. [Online]. Available: http://www.hydroone.com/HydroOneConditionsofService2013ENGLISH.pdf

[119] Waterloo Institute for Sustainable Energy, "Drive4data program," 2017. [Online]. Available: https://wise.uwaterloo.ca/drive4data

[120] M. Armstrong, M. Swinton, H. Ribberink, I. Beausoleil-Morrison, and J. Millette, "Synthetically derived profiles for representing occupant-driven electric loads in Canadian housing," *Journal of Building Performance Simulation*, vol. 2, no. 1, pp. 15–30, 2009.

[121] Schneider Electric Inc. (2017) Oil-immersed transformers. [Online]. Available: https://www.se.com/eg/en/download/mylist/permissible_overload.pdf

[122] T. Alharbi, K. Bhattacharya, and M. Kazerani, "A new approach for repurposed ev battery-based microgrid planning considering adequacy," *IEEE Transactions on Power Systems*, In review, 2020.

[123] T. Alharbi, M. Restrepo, M. Kazerani, and K. Bhattacharya, "Control and hardware-in-the-loop simulation of community energy storage systems based on repurposed electric vehicle batteries," *Electric Power System Research*, In review, 2020.

Appendices

Appendix A

Table A1: Battery cell specifications

Parameter	Value
Nominal voltage (V)	3.3
Charge capacity (Ah)	2.3
Nominal series resistance (mΩ)	10
Mass (g)	76

Table A2: Nissan Leaf parameters

Effective vehicle frontal area $A_f\,(\mathrm{m}^2)$	2.59
Aerodynamic drag coefficient C_D	0.28
Rolling resistance coefficient C_r	0.0125
Vehicle mass (excluding EVB) (kg)	1,177
Gearbox ratio N_g	7.94
Wheel radius r_w(m)	0.3
Air density $\rho\,(\mathrm{kg/m}^3)$	1.225
Gravitational acceleration $g\,(\mathrm{m/s}^2)$	9.81

Appendix B

Table B1: HIL System Data

Table B1: Power module specification

	Power Input ratings, (maximum)		Output Ratings, (maximum)	
	1 phase ac	3 phase ac	1 dc channel	3 dc channels
Voltage	$0 - 120\,\text{V}$	$0 - 208\,\text{V}$	$20 - 650\,\text{V}$	$20 - 650\,\text{V}$
Current	$2 \times 24\,\text{A}$	$3 \times 24\,\text{A}$	$72\,\text{A}$	$3 \times 24\,\text{A}$
Power	$2.88\,\text{kW}$ total	$8.65\,\text{kW}$ total	$8.65\,\text{kW}$	$8.65\,\text{kW}$

Figure B1: Power Module Schematic Diagram used for HIL System

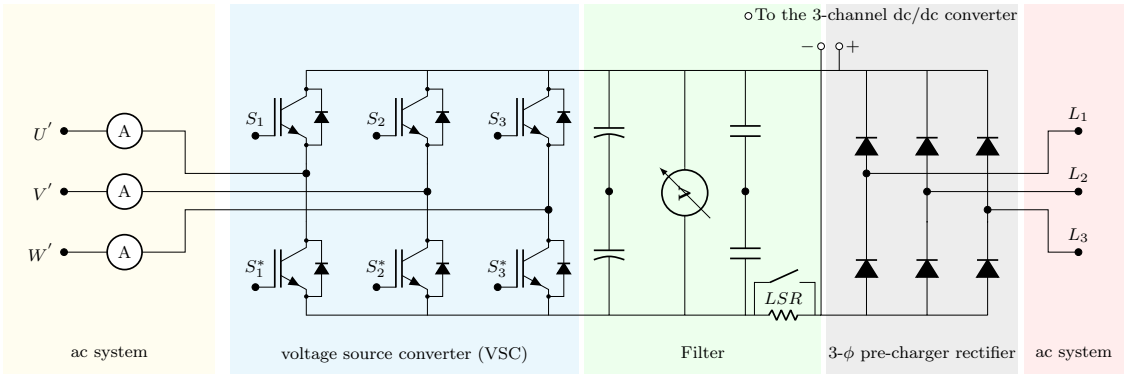

Figure B1: Power Module.